

The Role of Subsidence during the Development of North American Polar/Subtropical Jet Superpositions

Daniel Keyser

University at Albany, SUNY

Andrew C. Winters

University of Colorado Boulder

Lance F. Bosart

University at Albany, SUNY

Department of Meteorology and

Atmospheric Science

The Pennsylvania State University

29 January 2020



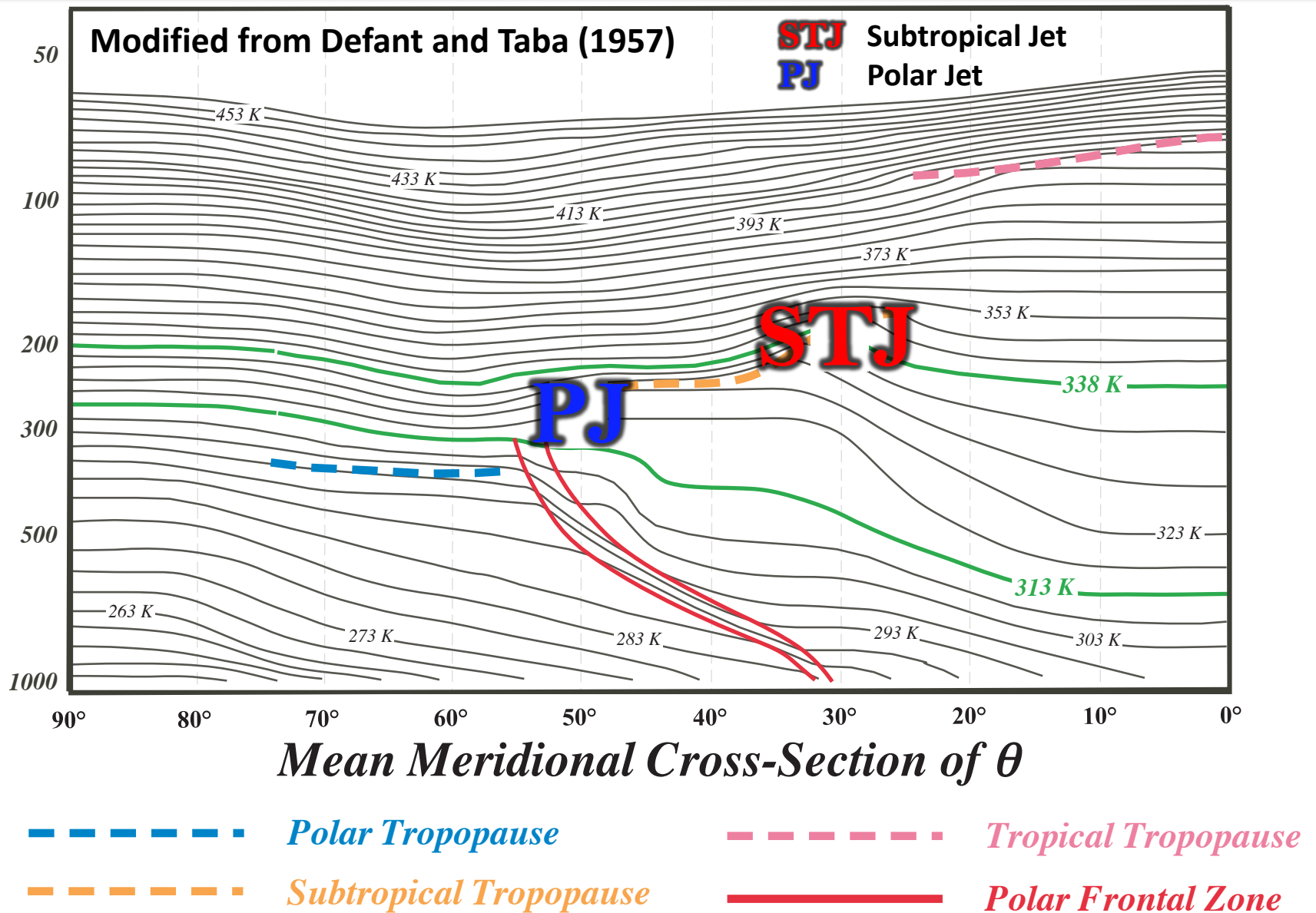
This work was funded by an NSF-PRF (AGS-1624316)

Outline

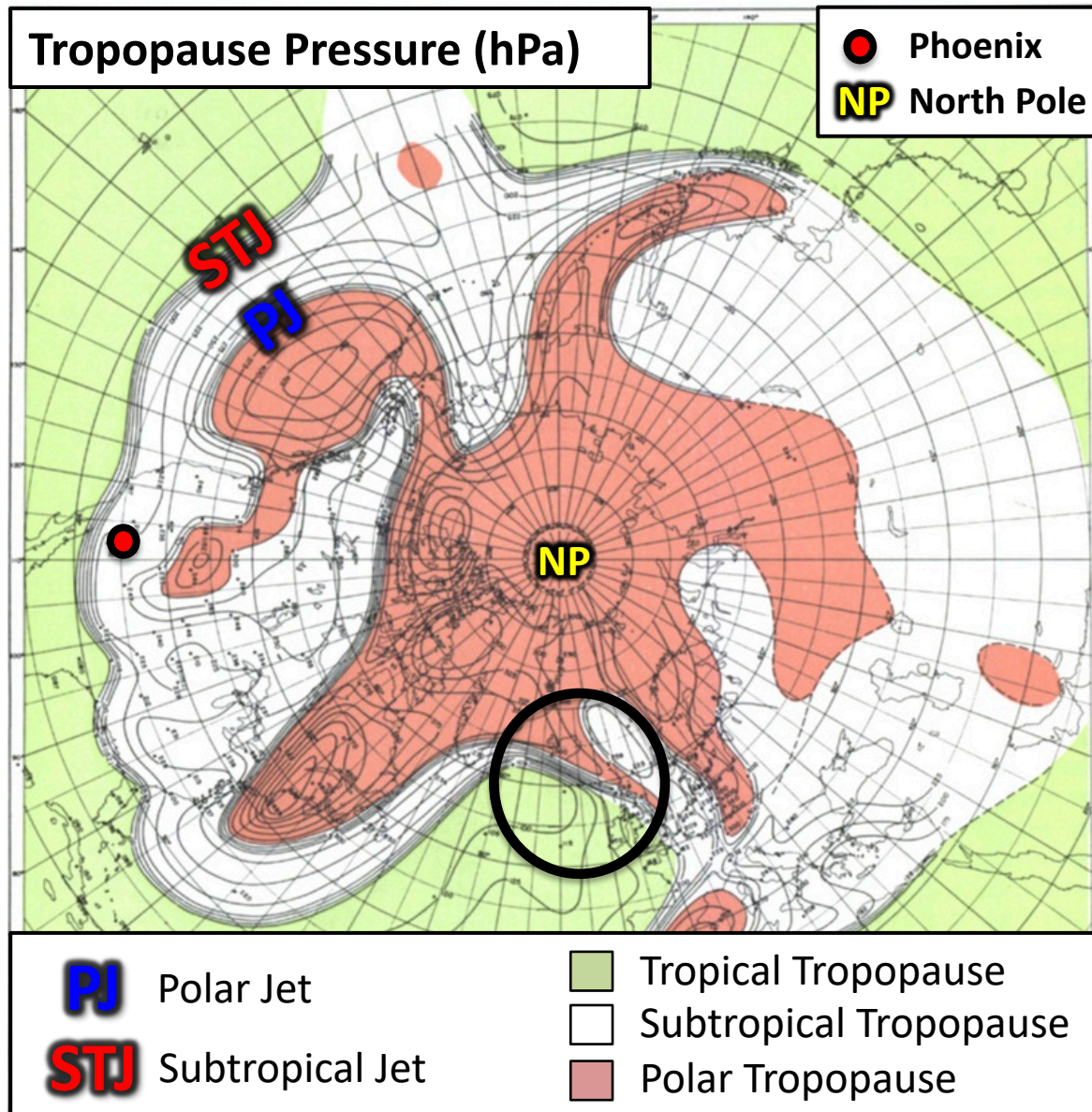
- Background
- Jet Superposition Event Identification and Classification
- Jet Superposition Event Composites
- Piecewise QGPV Inversion
- Along- and Across-Front Vertical Motion
- Summary

Background

Background



Background



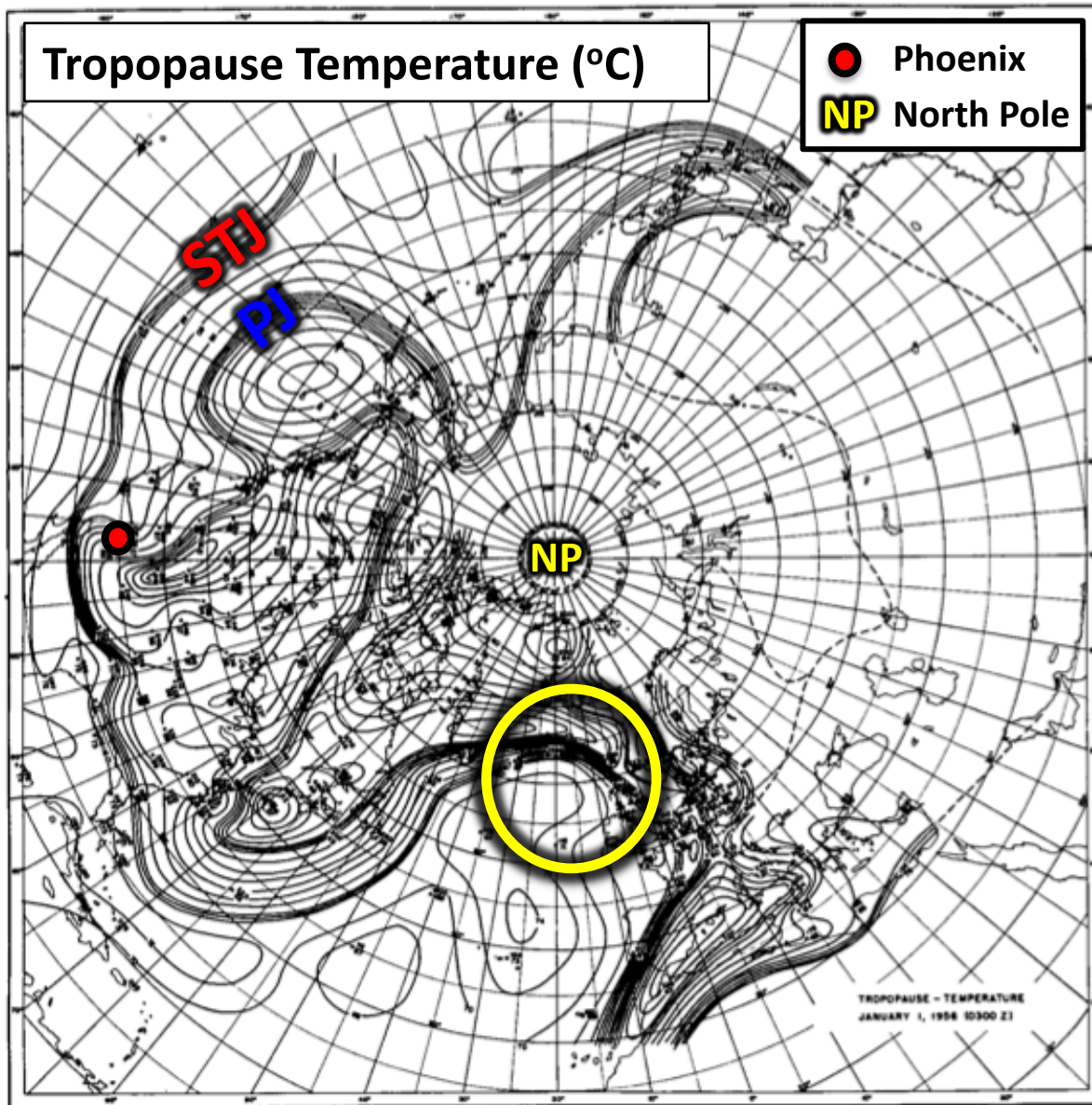
Maps of tropopause pressure help to identify the location of the jets.

While each jet occupies its own climatological latitude band, substantial meanders are common.

Occasionally, the latitudinal separation between the jets can vanish resulting in a vertical **jet superposition**.

Modified from Defant and Taba (1957)

Background



The pole-to-equator baroclinicity is combined into a much narrower zone of contrast in the vicinity of a jet superposition.

Intensified frontal structure is often accompanied by a strengthening of the transverse circulation associated with the superposed jet.

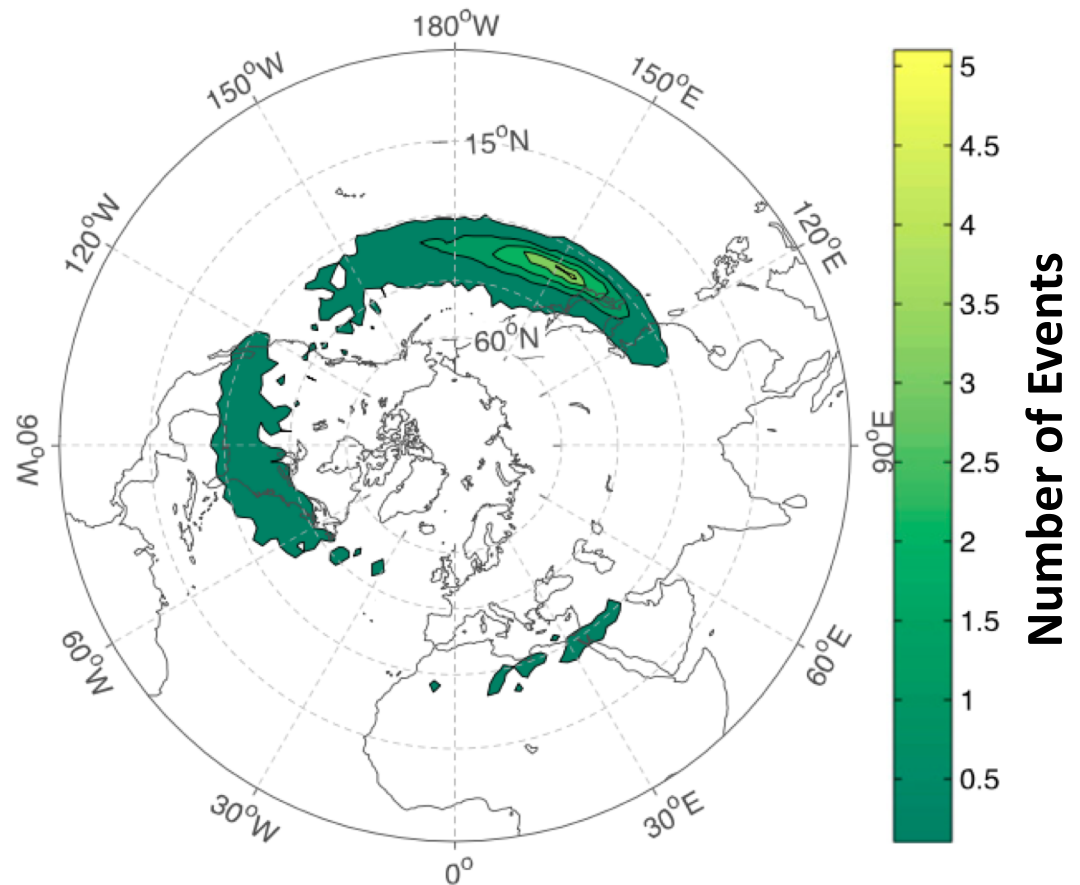
Modified from Defant and Taba (1957)

Background

Christenson et al. (2017) highlight three locations that experience the greatest frequency of jet superpositions:

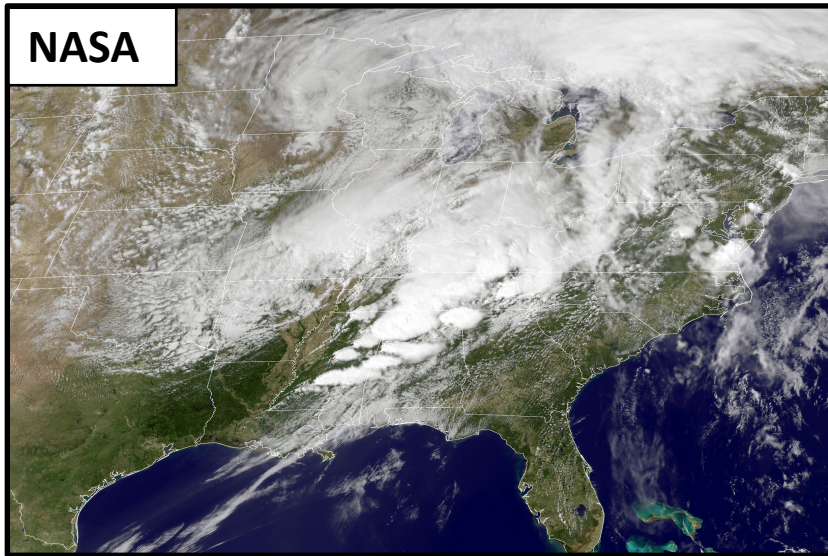
- 1) Western Pacific
- 2) North America
- 3) Northern Africa

Climatological frequency of Northern Hemisphere jet superposition events per cold season (Nov–Mar) 1960–2010



Christenson et al. (2017)

Jet Superpositions and High-Impact Weather



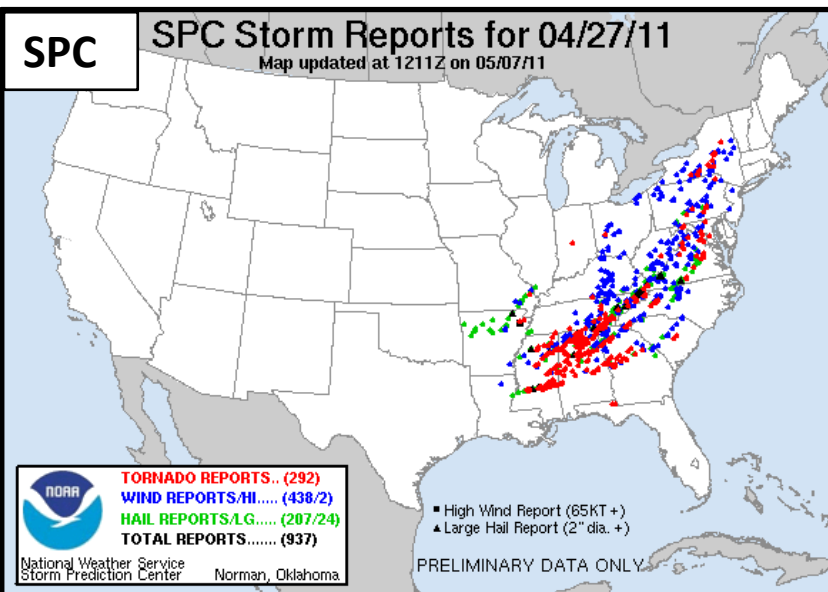
Jet superpositions can be an element of high-impact weather events

1–3 May 2010 Nashville Flood

- Jet superposition enhanced the poleward moisture transport via its ageostrophic circulation (Winters and Martin 2014; 2016).

18–20 December 2009 Mid-Atlantic Blizzard

- Jet superposition was associated with a rapidly deepening East Coast cyclone (Winters and Martin 2016; 2017).



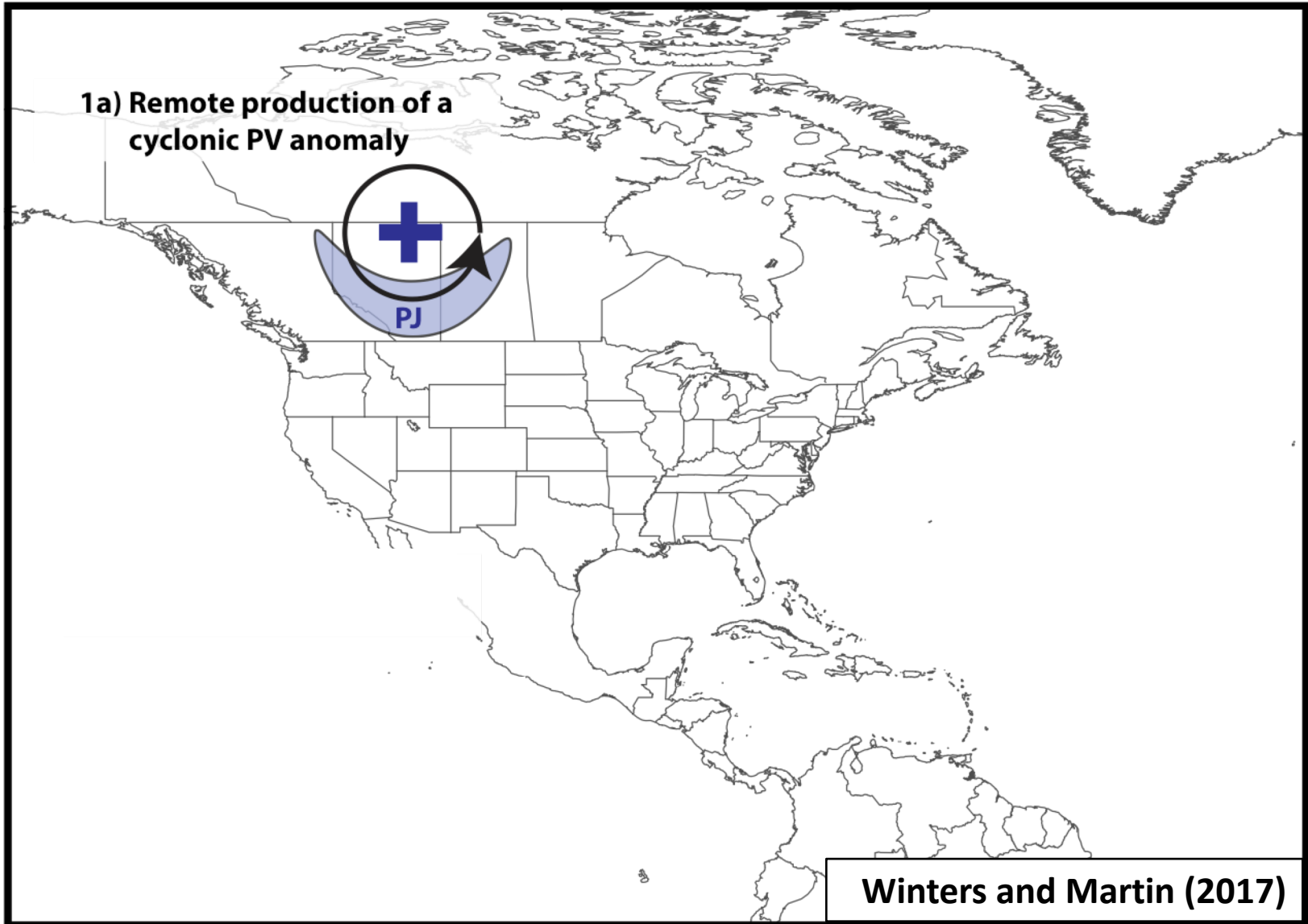
26 October 2010: Explosive Cyclogenesis Event

- Jet superposition over the West Pacific preceded the development of an intense Midwest U.S. cyclone.

25–28 April 2011 Tornado Outbreak

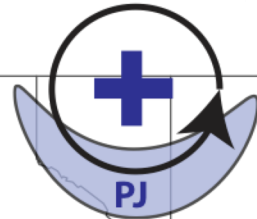
- Jet superposition occurred over the West Pacific prior to the outbreak (Knupp et al. 2014; Christenson and Martin 2012).

Jet Superposition Conceptual Model



Jet Superposition Conceptual Model

1a) Remote production of a cyclonic PV anomaly

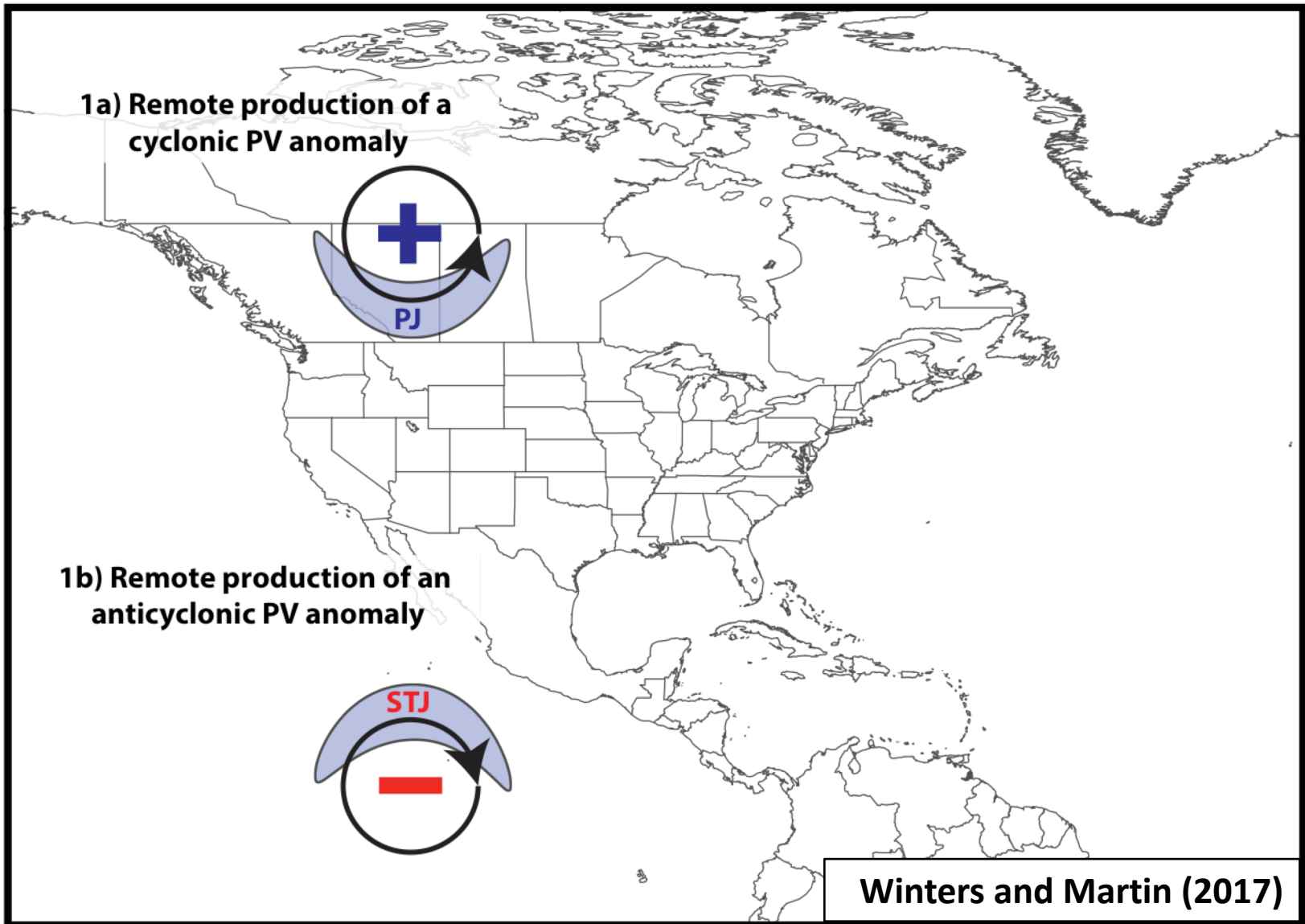


Polar cyclonic PV anomalies:

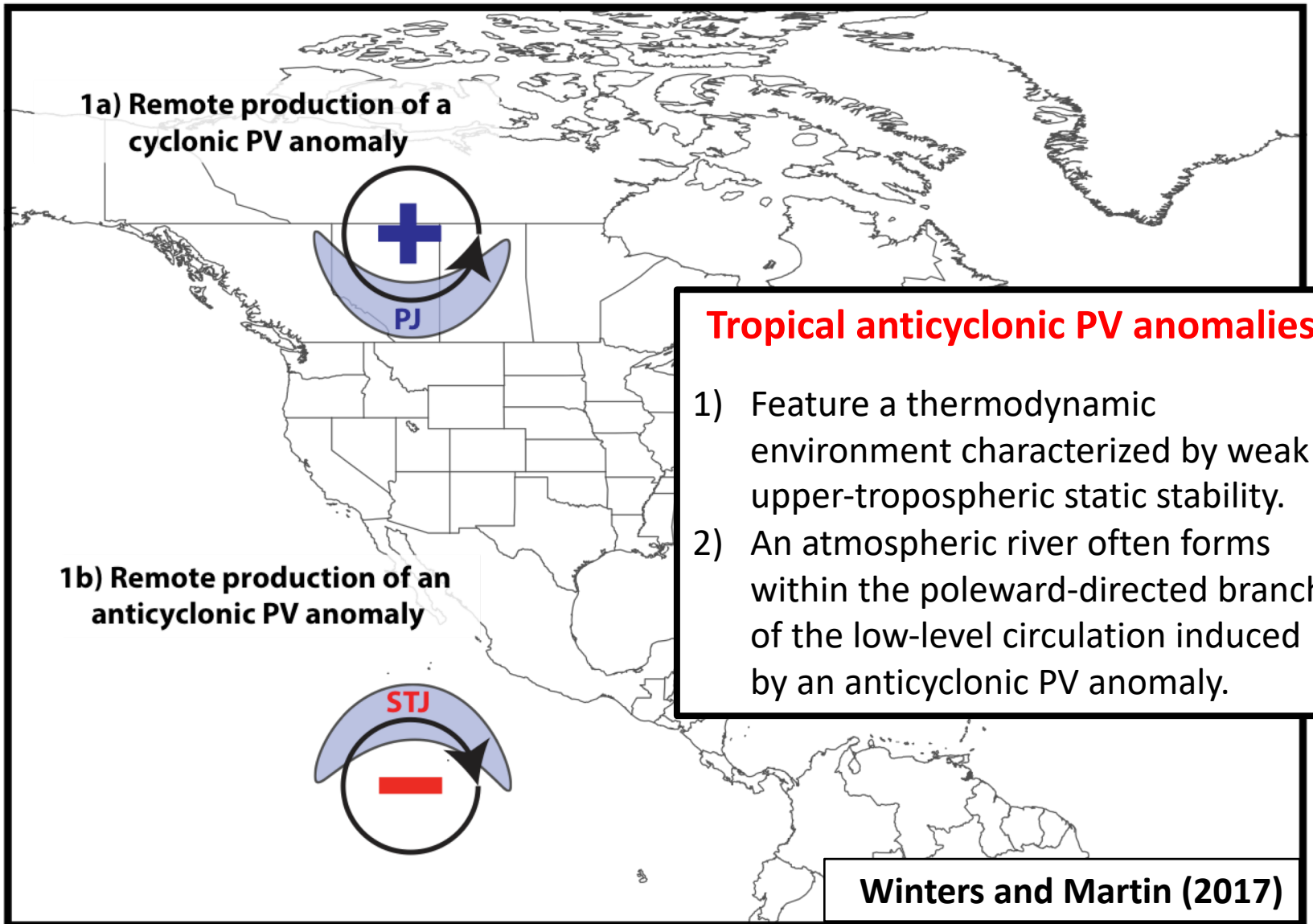
- 1) Often referred to as coherent tropopause disturbances (Pyle et al. 2004) or tropopause polar vortices (Cavallo and Hakim 2010).
- 2) Characterize a dynamical environment conducive to midlatitude cyclogenesis.

Winters and Martin (2017)

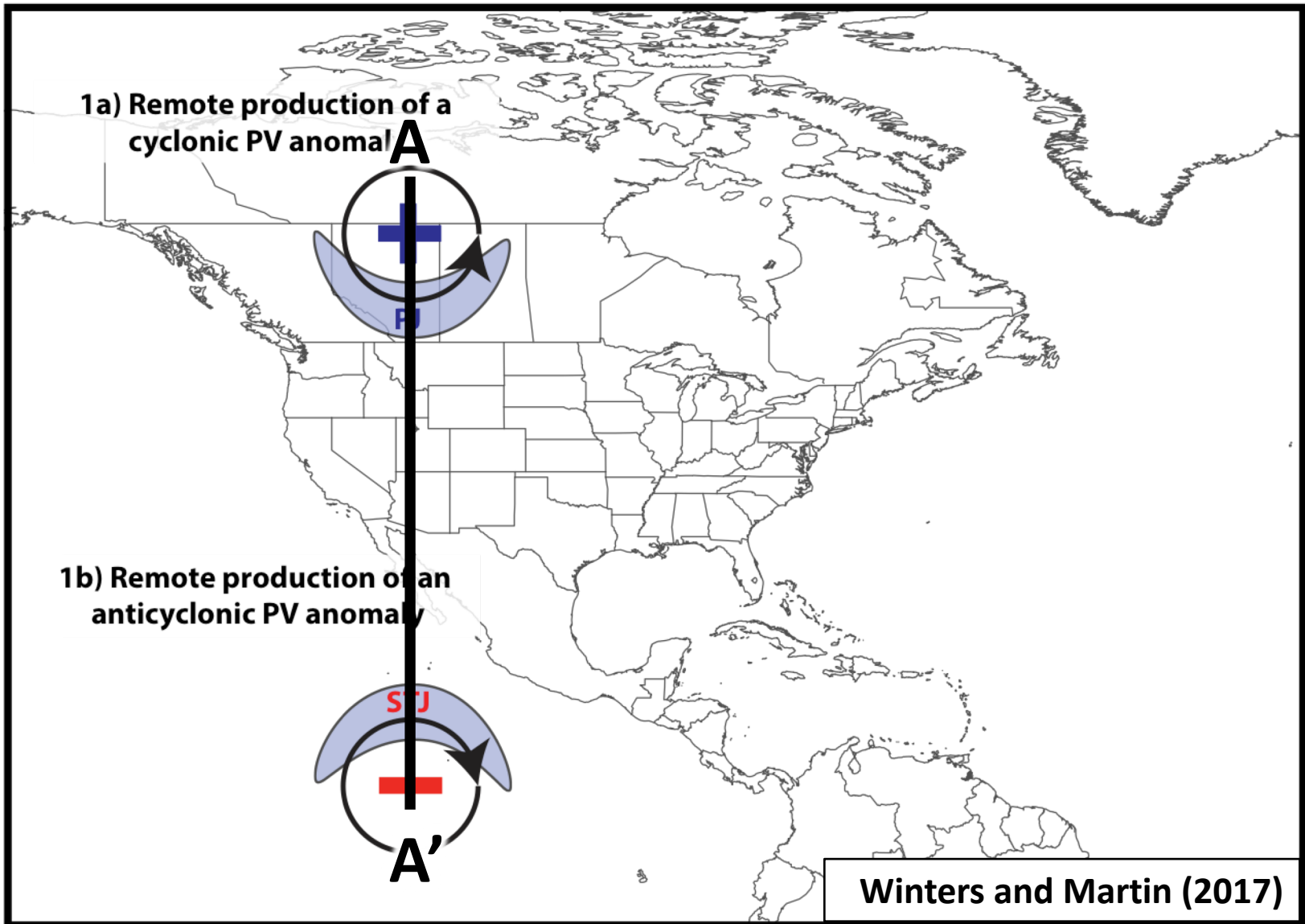
Jet Superposition Conceptual Model



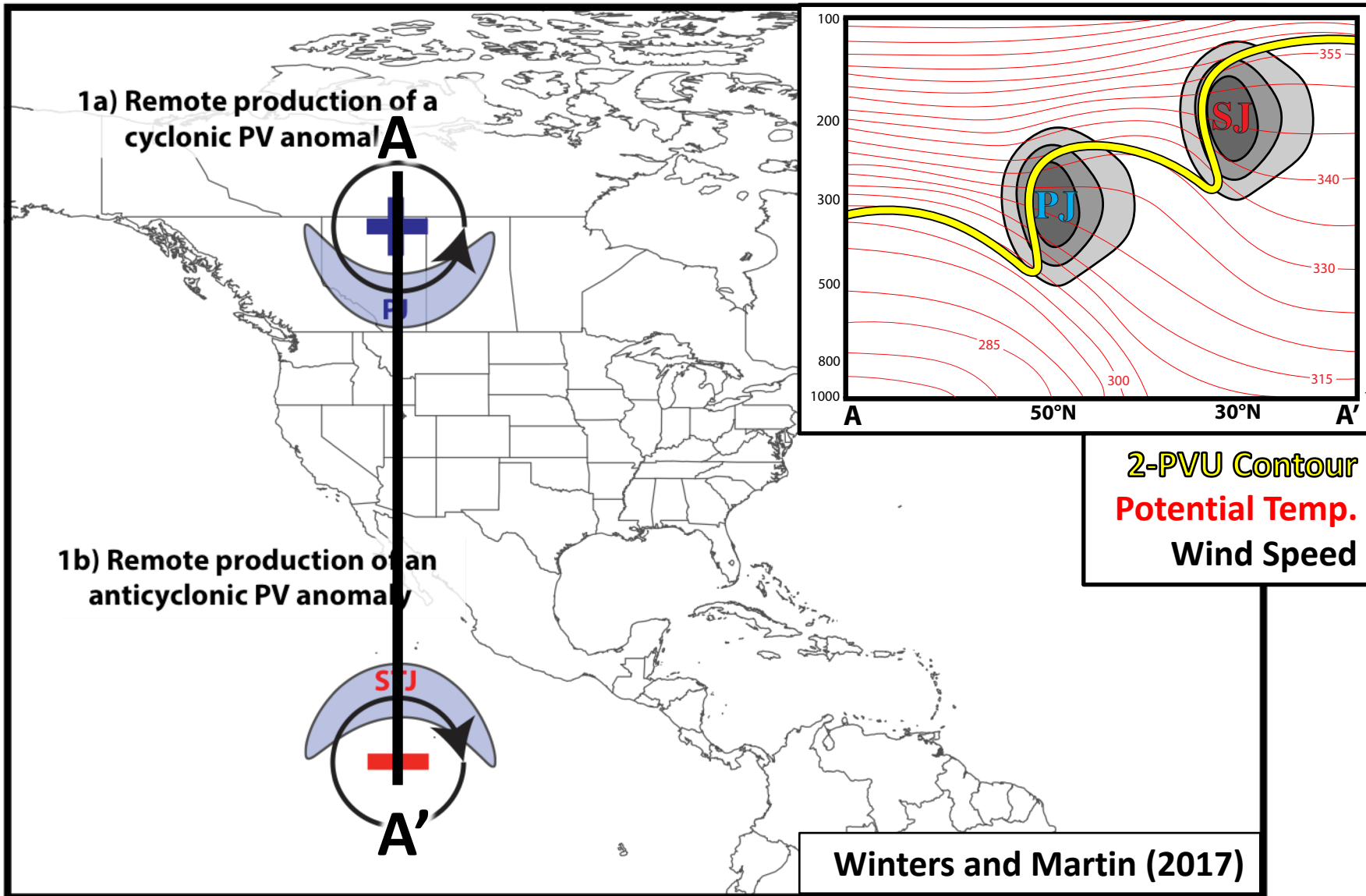
Jet Superposition Conceptual Model



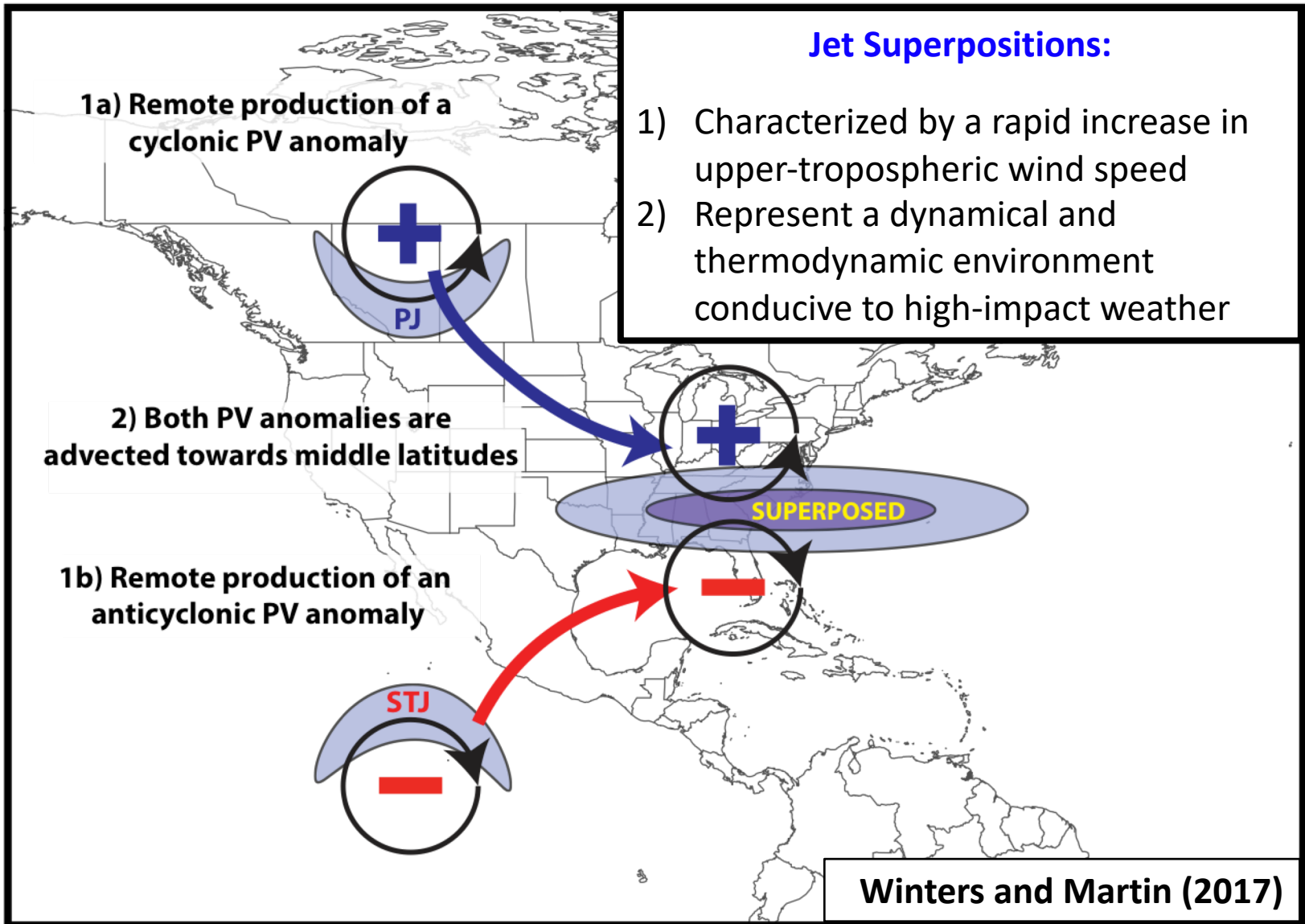
Jet Superposition Conceptual Model



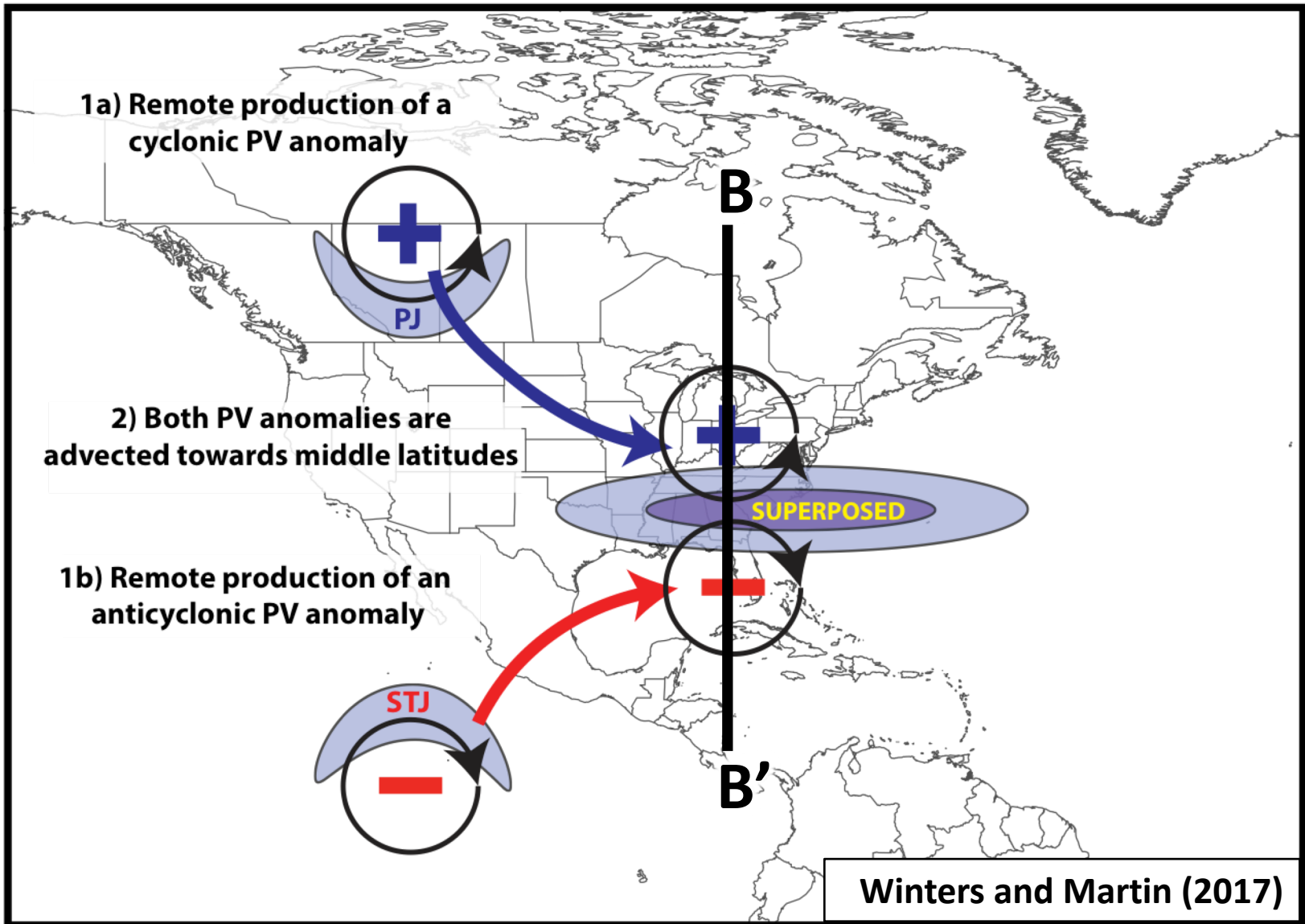
Jet Superposition Conceptual Model



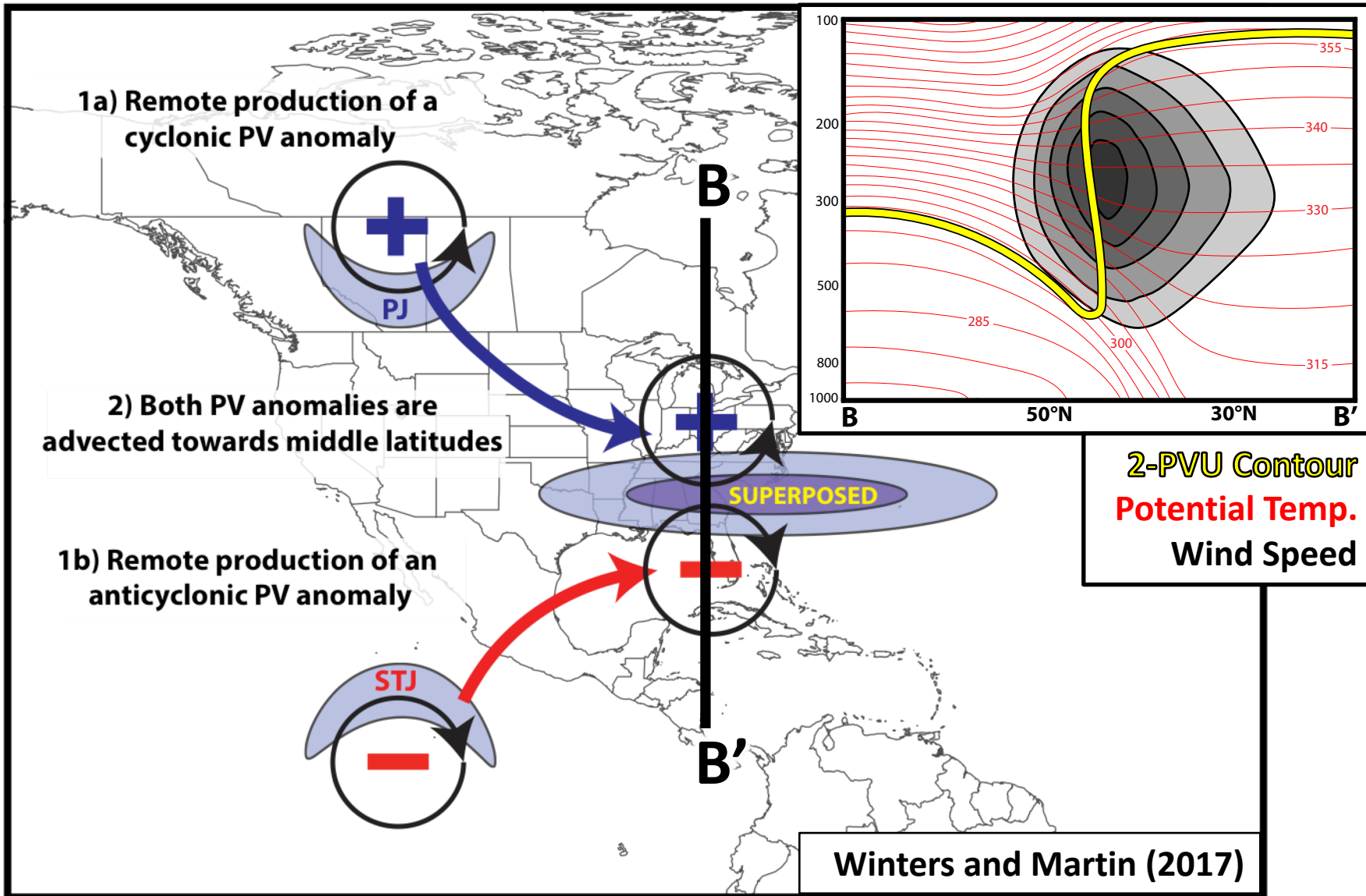
Jet Superposition Conceptual Model



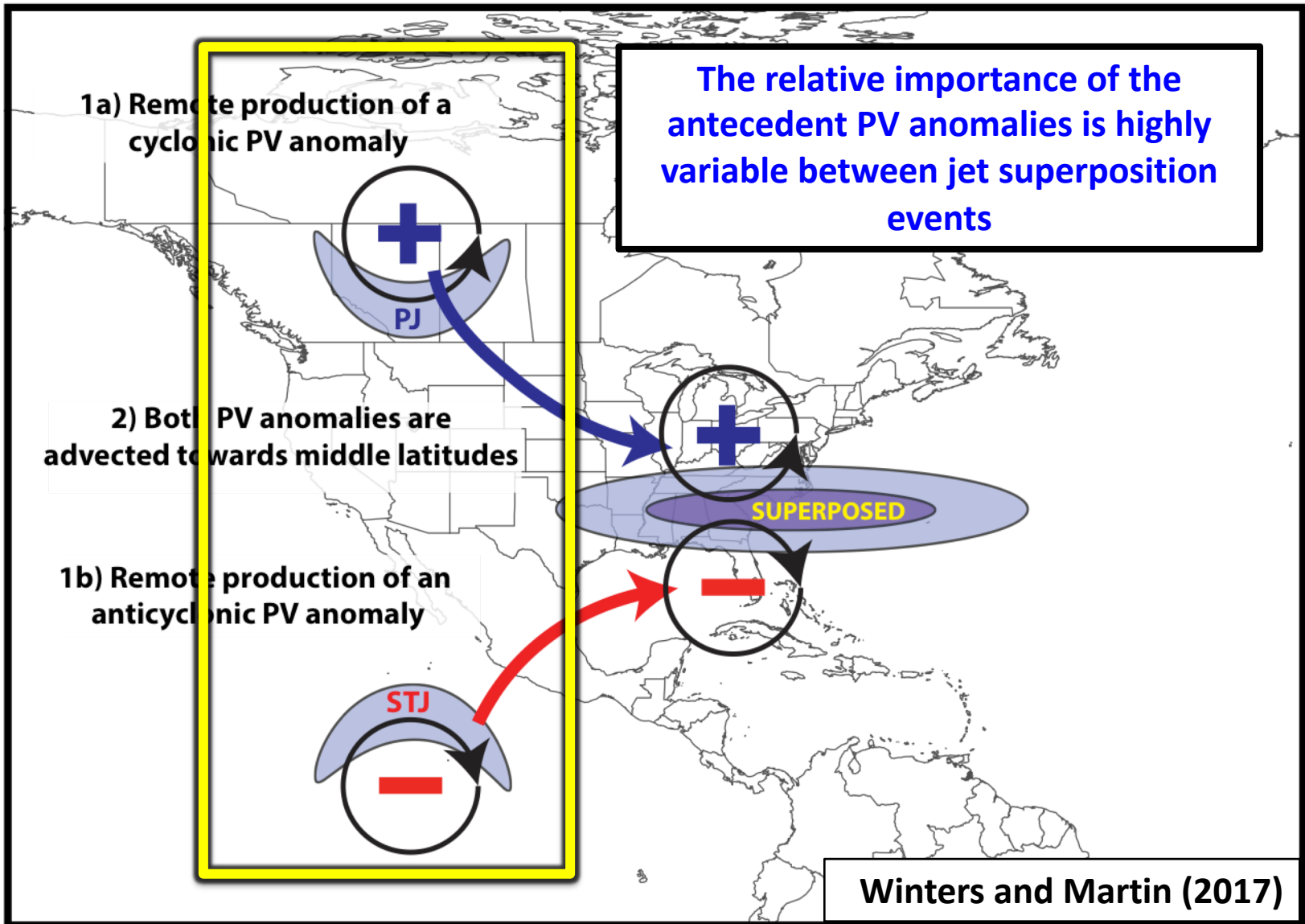
Jet Superposition Conceptual Model



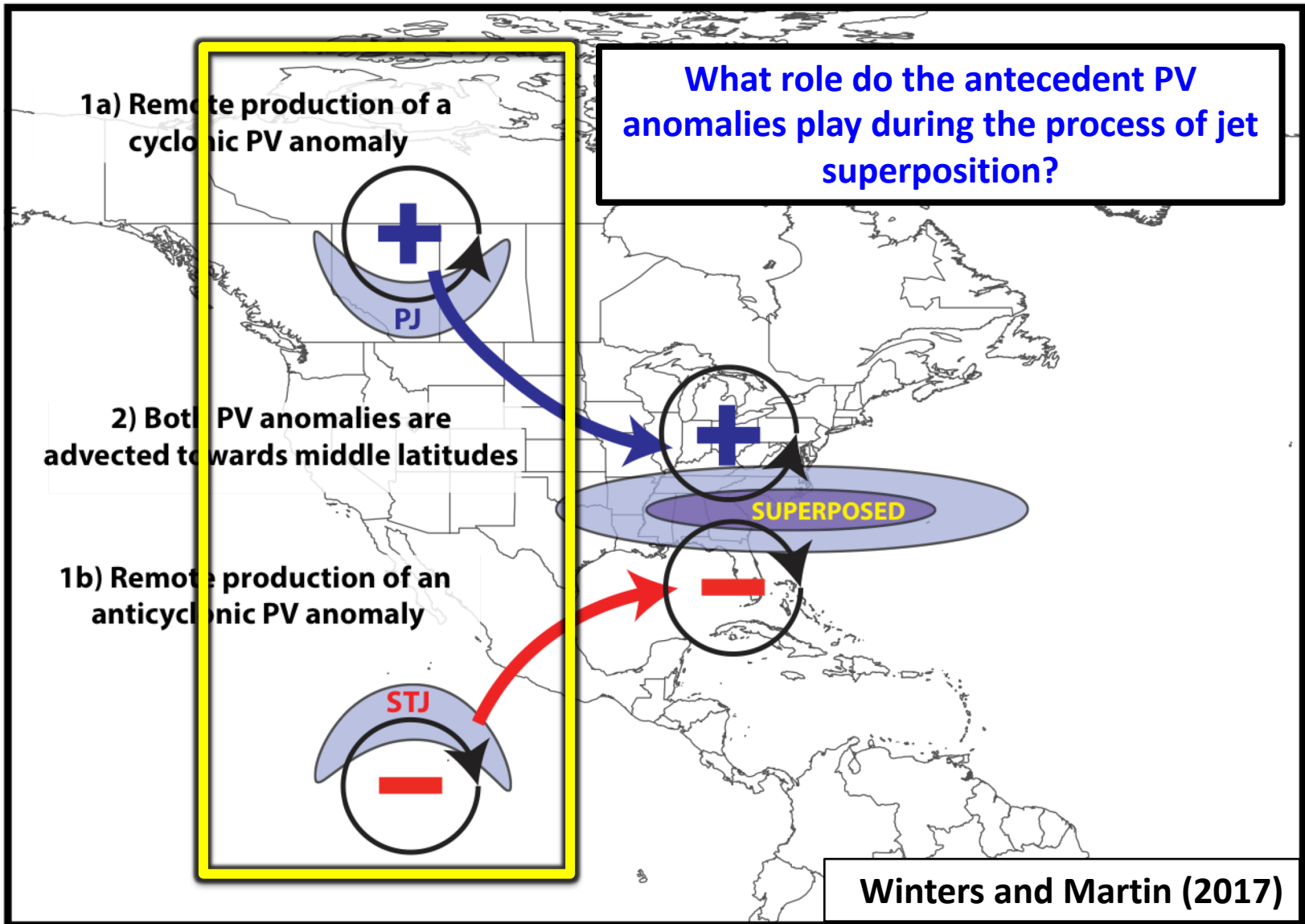
Jet Superposition Conceptual Model



Jet Superposition Conceptual Model



Jet Superposition Conceptual Model



Jet Superposition Event Identification and Classification

Jet Superposition Event Identification

- Isolated NCEP CFSR (Saha et al. 2014) grid points over North America characterized by a jet superposition during Nov.–Mar. 1979–2010 using the Christenson et al. (2017) scheme.
- Retained analysis times that rank in the top 10% in terms of the number of grid points characterized by a jet superposition.
- Filtered retained analysis times to group together jet superpositions that are < 30 h and < 1500 km apart.

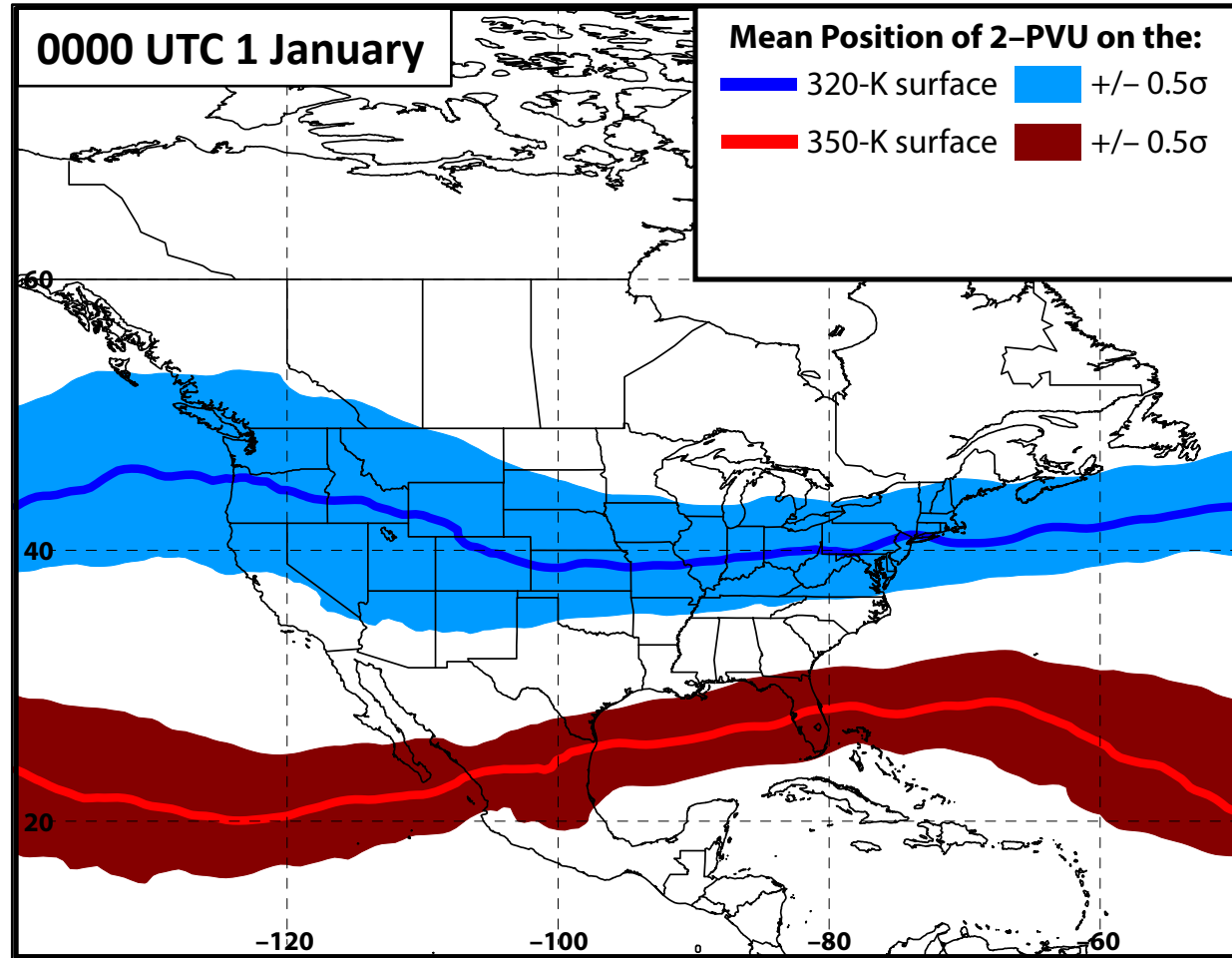
326 jet superposition events

Jet Superposition Event Identification

- Isolated NCEP CFSR (Saha et al. 2014) grid points over North America characterized by a jet superposition during Nov.–Mar. 1979–2010 using the Christenson et al. (2017) scheme.
- Retained analysis times that rank in the top 10% in terms of the number of grid points characterized by a jet superposition.
- Filtered retained analysis times to group together jet superpositions that are < 30 h and < 1500 km apart.
- Classified jet superposition events based on the deviations of the polar and subtropical jets from their respective climatological latitude bands at the time of jet superposition.

Jet Superposition Event Classification

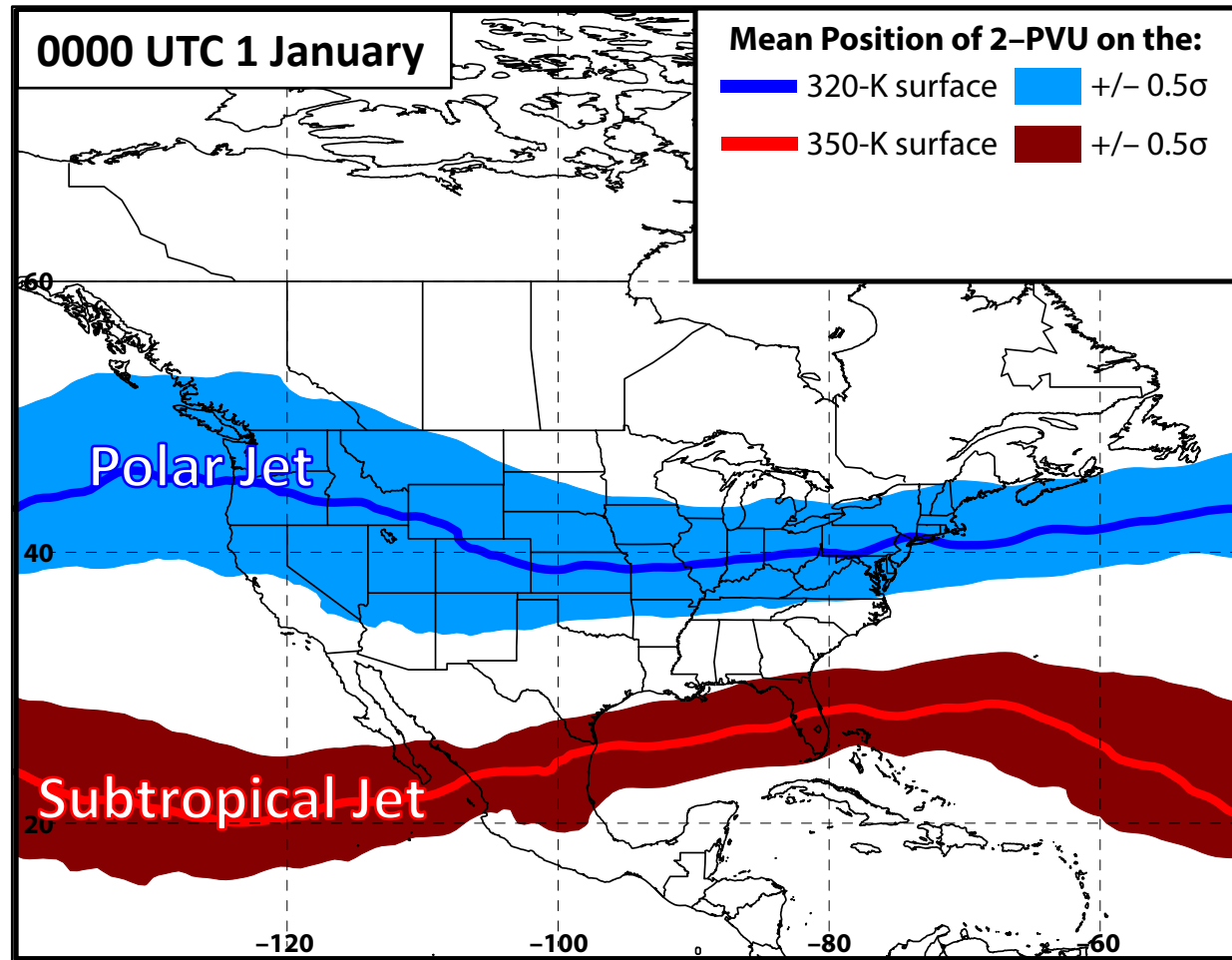
1. Determined the mean position of the 2-PVU contour on the 320-K and 350-K surfaces at each analysis time in the CFSR.



Winters et al. (2020, *in revision*)

Jet Superposition Event Classification

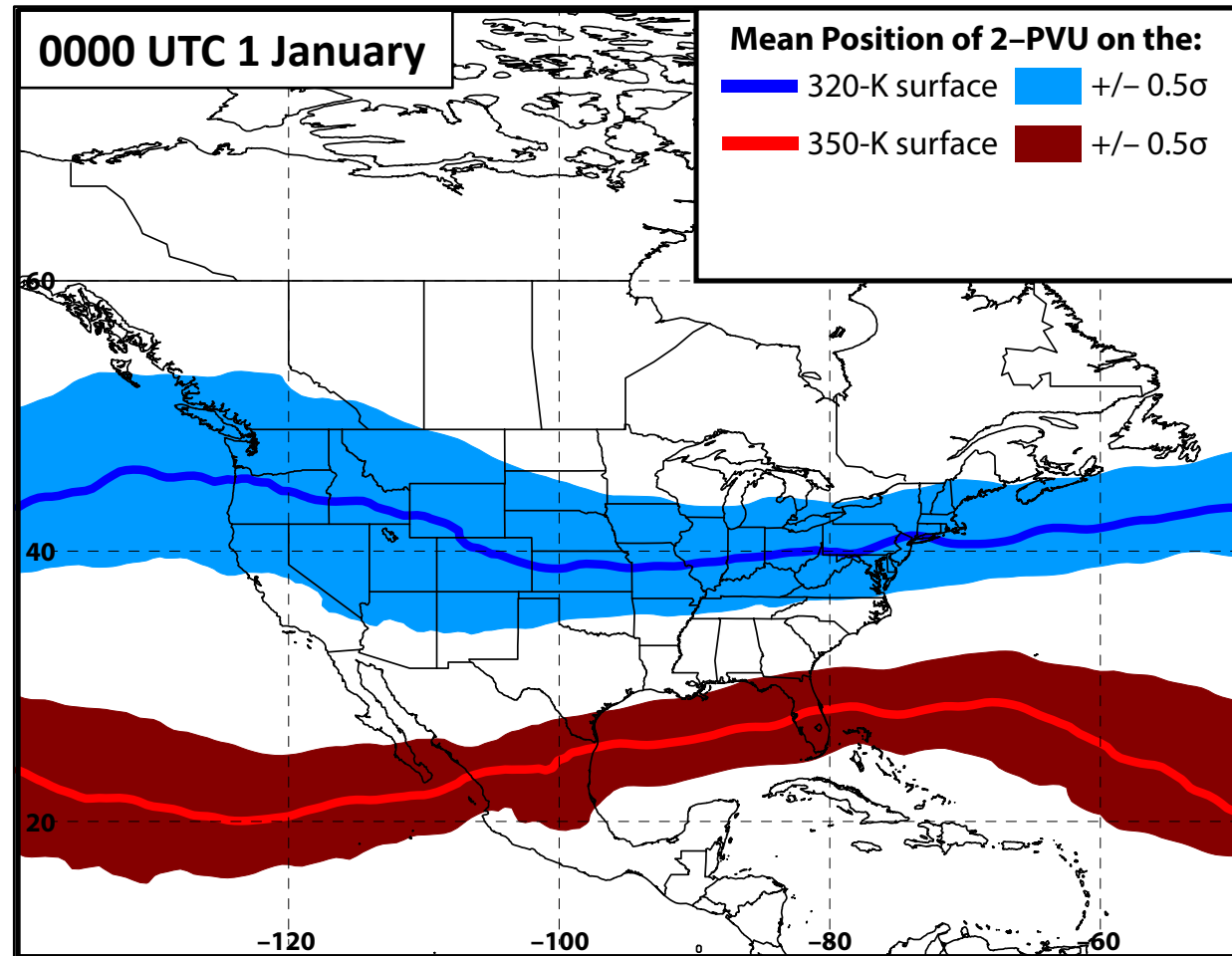
1. Determined the mean position of the 2-PVU contour on the 320-K and 350-K surfaces at each analysis time in the CFSR.



Winters et al. (2020, *in revision*)

Jet Superposition Event Classification

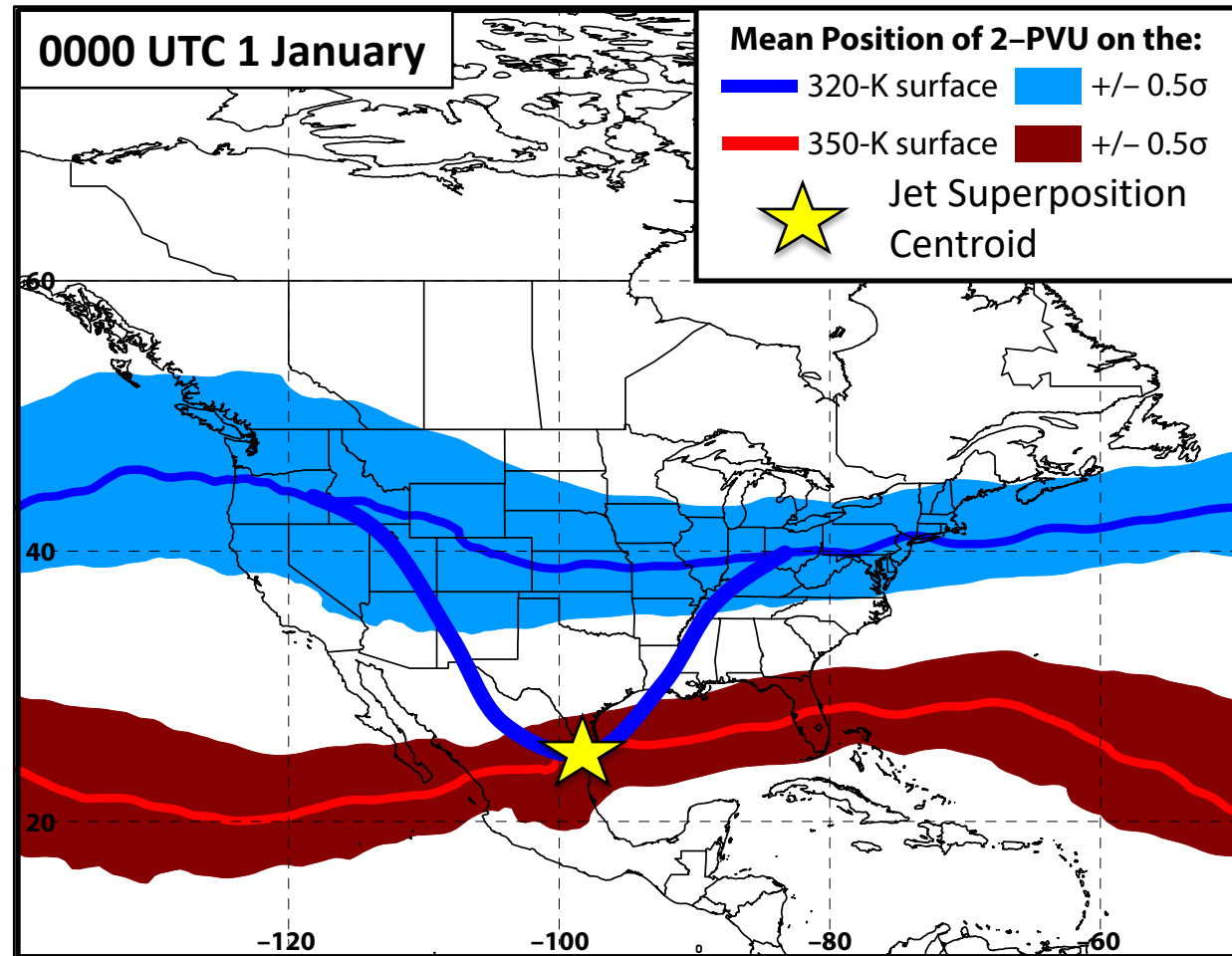
1. Determined the mean position of the 2-PVU contour on the 320-K and 350-K surfaces at each analysis time in the CFSR.
2. Compared the position of the jet superposition centroid at the start of each event against the climatological position of the 2-PVU contour.



Winters et al. (2020, *in revision*)

Jet Superposition Event Classification

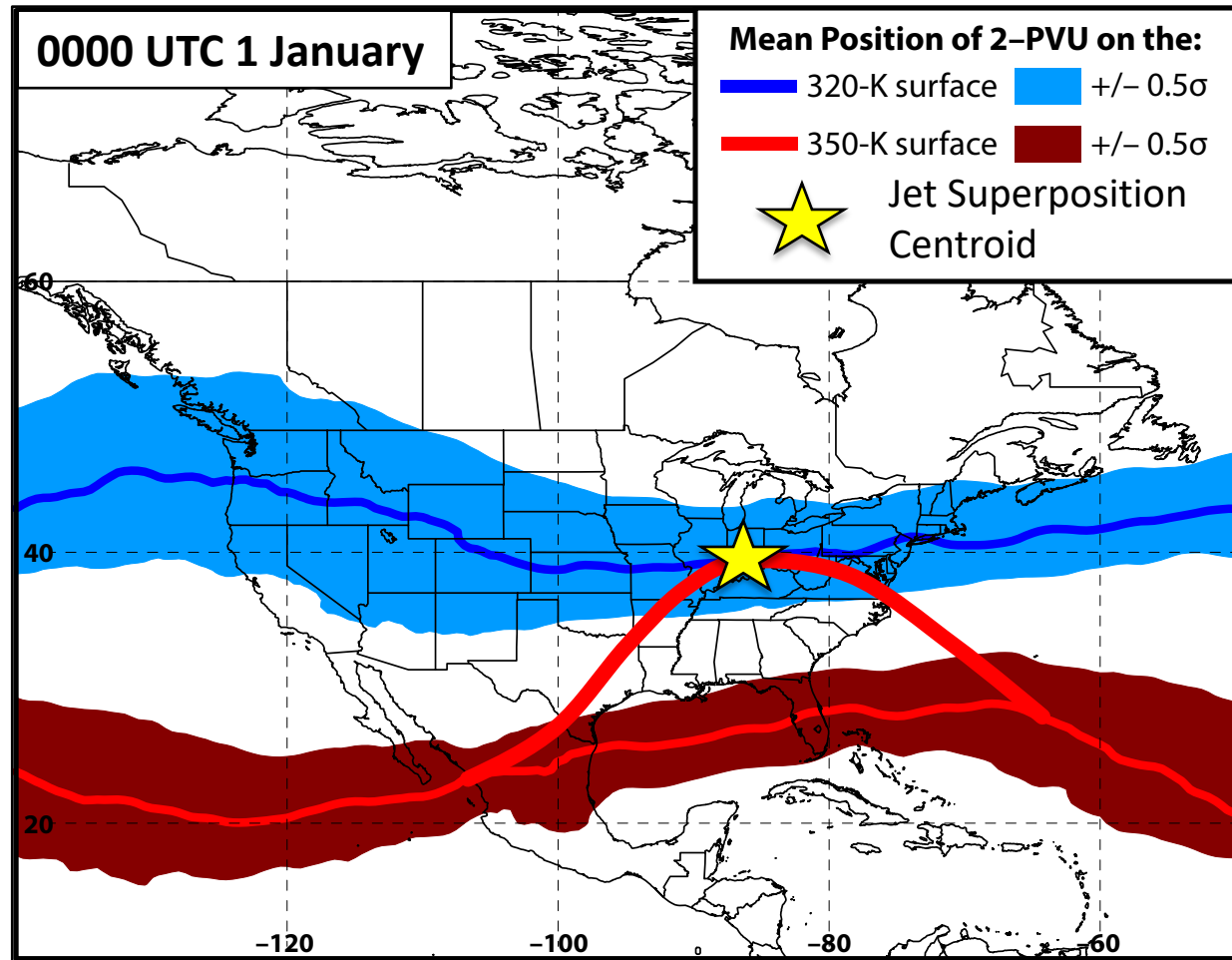
1. Determined the mean position of the 2-PVU contour on the 320-K and 350-K surfaces at each analysis time in the CFSR.
 2. Compared the position of the jet superposition centroid at the start of each event against the climatological position of the 2-PVU contour.
- **Polar Dominant**



Winters et al. (2020, *in revision*)

Jet Superposition Event Classification

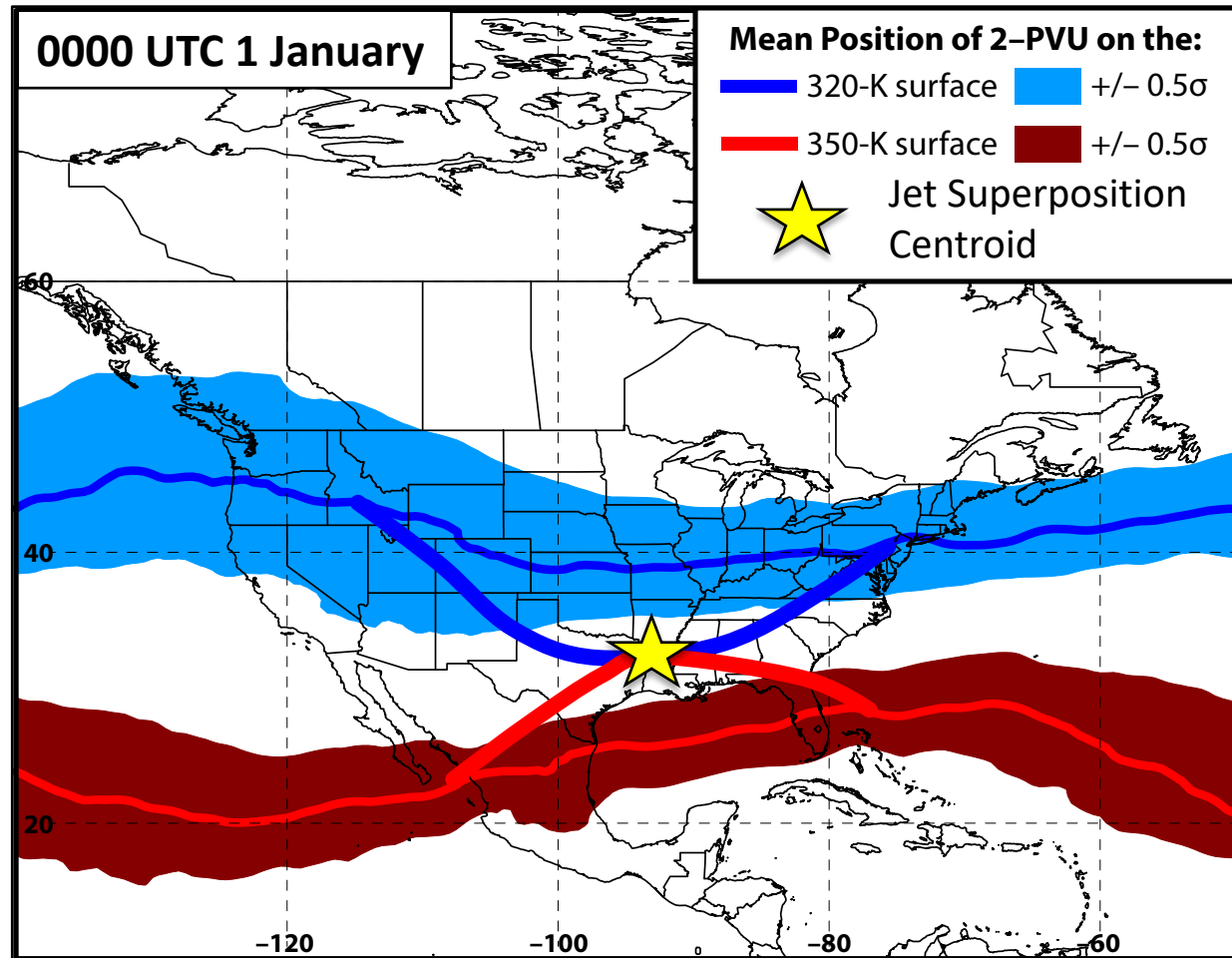
1. Determined the mean position of the 2-PVU contour on the 320-K and 350-K surfaces at each analysis time in the CFSR.
 2. Compared the position of the jet superposition centroid at the start of each event against the climatological position of the 2-PVU contour.
- Polar Dominant
 - **Subtropical Dominant**



Winters et al. (2020, *in revision*)

Jet Superposition Event Classification

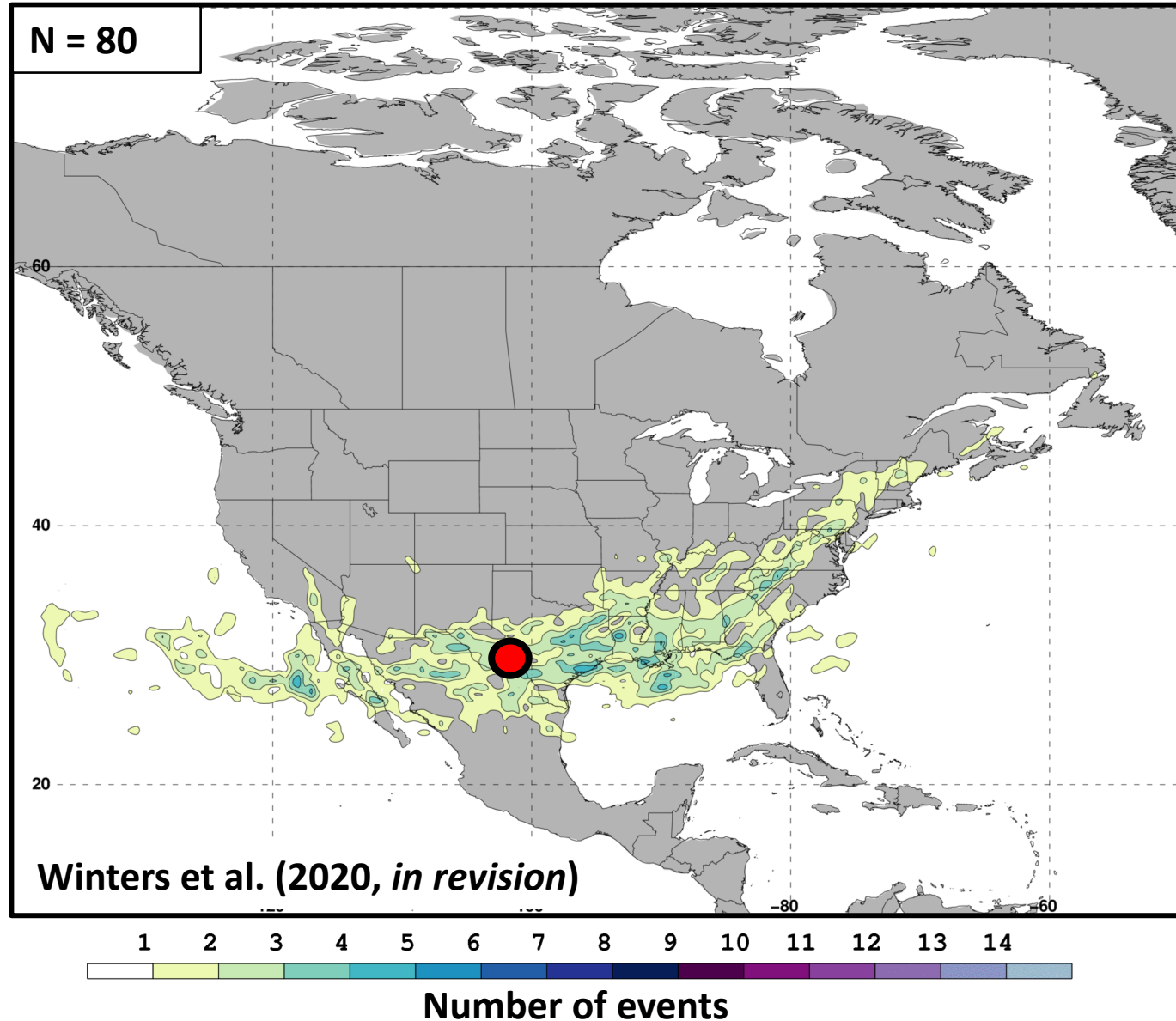
1. Determined the mean position of the 2-PVU contour on the 320-K and 350-K surfaces at each analysis time in the CFSR.
 2. Compared the position of the jet superposition centroid at the start of each event against the climatological position of the 2-PVU contour.
- Polar Dominant
 - Subtropical Dominant
 - **Hybrid**



Winters et al. (2020, *in revision*)

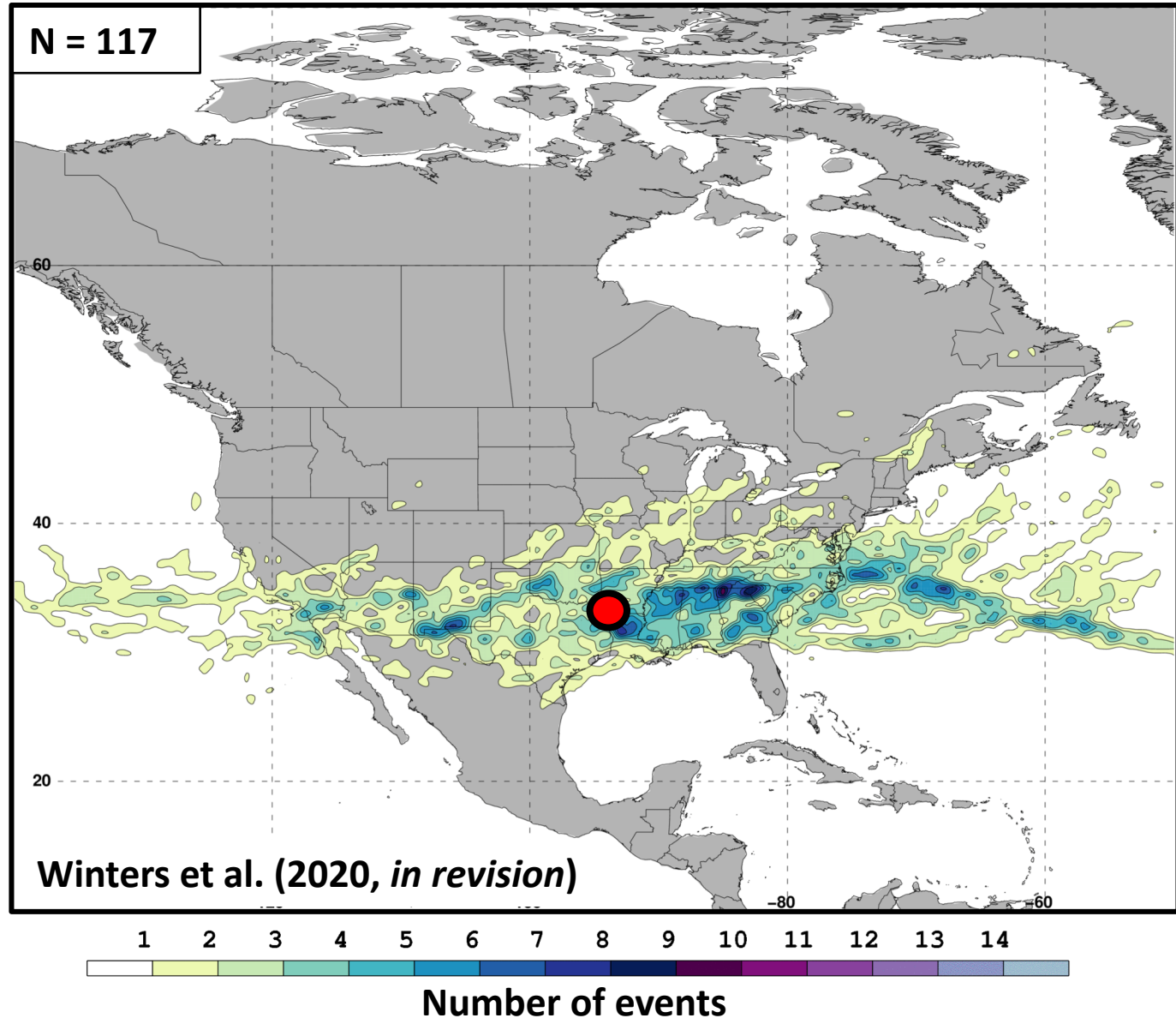
Jet Superposition Event Classification

Frequency of
Polar Dominant
Jet
Superposition
Events



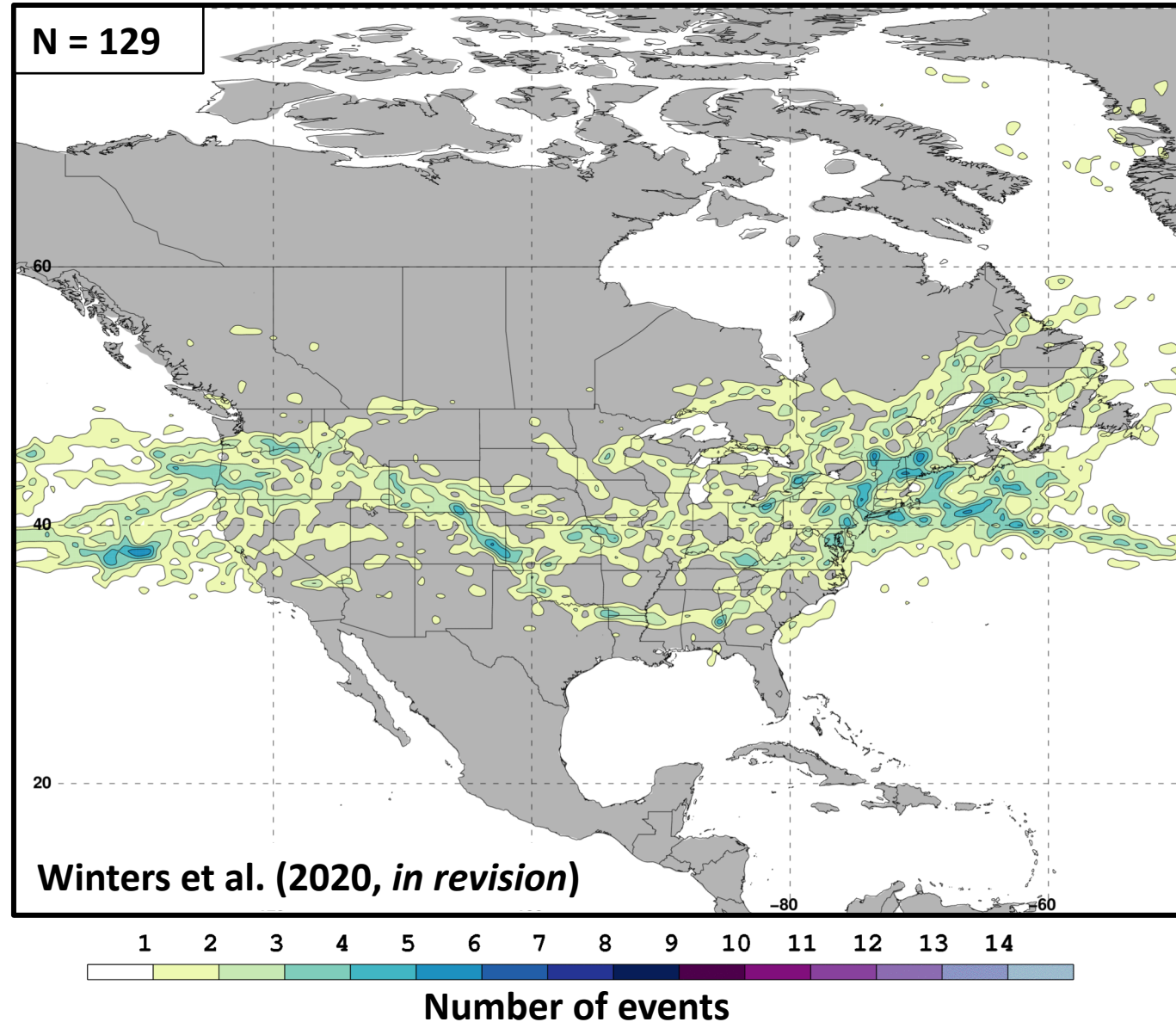
Jet Superposition Event Classification

Frequency of
Hybrid
Jet
Superposition
Events



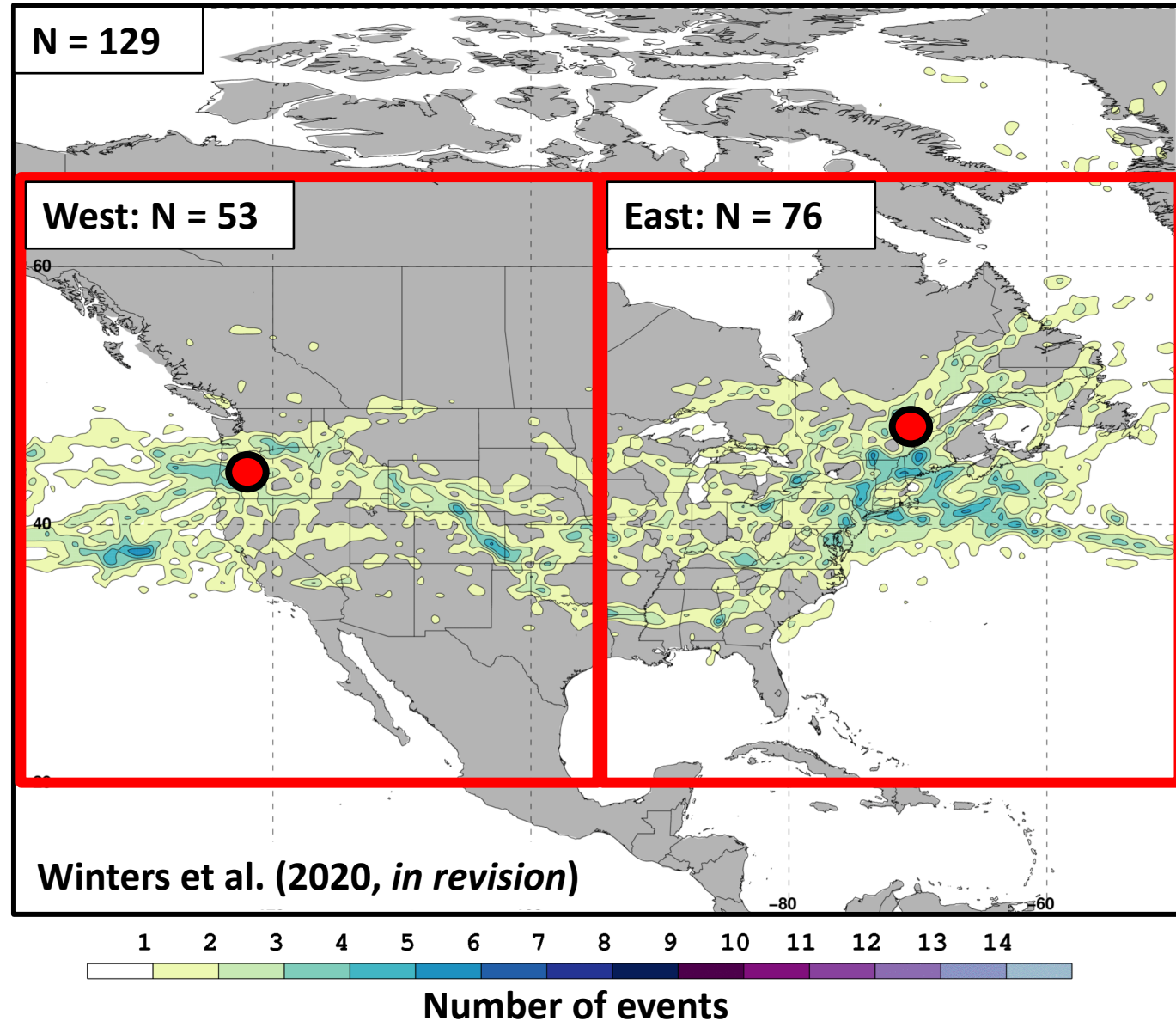
Jet Superposition Event Classification

Frequency of
**Subtropical
Dominant** Jet
Superposition
Events



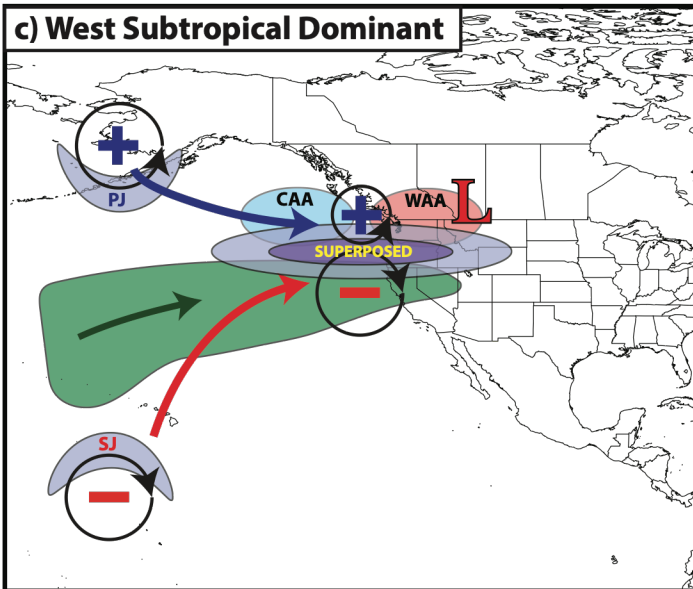
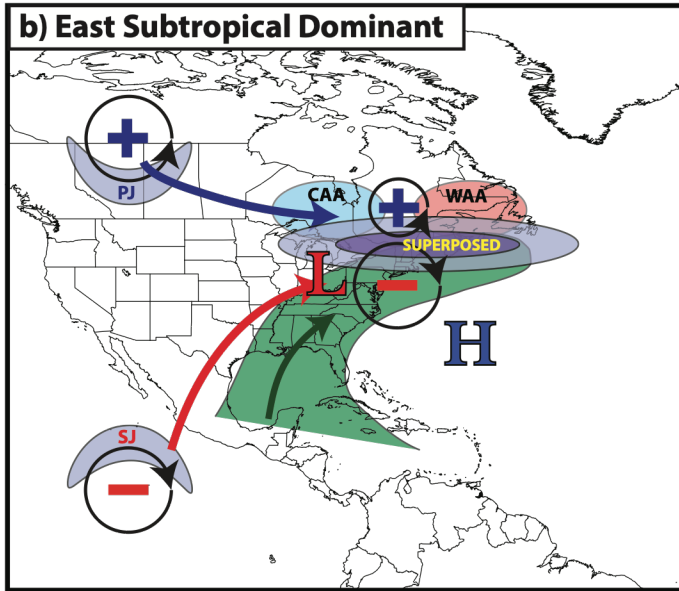
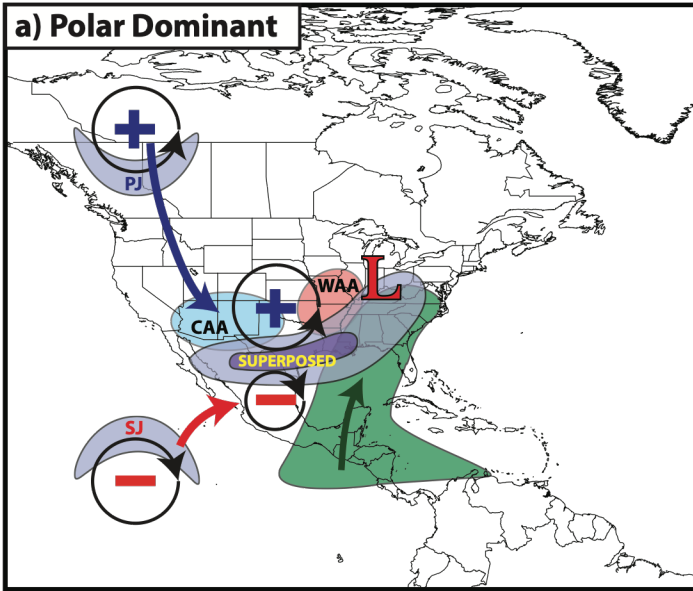
Jet Superposition Event Classification

Frequency of
Subtropical
Dominant Jet
Superposition
Events



Jet Superposition Event Composites

Jet Superposition Event Composites

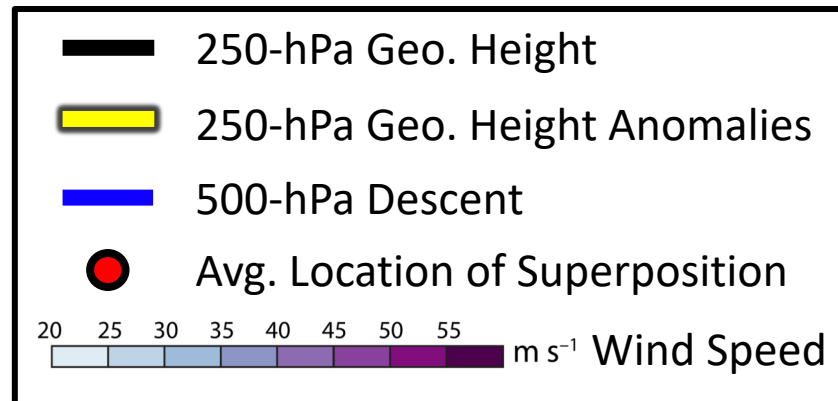
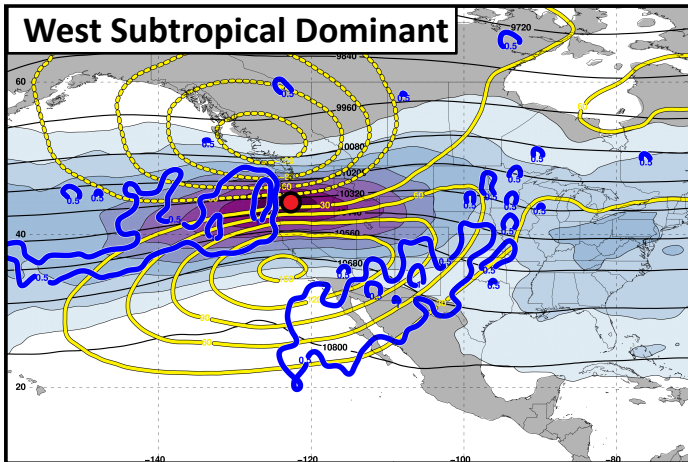
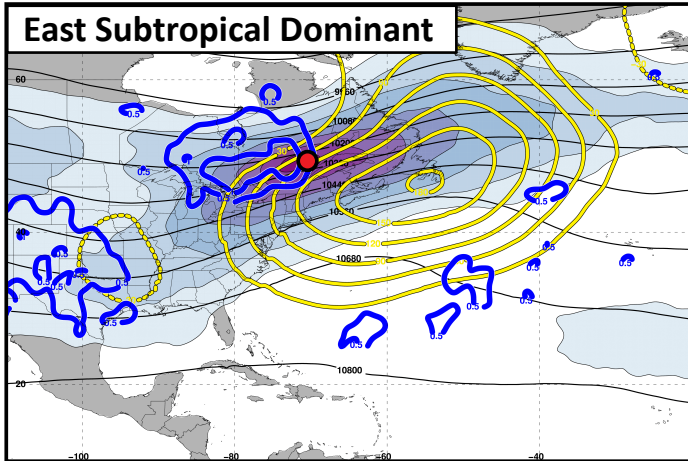
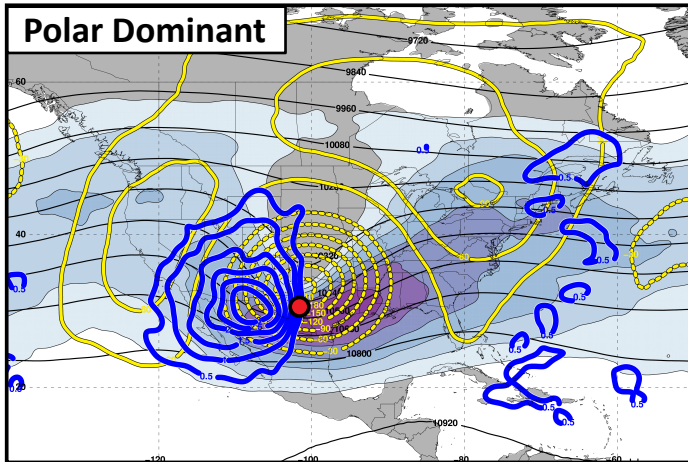


Legend

- L** Surface Cyclone
- H** Surface Anticyclone
- 300-hPa Geo. Warm-air Advection
- 300-hPa Geo. Cold-air Advection
- Precipitable Water Anomalies
- 250-hPa Jet Streak
- + Polar Cyclonic PV Anomaly
- Tropical Anticyclonic PV Anomaly
- Direction of Moisture Transport
- Movement of Polar Cyclonic PV Anomaly
- Movement of Tropical Anticyclonic PV Anomaly

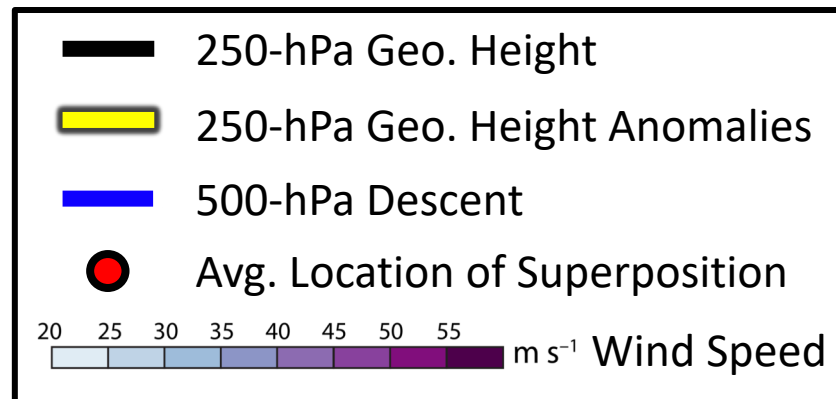
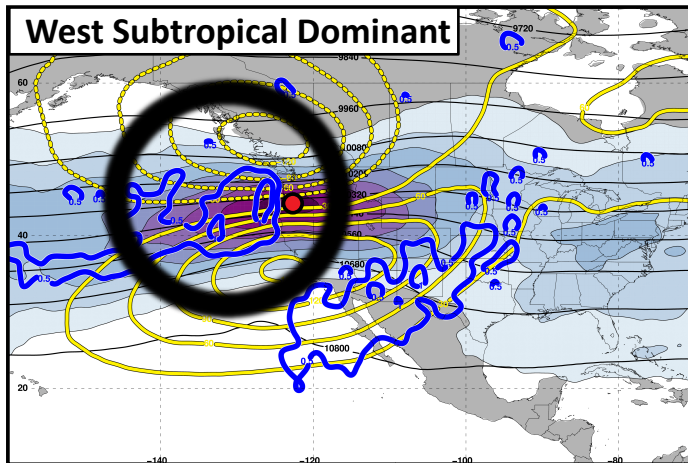
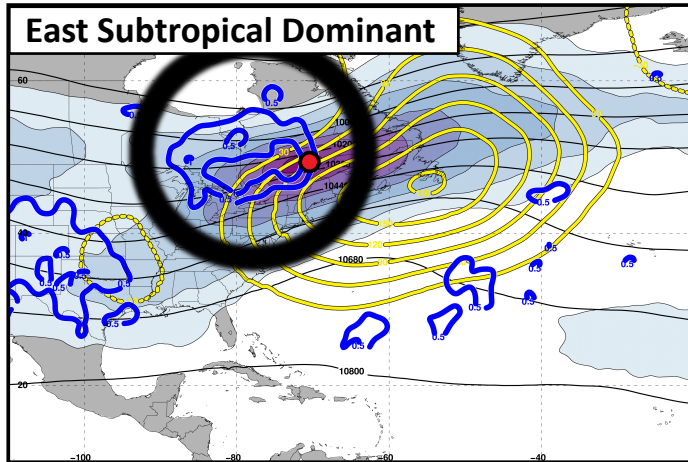
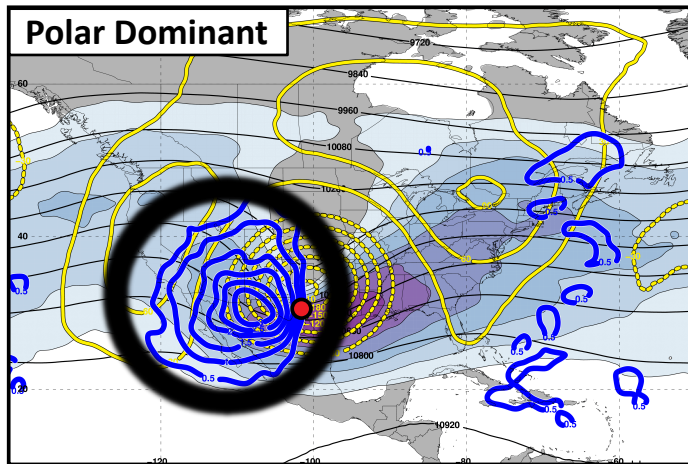
Winters et al.
(2020, *in revision*)

Jet Superposition Event Composites



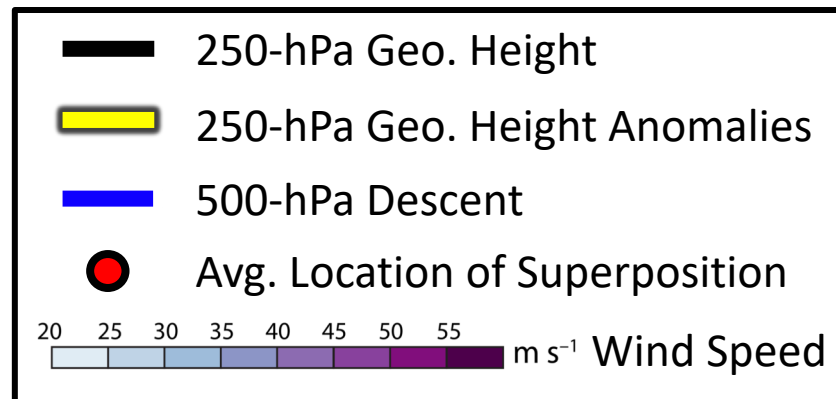
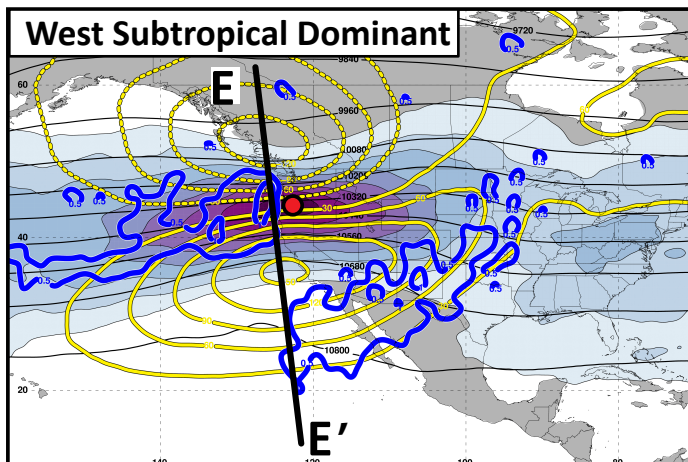
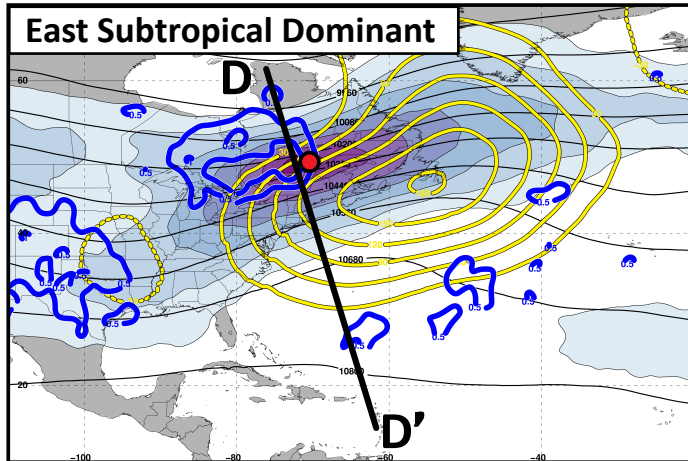
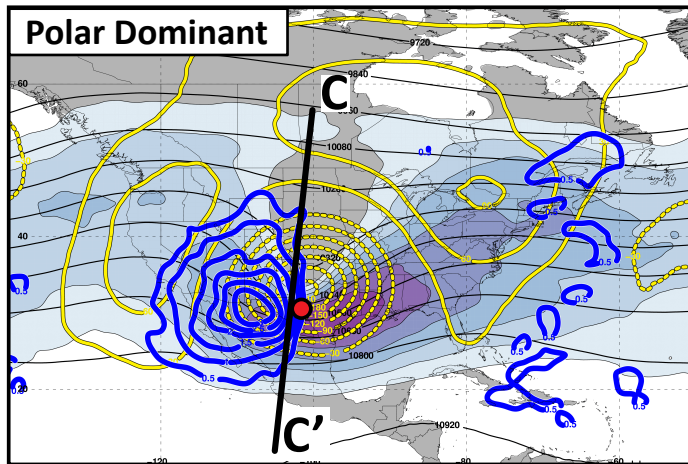
Jet Superposition Event Composites

- Descent beneath the jet-entrance region is a common element among the jet superposition event composites.

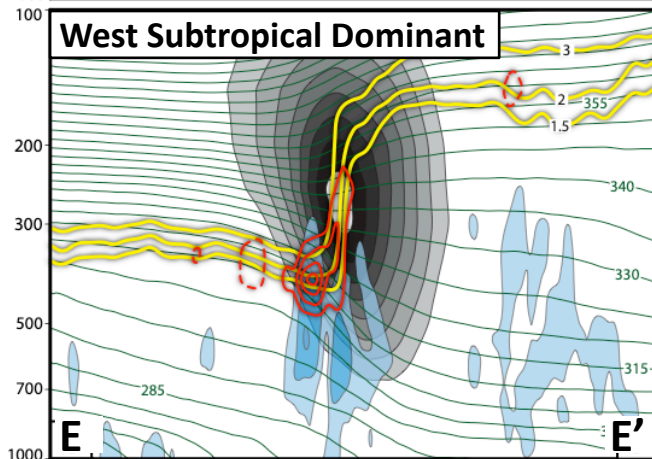
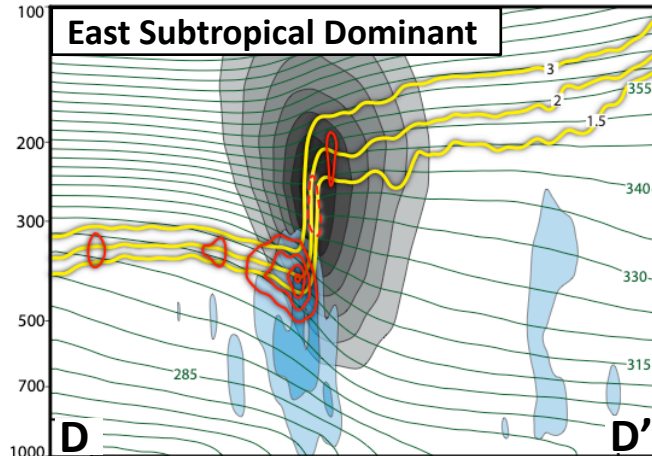
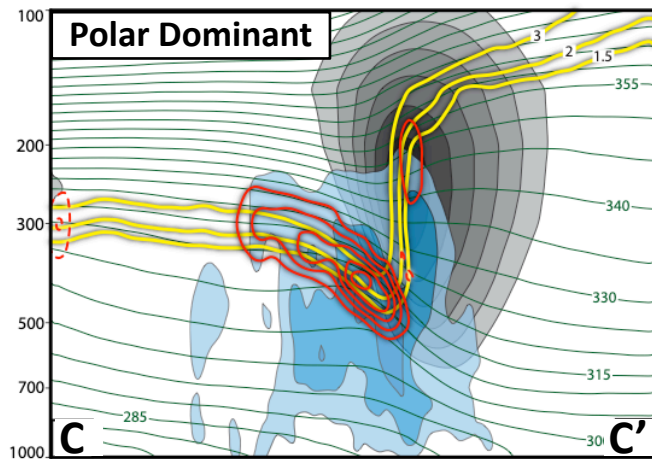


Jet Superposition Event Composites

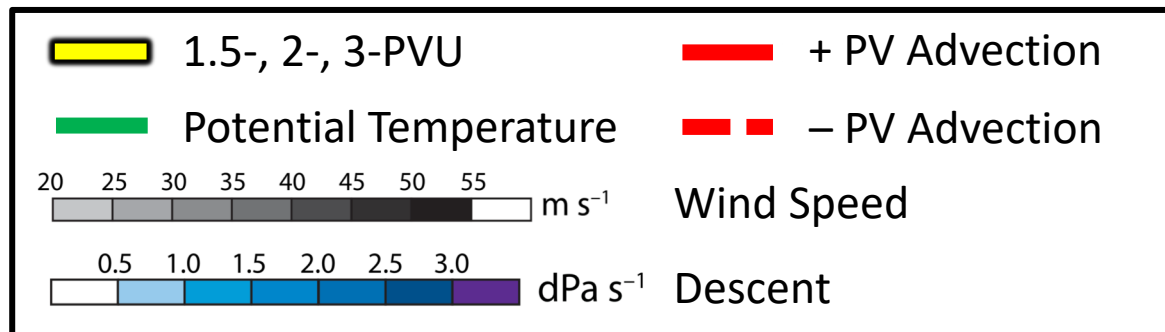
- Descent beneath the jet-entrance region is a common element among the jet superposition event composites.



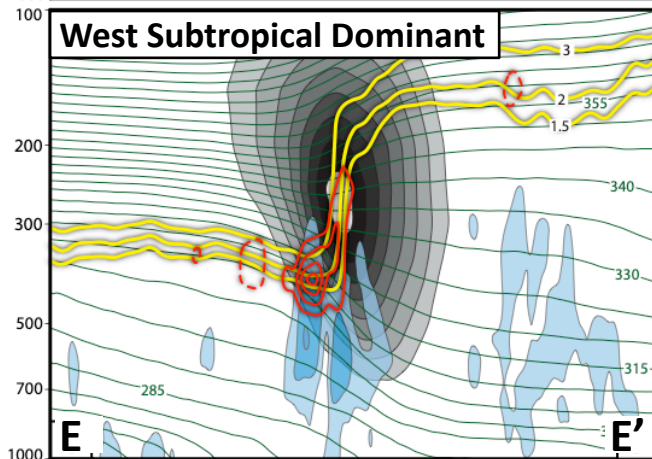
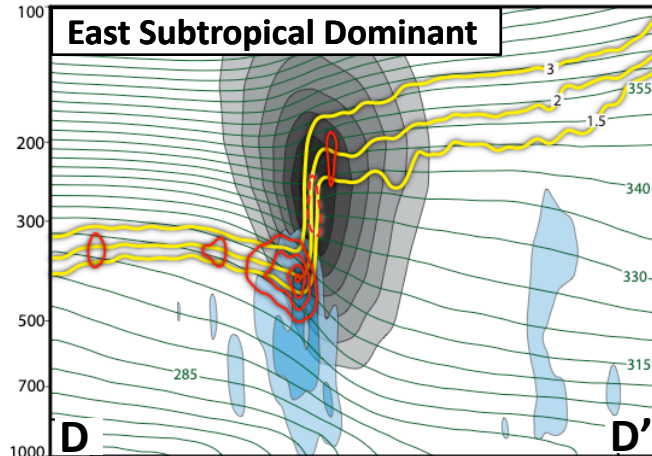
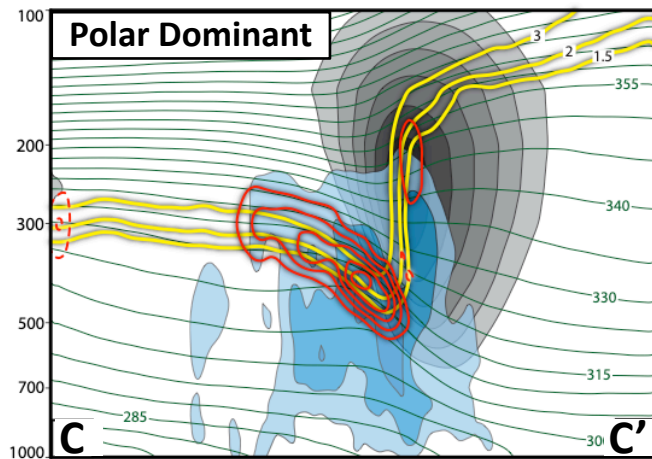
Jet Superposition Event Composites



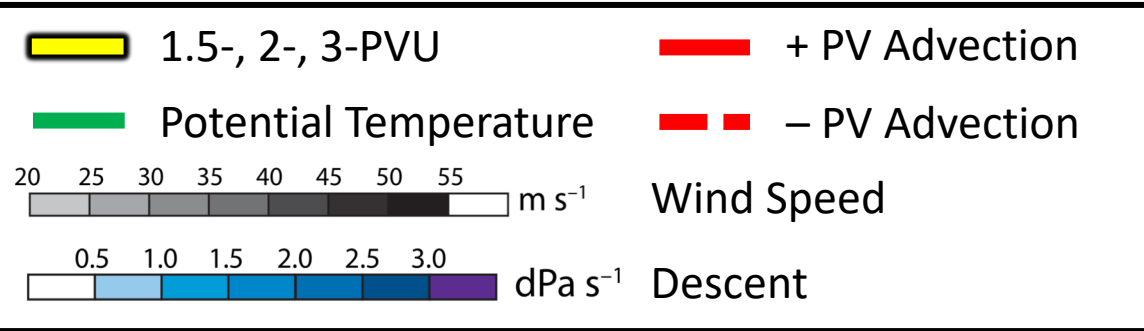
- Descent beneath the jet-entrance region is a common element among the jet superposition event composites.
- Descent results in downward PV advection within the developing tropopause fold, which steepens the tropopause.



Jet Superposition Event Composites

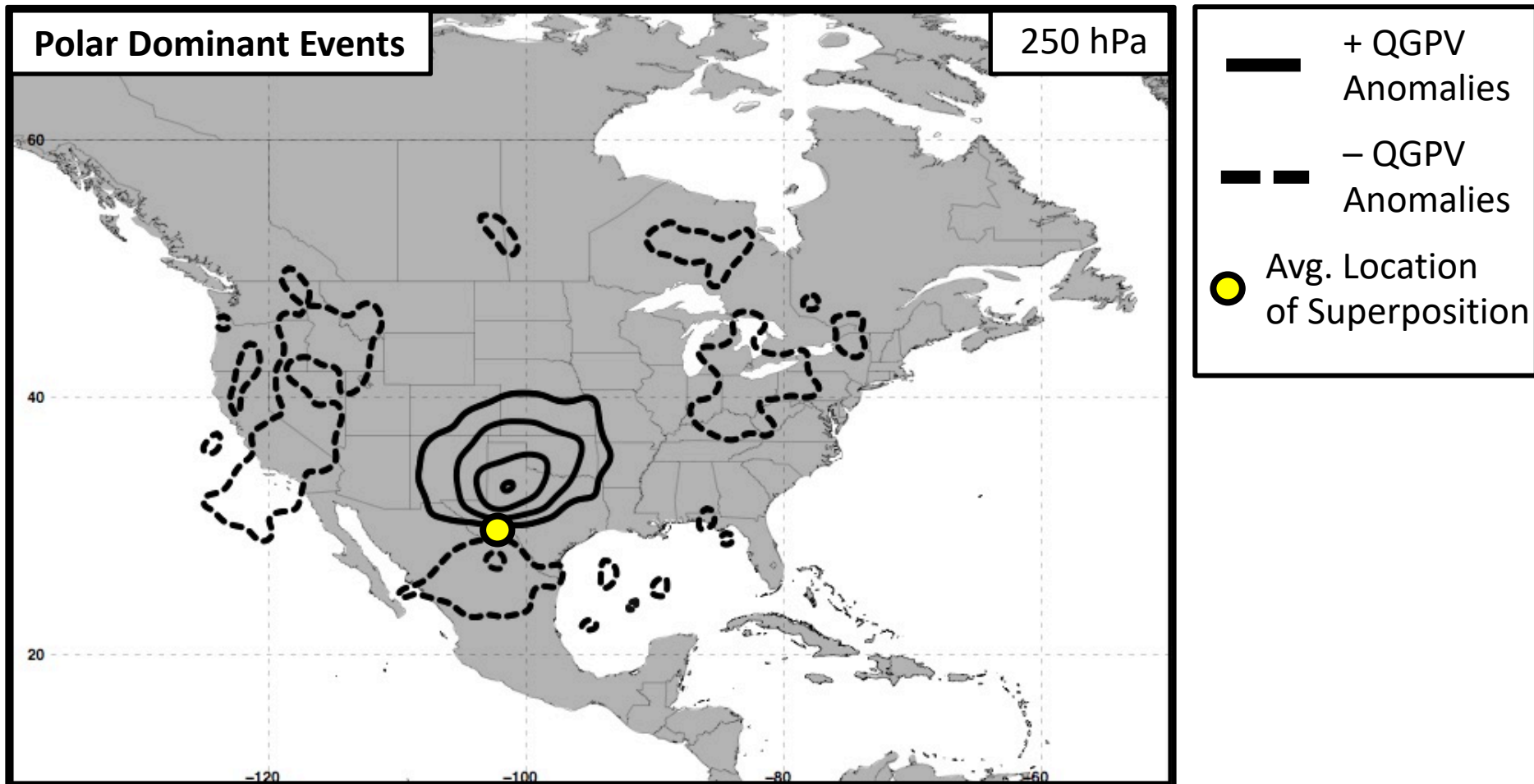


- Descent beneath the jet-entrance region is a common element among the jet superposition event composites.
- Descent results in downward PV advection within the developing tropopause fold, which steepens the tropopause.
- The consistent role of descent motivates further investigation of the dynamical mechanisms responsible for the descent.



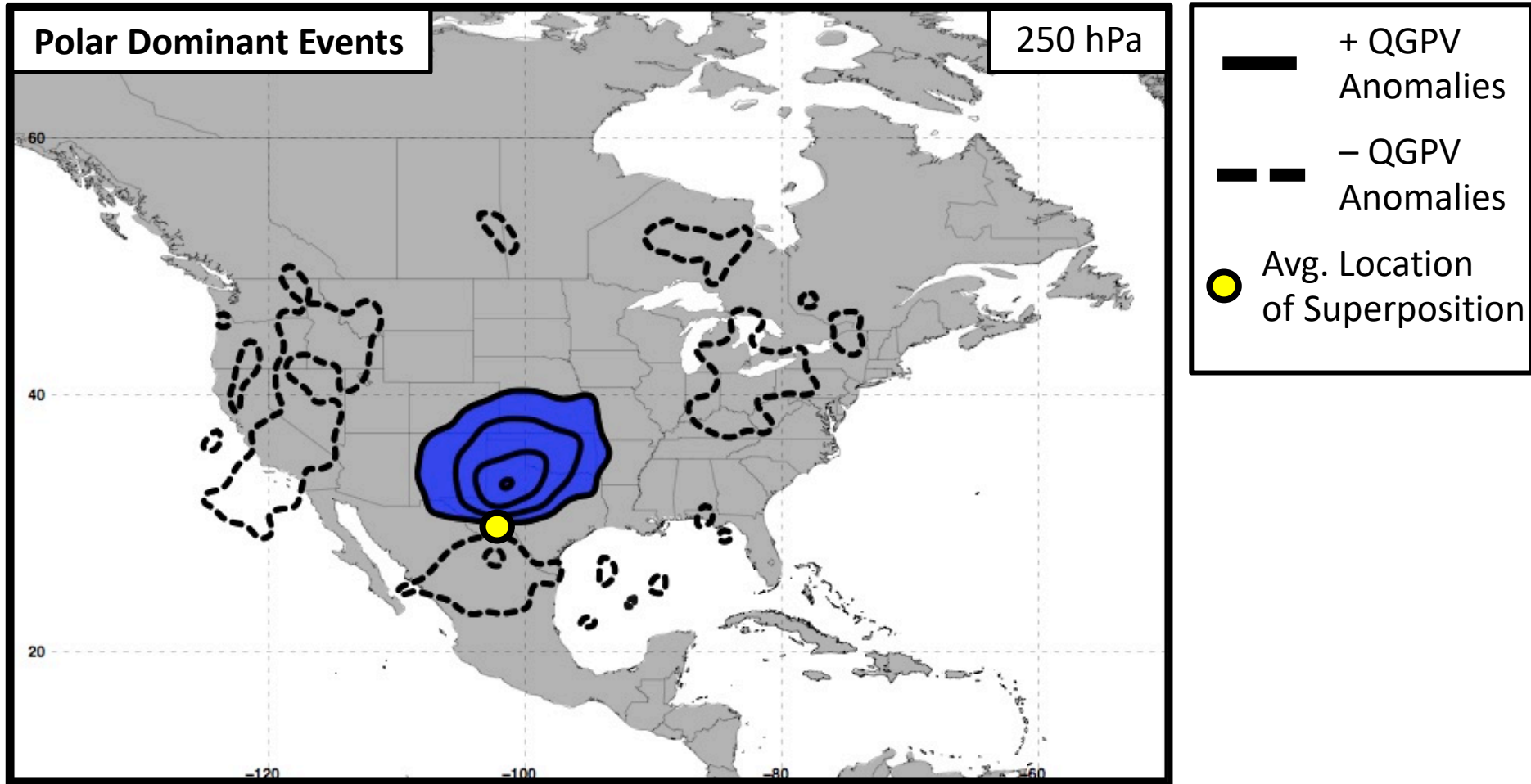
Piecewise QGPV Inversion

Piecewise QGPV Inversion

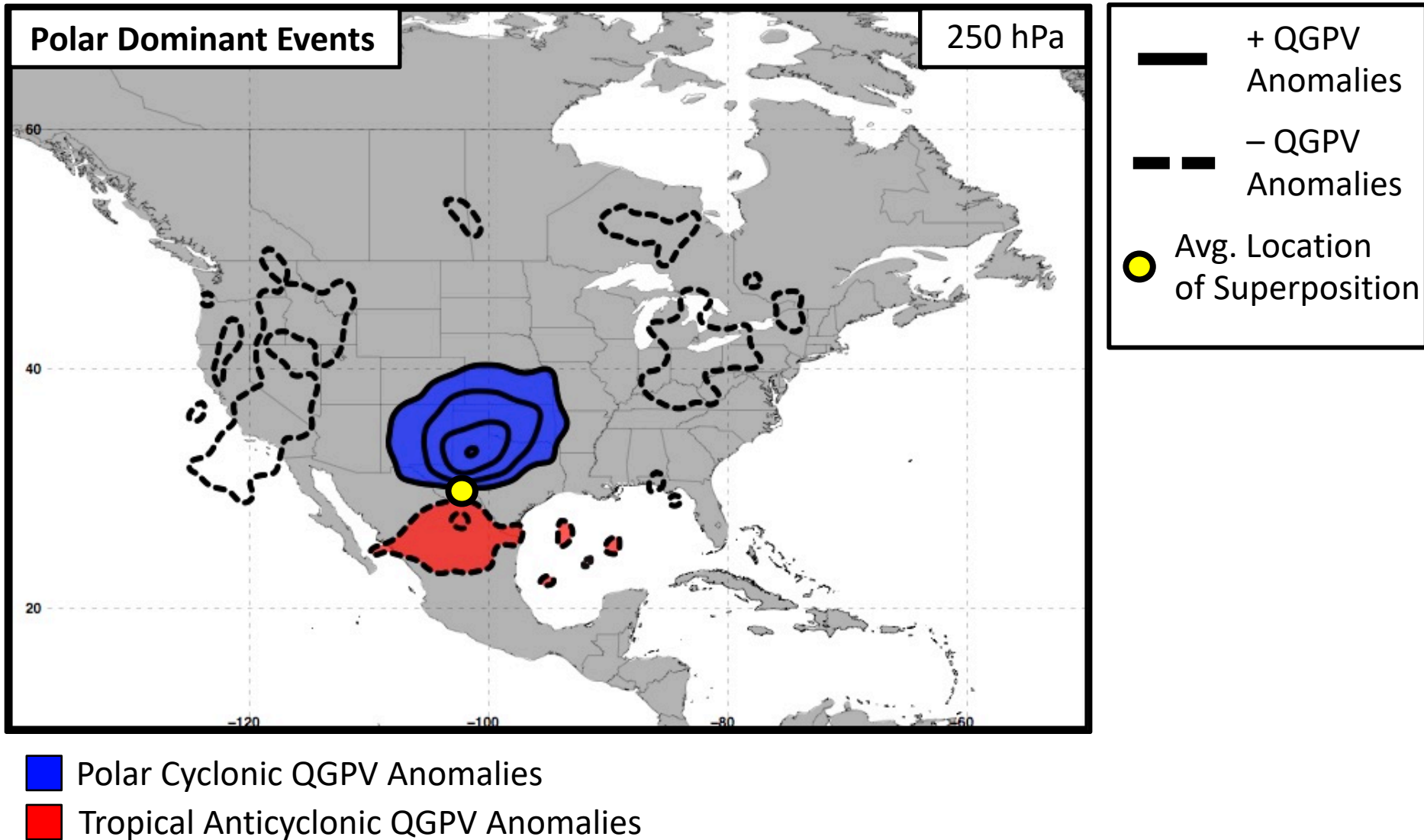


The descent characterizing each jet superposition event composite is examined further by isolating quasi-geostrophic (QG) PV anomalies in the vicinity of the jet superposition.

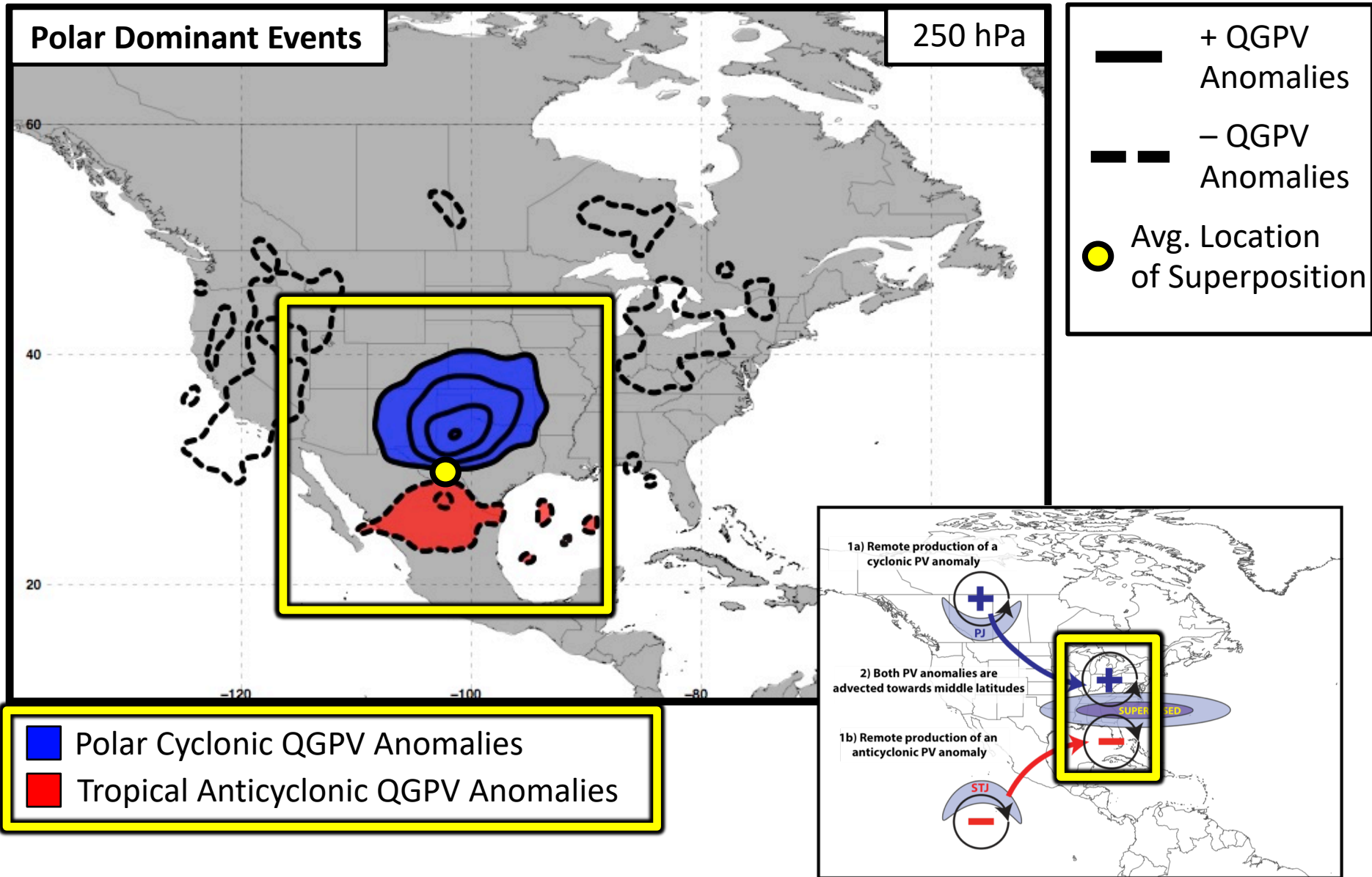
Piecewise QGPV Inversion



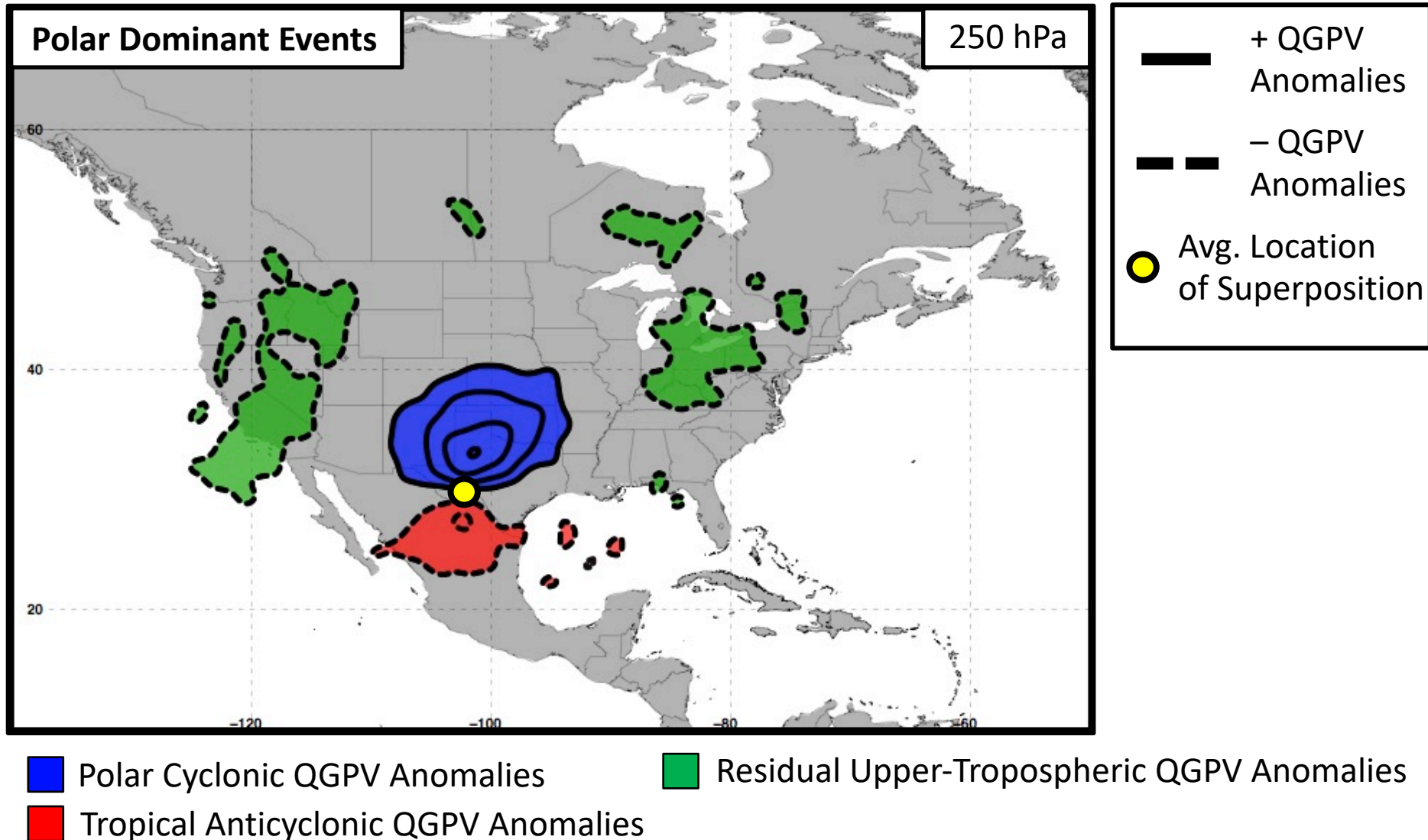
Piecewise QGPV Inversion



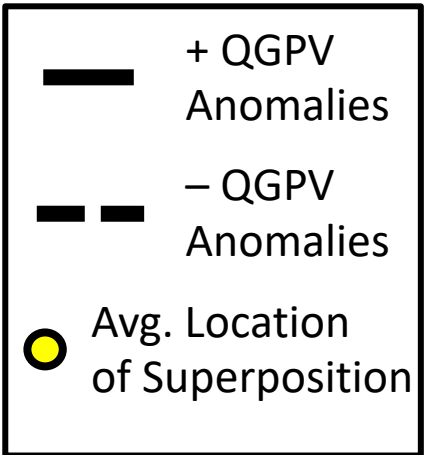
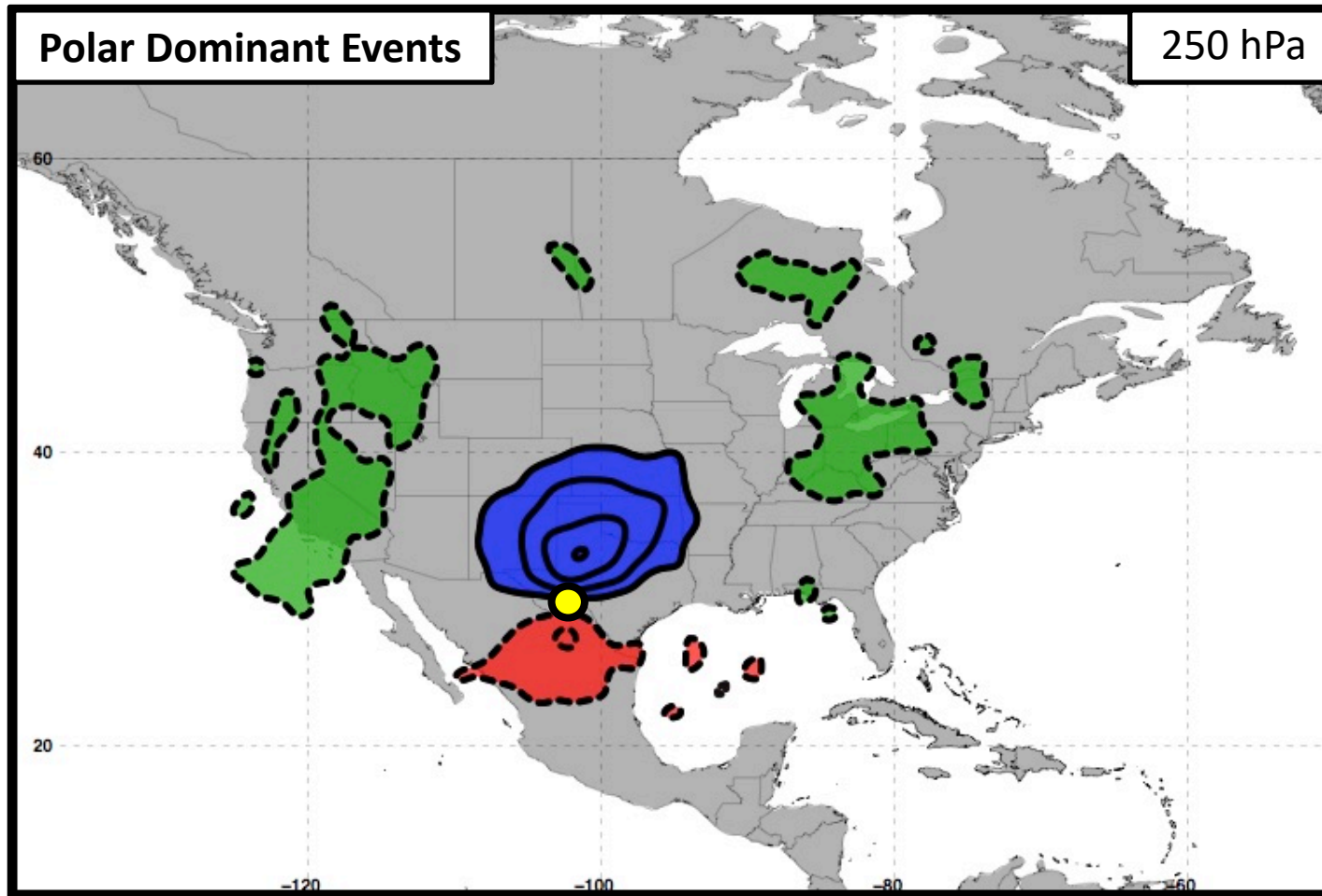
Piecewise QGPV Inversion



Piecewise QGPV Inversion

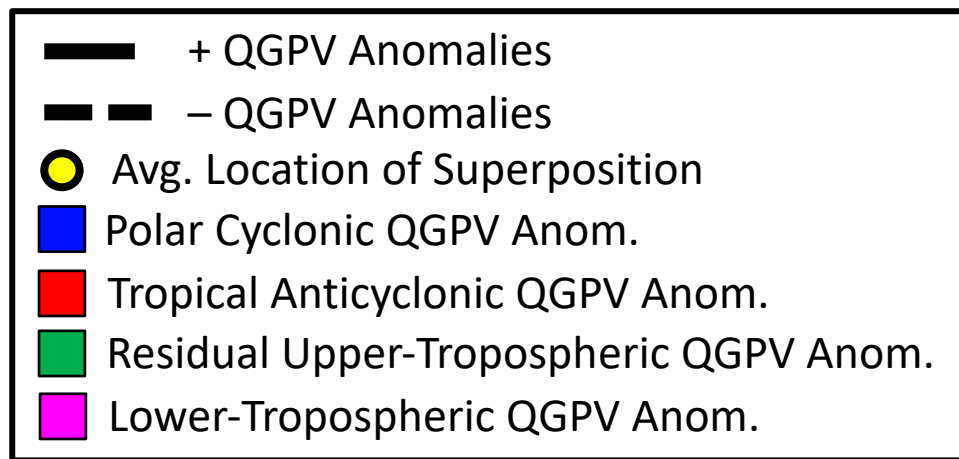
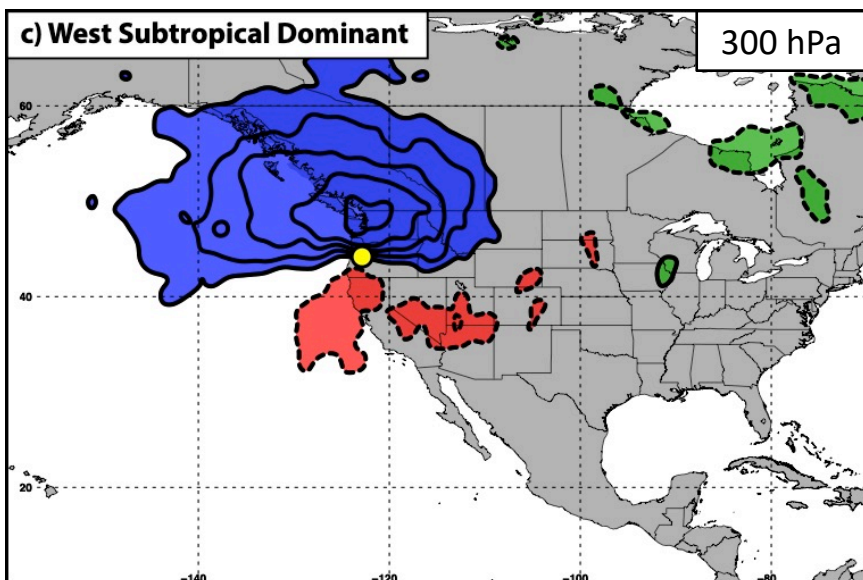
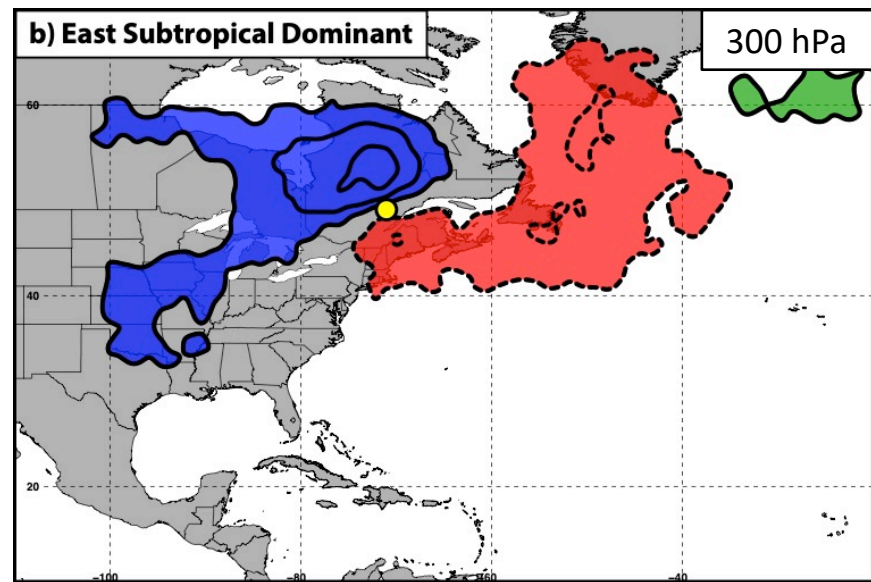
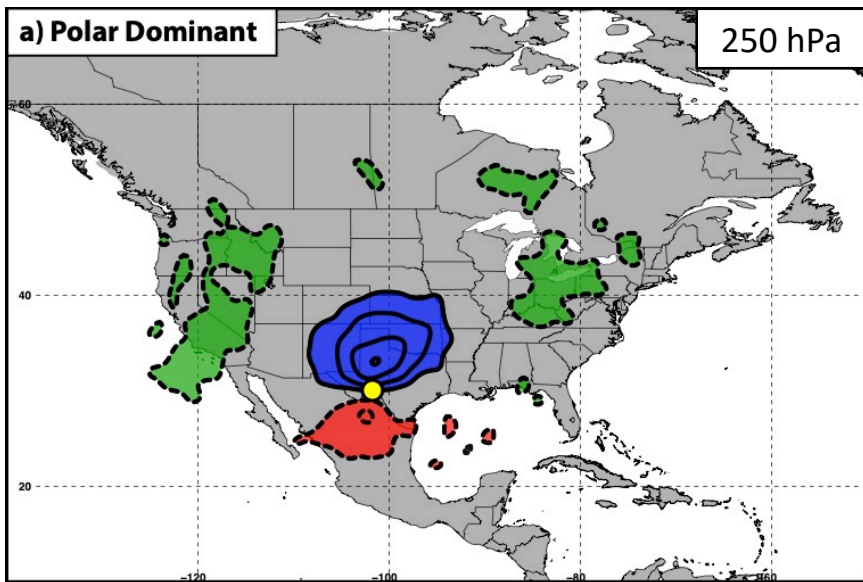


Piecewise QGPV Inversion



- Polar Cyclonic QGPV Anomalies
- Residual Upper-Tropospheric QGPV Anomalies
- Tropical Anticyclonic QGPV Anomalies
- Lower-Tropospheric QGPV Anomalies

Piecewise QGPV Inversion



Piecewise QGPV Inversion

Each category of QGPV anomalies (q'_i) is inverted to determine its associated perturbation geopotential (ϕ'_i) field:

$$q'_i = \frac{1}{f_0} \nabla^2 \phi'_i + f_0 \frac{\partial}{\partial p} \left(\frac{1}{\sigma_r} \frac{\partial \phi'_i}{\partial p} \right) \quad \text{where} \quad \begin{array}{l} f_0 = \text{Reference Coriolis Parameter} \\ \sigma_r = \text{Static Stability of the U.S. Std. Atm.} \end{array}$$

Piecewise QGPV Inversion

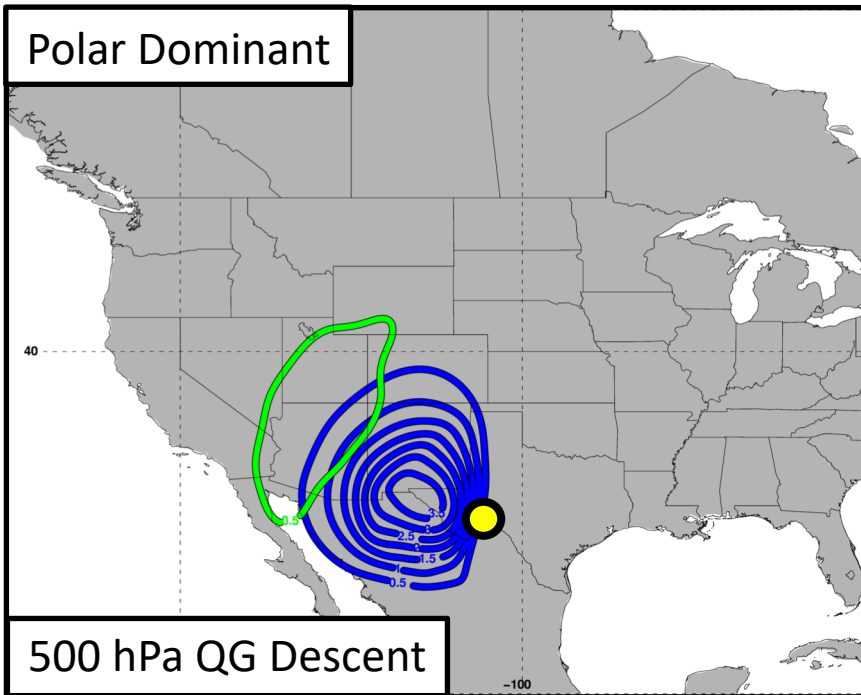
Each category of QGPV anomalies (q'_i) is inverted to determine its associated perturbation geopotential (ϕ'_i) field:

$$q'_i = \frac{1}{f_0} \nabla^2 \phi'_i + f_0 \frac{\partial}{\partial p} \left(\frac{1}{\sigma_r} \frac{\partial \phi'_i}{\partial p} \right) \quad \text{where} \quad \begin{array}{l} f_0 = \text{Reference Coriolis Parameter} \\ \sigma_r = \text{Static Stability of the U.S. Std. Atm.} \end{array}$$

The perturbation geopotential fields and the composite temperature (T) field are used to determine the QG vertical motion (ω_i) associated with each category of QGPV:

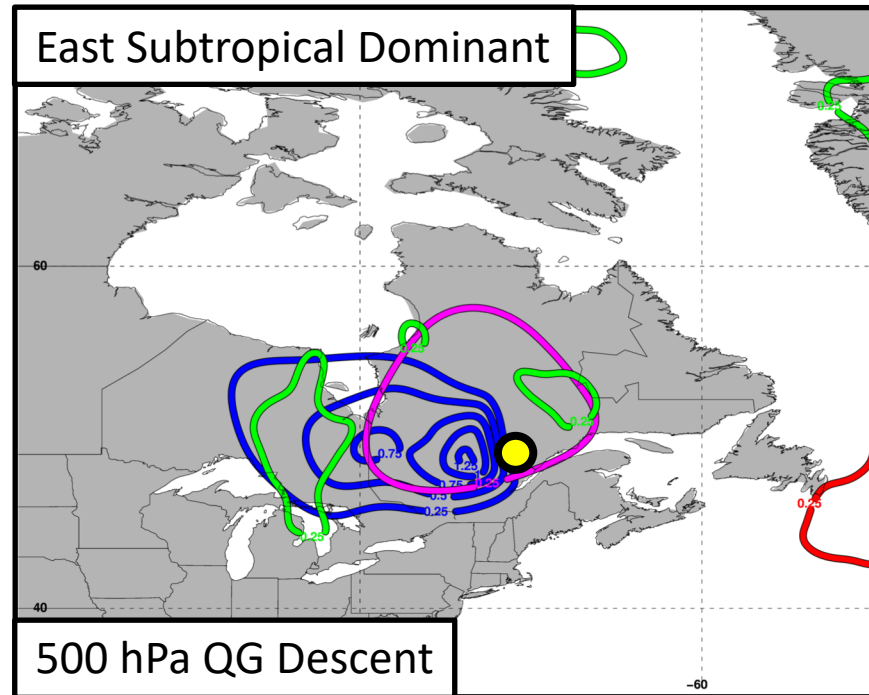
$$\sigma_r \nabla^2 \omega_i + f_0^2 \frac{\partial^2 \omega_i}{\partial p^2} = -2 \nabla \cdot \vec{Q}_i \quad \text{where} \quad \begin{array}{l} \vec{V}'_{gi} = -(1/f_0)(\hat{k} \times \nabla \phi'_i) \\ \vec{Q}_i = -\frac{R}{p} \left[\left(\frac{\partial \vec{V}'_{gi}}{\partial x} \cdot \nabla T \right), \left(\frac{\partial \vec{V}'_{gi}}{\partial y} \cdot \nabla T \right) \right] \end{array}$$

Polar Dominant



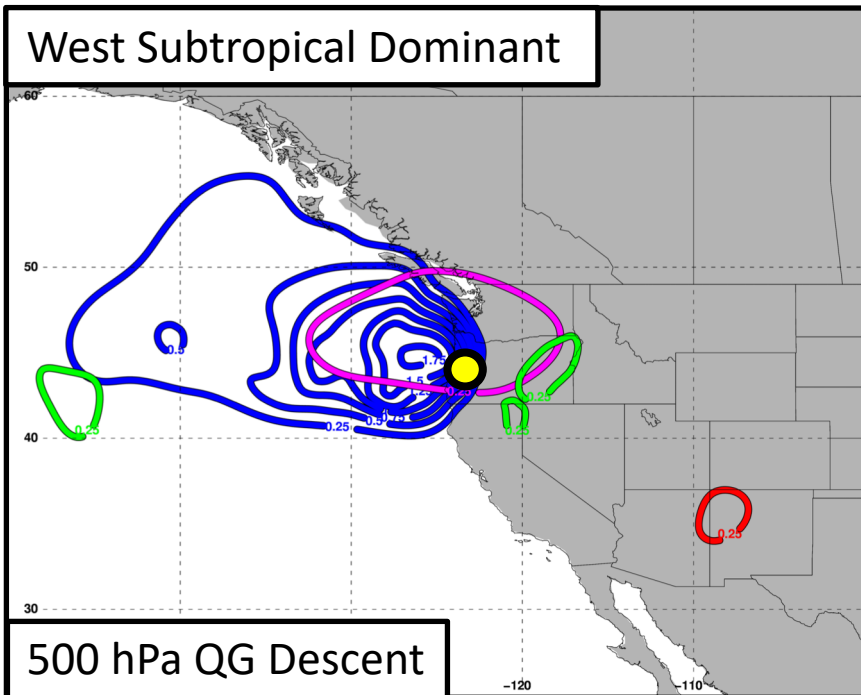
500 hPa QG Descent

East Subtropical Dominant



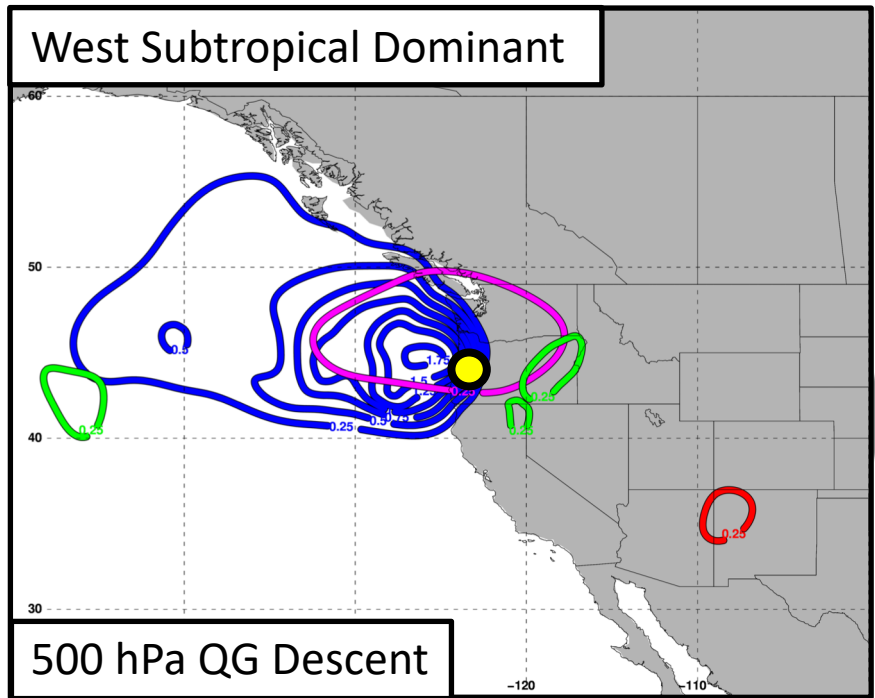
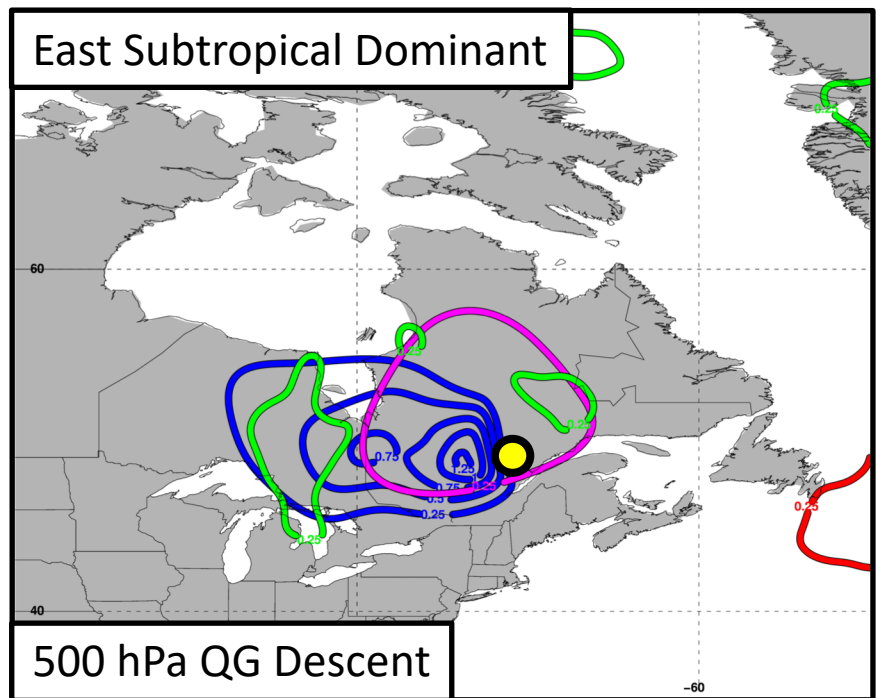
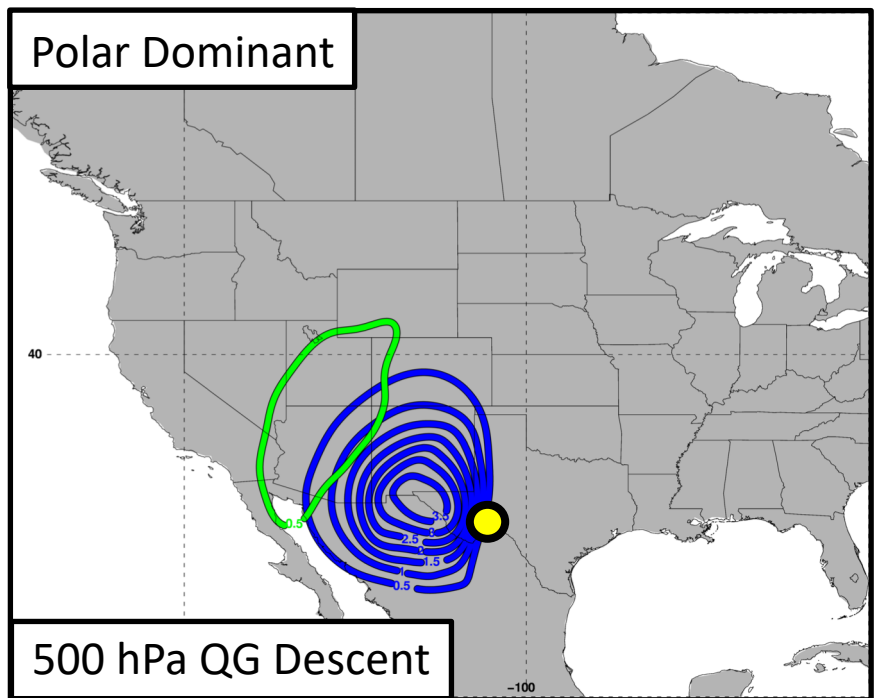
500 hPa QG Descent

West Subtropical Dominant



500 hPa QG Descent

- Blue square: Polar Cyclonic QGPV Anomalies
- Red square: Tropical Anticyclonic QGPV Anomalies
- Green square: Residual Upper-Tropospheric QGPV Anomalies
- Magenta square: Lower-Tropospheric QGPV Anomalies
- Yellow circle: Avg. Location of Jet Superposition



Descent is primarily associated with polar cyclonic QGPV anomalies.

- Polar Cyclonic QGPV Anomalies
- Tropical Anticyclonic QGPV Anomalies
- Residual Upper-Tropospheric QGPV Anomalies
- Lower-Tropospheric QGPV Anomalies
- Avg. Location of Jet Superposition

Piecewise QGPV Inversion

$$\sigma_r \nabla^2 \omega_i + f_0^2 \frac{\partial^2 \omega_i}{\partial p^2} = -2 \nabla \cdot \vec{Q}_i \quad \text{where} \quad \vec{V}'_{gi} = -(1/f_0)(\hat{k} \times \nabla \phi'_i)$$
$$\vec{Q}_i = -\frac{R}{p} \left[\left(\frac{\partial \vec{V}'_{gi}}{\partial x} \cdot \nabla T \right), \left(\frac{\partial \vec{V}'_{gi}}{\partial y} \cdot \nabla T \right) \right]$$

The prior analyses only consider the interaction of each perturbation geostrophic wind (\vec{V}'_{gi}) field with the composite temperature field (T).

Piecewise QGPV Inversion

$$\sigma_r \nabla^2 \omega_i + f_0^2 \frac{\partial^2 \omega_i}{\partial p^2} = -2 \nabla \cdot \vec{Q}_i \quad \text{where} \quad \begin{aligned} \vec{V}'_{gi} &= -(1/f_0)(\hat{k} \times \nabla \phi'_i) \\ \vec{Q}_i &= -\frac{R}{p} \left[\left(\frac{\partial \vec{V}'_{gi}}{\partial x} \cdot \nabla T \right), \left(\frac{\partial \vec{V}'_{gi}}{\partial y} \cdot \nabla T \right) \right] \end{aligned}$$

The prior analyses only consider the interaction of each perturbation geostrophic wind (\vec{V}'_{gi}) field with the composite temperature field (T).

Each perturbation geopotential field (ϕ'_i) is also accompanied by a perturbation temperature field (T'_i).

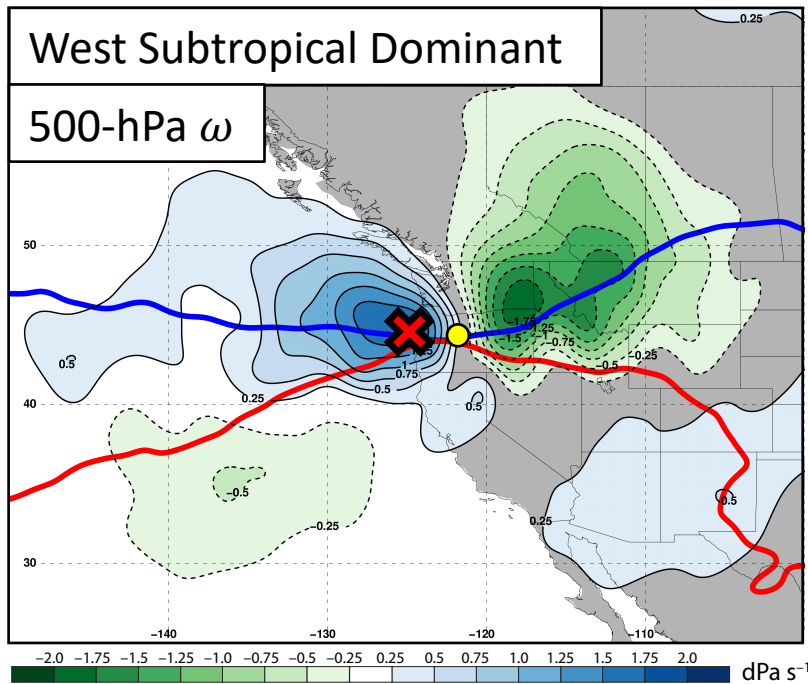
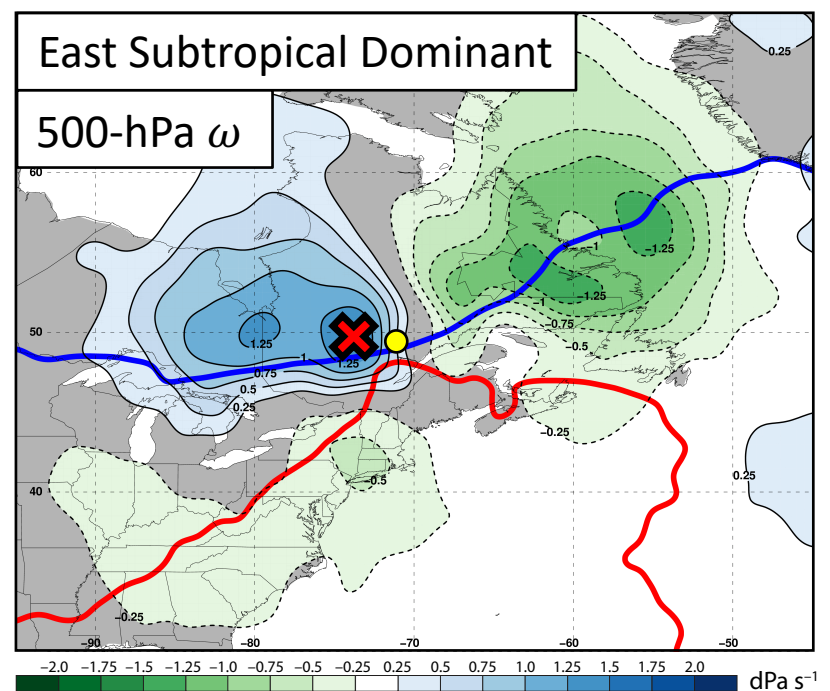
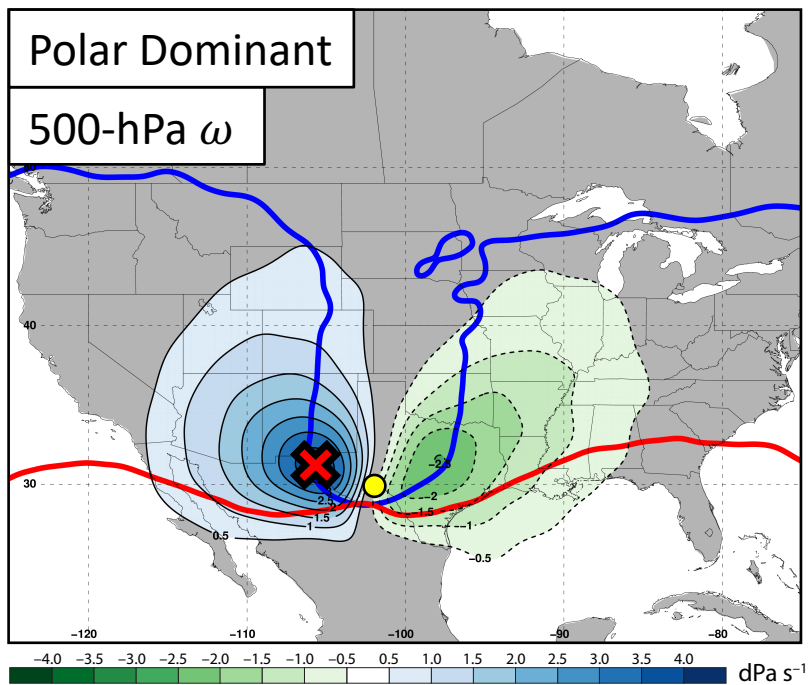
Piecewise QGPV Inversion

$$\sigma_r \nabla^2 \omega_i + f_0^2 \frac{\partial^2 \omega_i}{\partial p^2} = -2 \nabla \cdot \vec{Q}_i \quad \text{where} \quad \begin{aligned} \vec{V}_{gi}' &= -(1/f_0)(\hat{k} \times \nabla \phi_i') \\ \vec{Q}_i &= -\frac{R}{p} \left[\left(\frac{\partial \vec{V}_{gi}'}{\partial x} \cdot \nabla T_i' \right), \left(\frac{\partial \vec{V}_{gi}'}{\partial y} \cdot \nabla T_i' \right) \right] \end{aligned}$$





The prior analyses only consider the interaction of each perturbation geostrophic wind (\vec{V}_{gi}') field with the composite temperature field (T).

Each perturbation geopotential field (ϕ_i') is also accompanied by a perturbation temperature field (T_i').

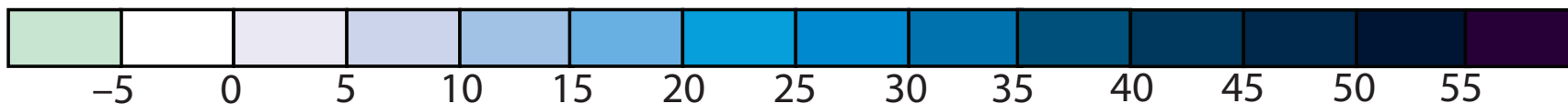
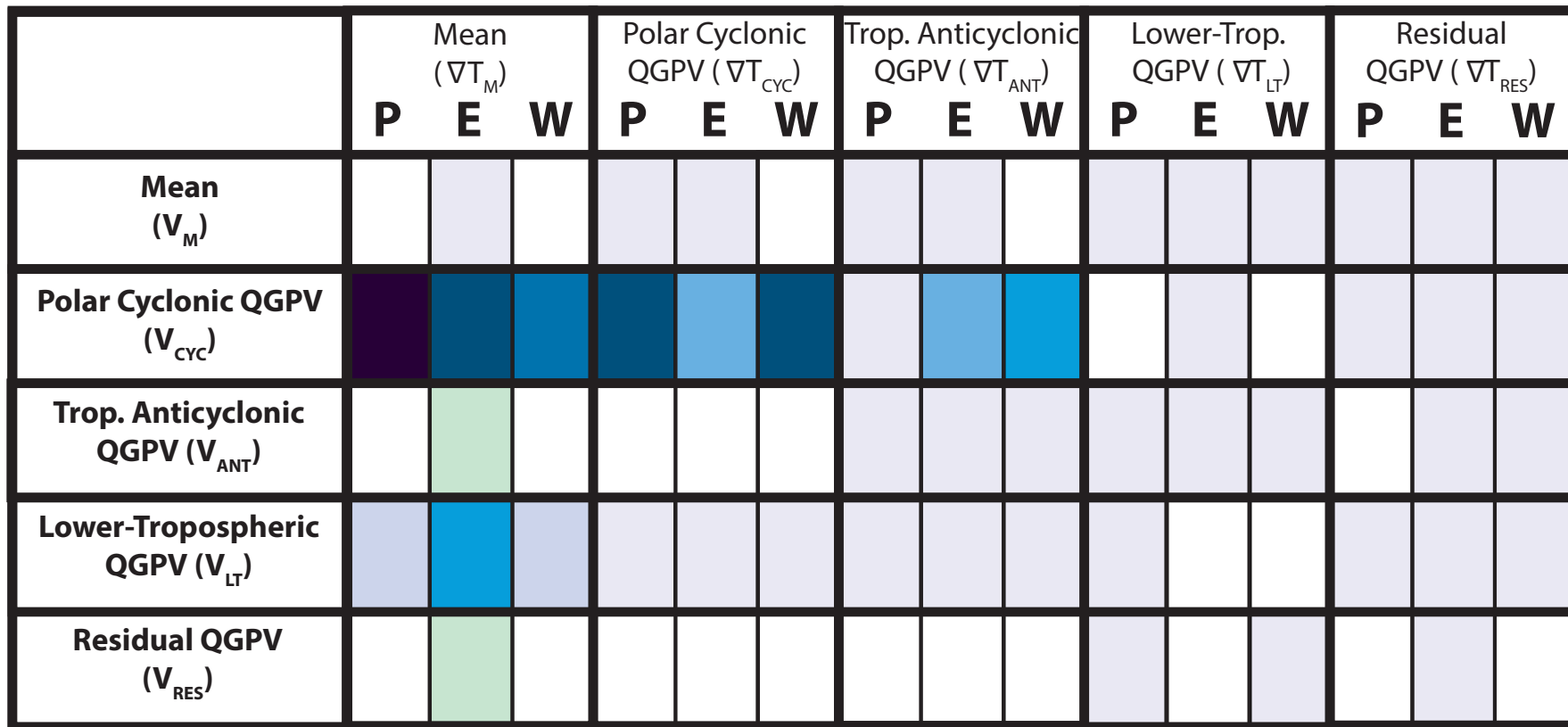
Substituting the perturbation temperature fields (T_i') into the QG- ω equation permits diagnosis of the QG vertical motion that results from interactions between each category of QGPV anomalies.



Consider the QG ω associated with each interaction term at the location of maximum descent.

-  Location of Maximum Descent
-  2 PVU on the 320-K surface
-  2 PVU on the 345-K surface
-  Avg. Location of Jet Superposition

Piecewise QGPV Inversion



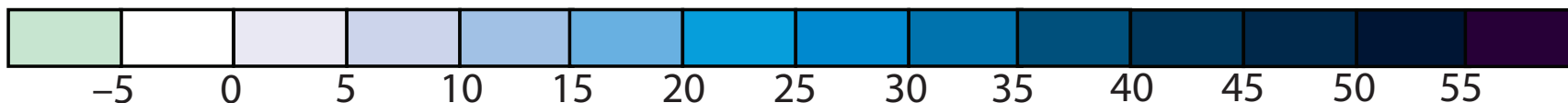
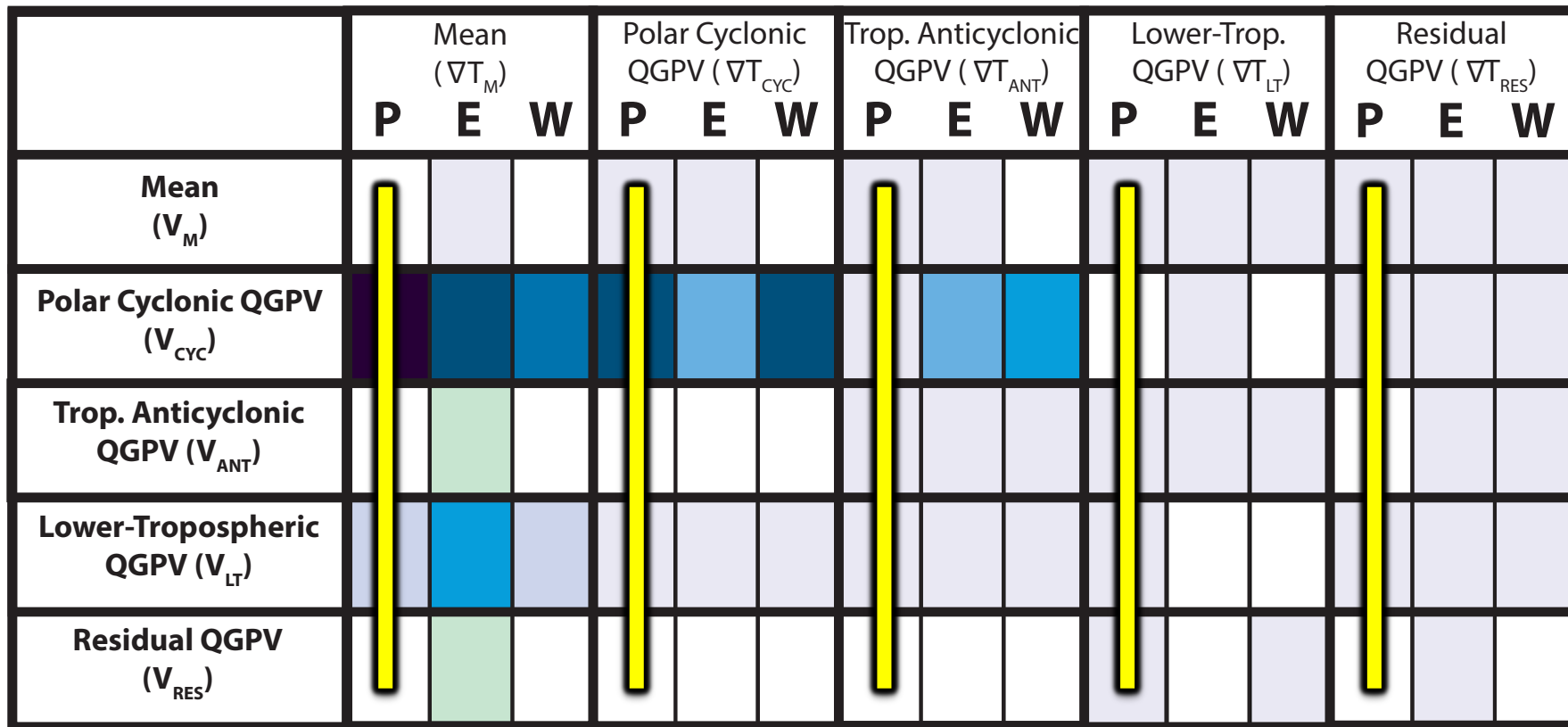
P = Polar Dominant

E = East Subtropical Dominant

W = West Subtropical Dominant

Percent of QG Descent

Piecewise QGPV Inversion



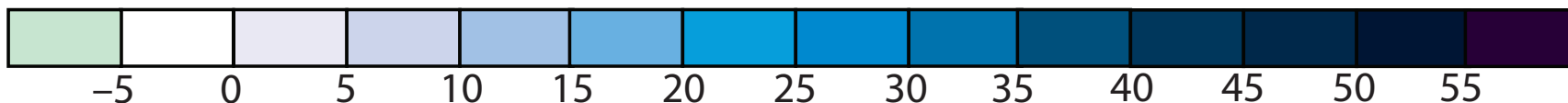
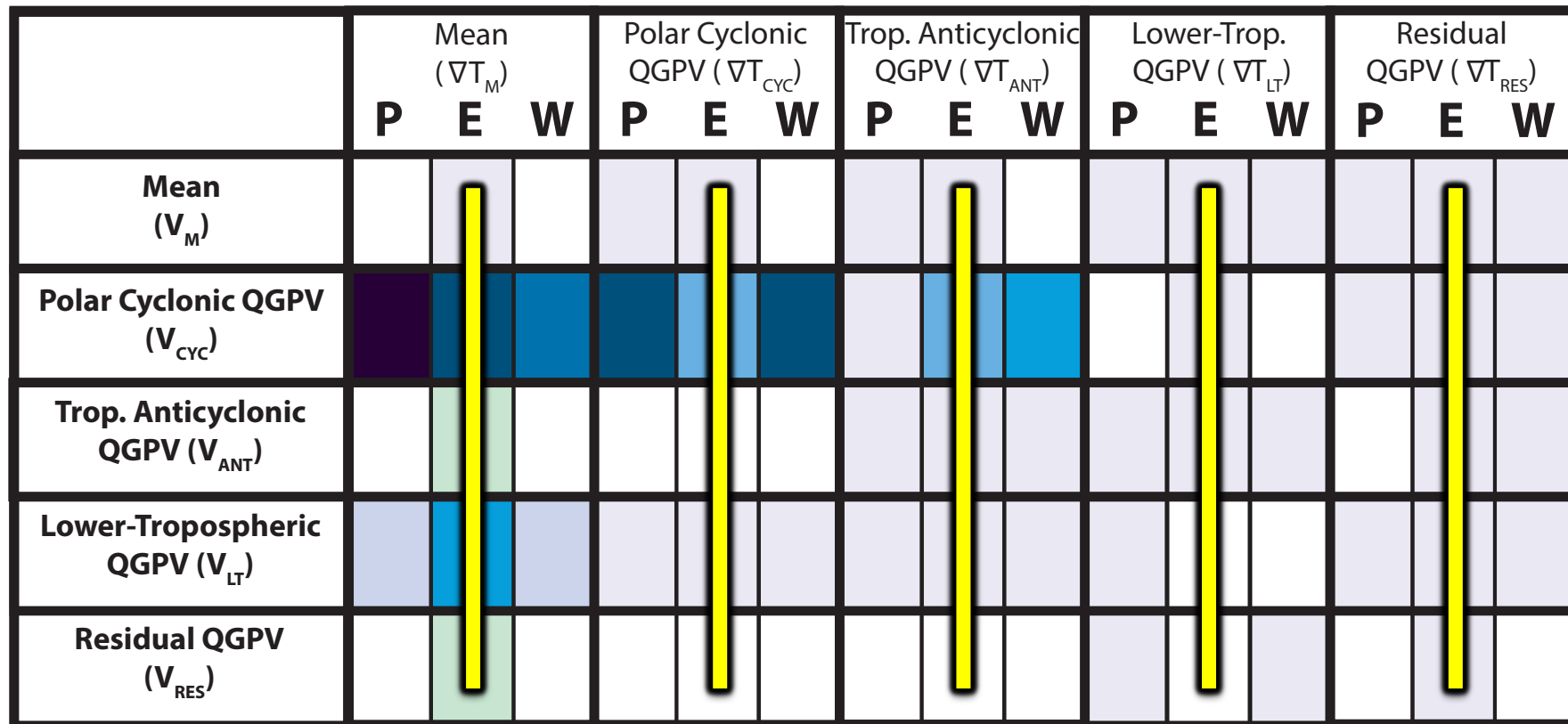
Percent of QG Descent

P = Polar Dominant

E = East Subtropical Dominant

W = West Subtropical Dominant

Piecewise QGPV Inversion



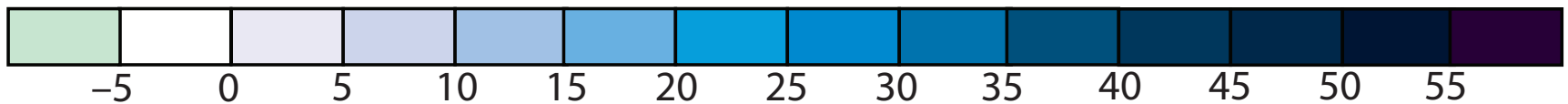
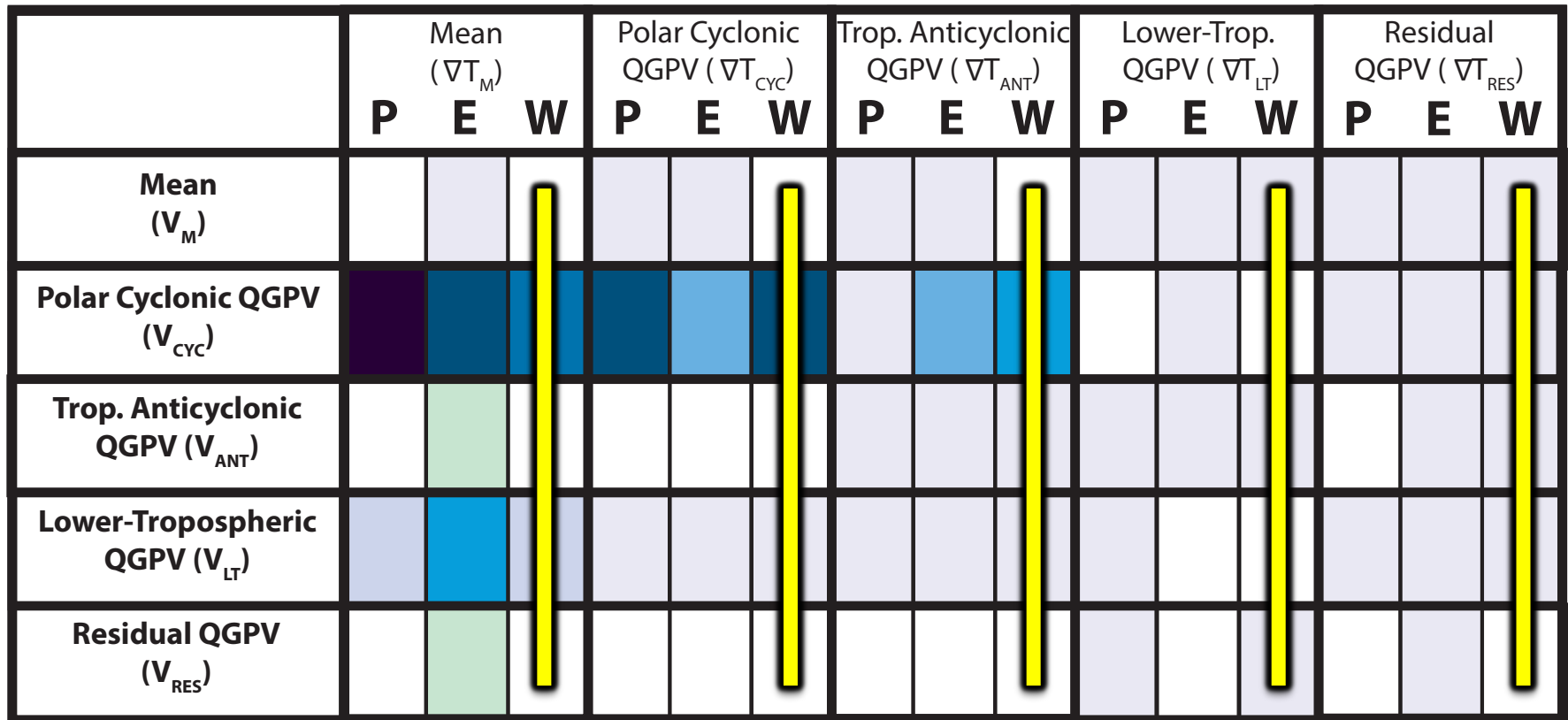
Percent of QG Descent

P = Polar Dominant

E = East Subtropical Dominant

W = West Subtropical Dominant

Piecewise QGPV Inversion



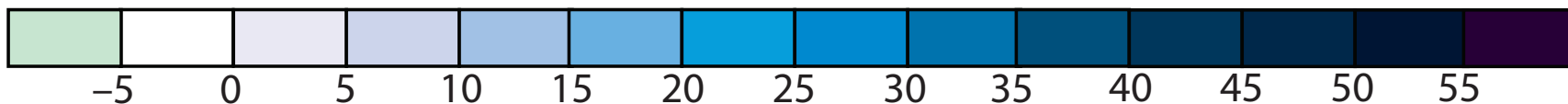
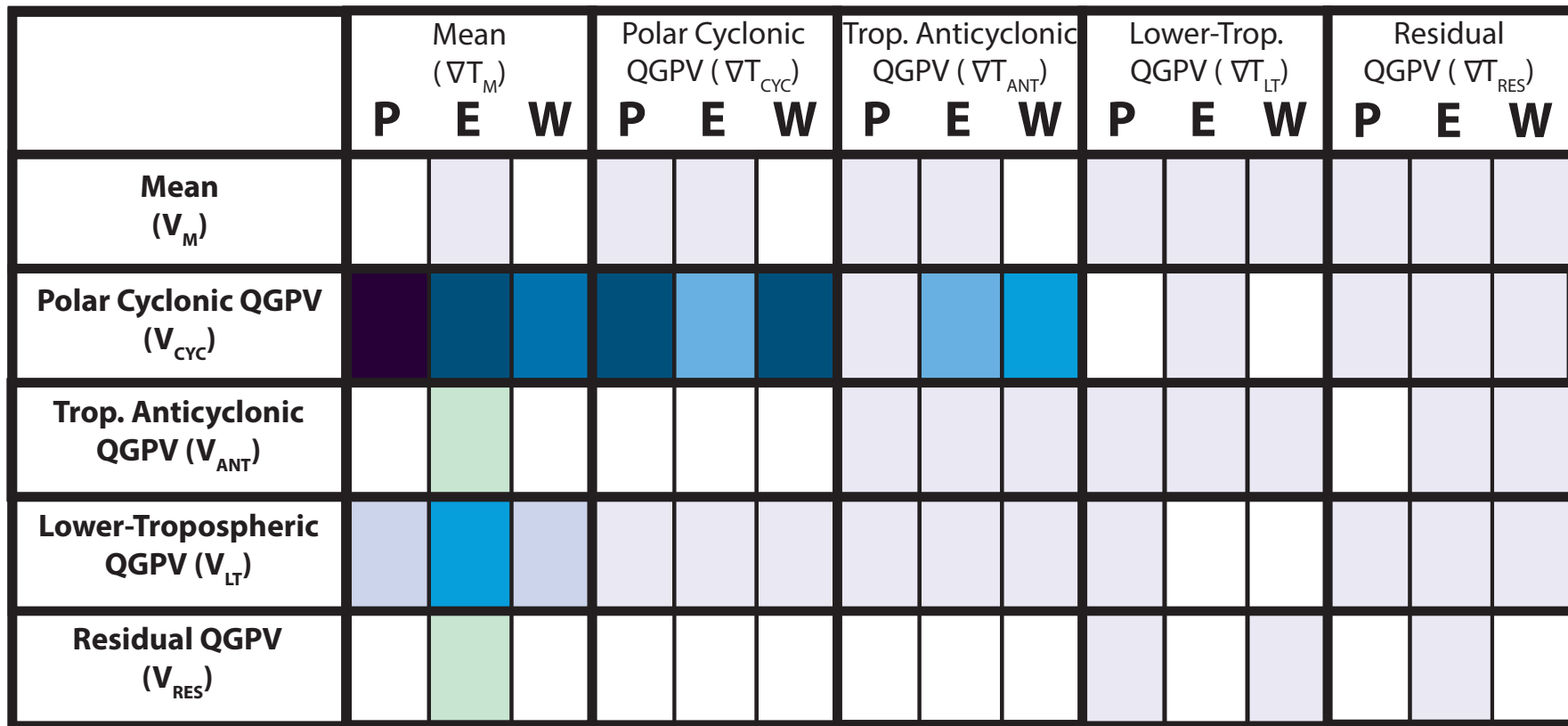
Percent of QG Descent

P = Polar Dominant

E = East Subtropical Dominant

W = West Subtropical Dominant

Piecewise QGPV Inversion



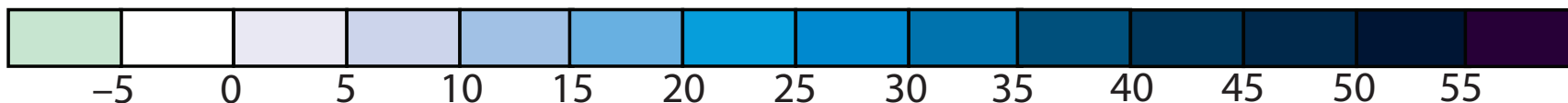
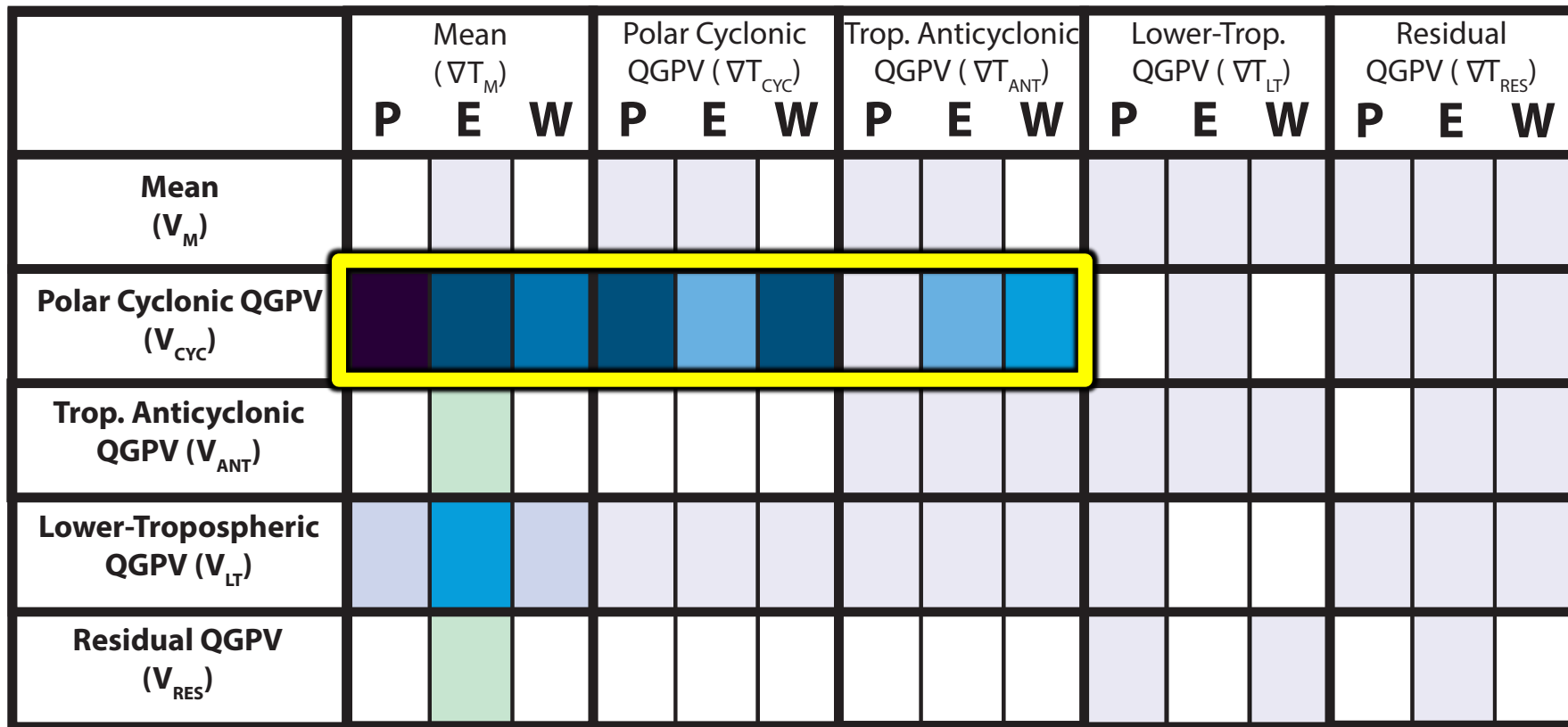
P = Polar Dominant

E = East Subtropical Dominant

W = West Subtropical Dominant

Percent of QG Descent

Piecewise QGPV Inversion



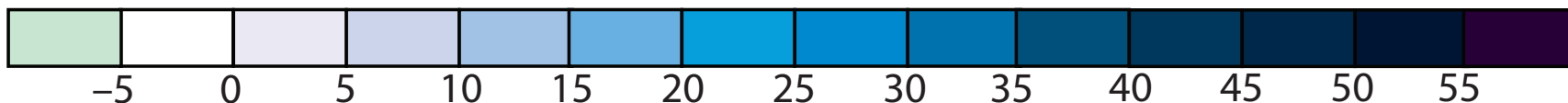
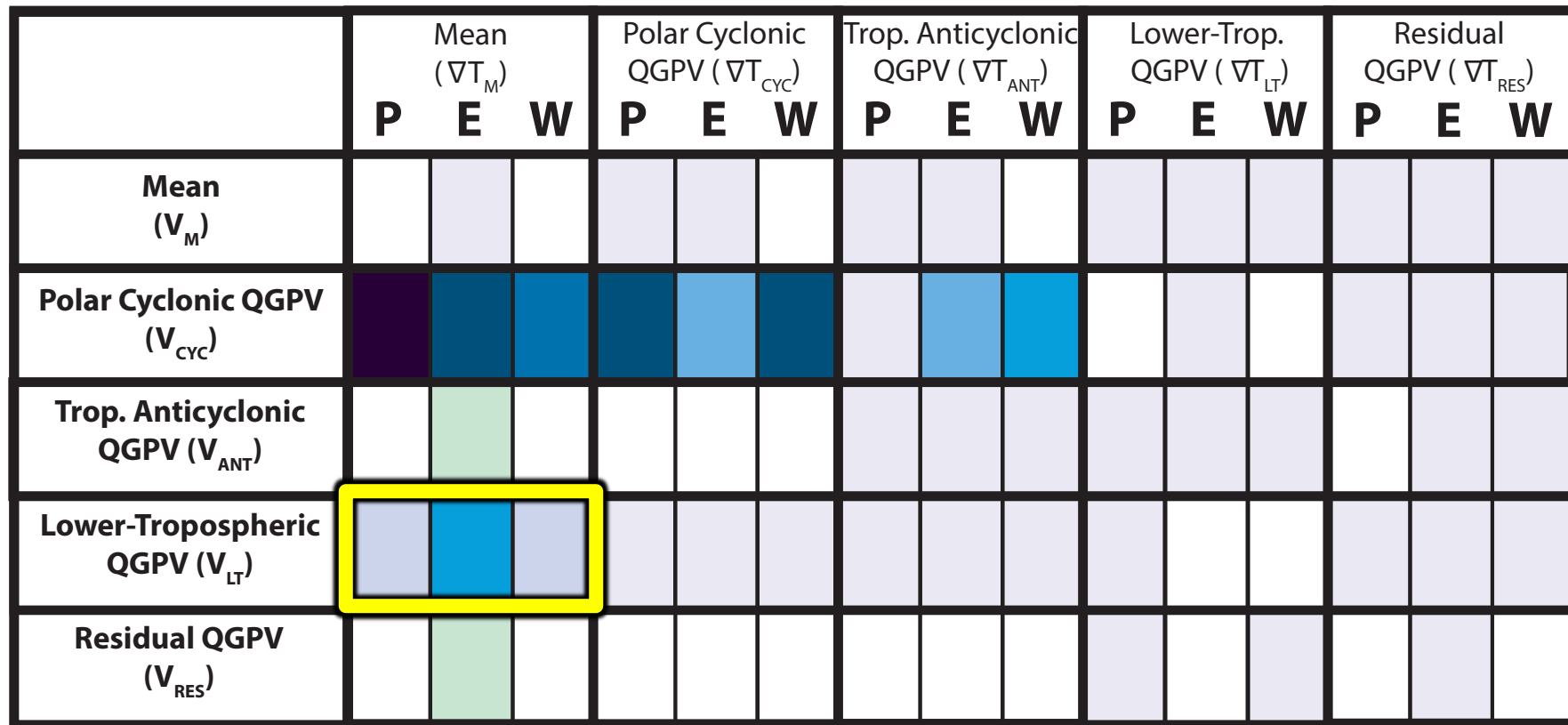
P = Polar Dominant

E = East Subtropical Dominant

W = West Subtropical Dominant

Percent of QG Descent

Piecewise QGPV Inversion



P = Polar Dominant

E = East Subtropical Dominant

W = West Subtropical Dominant

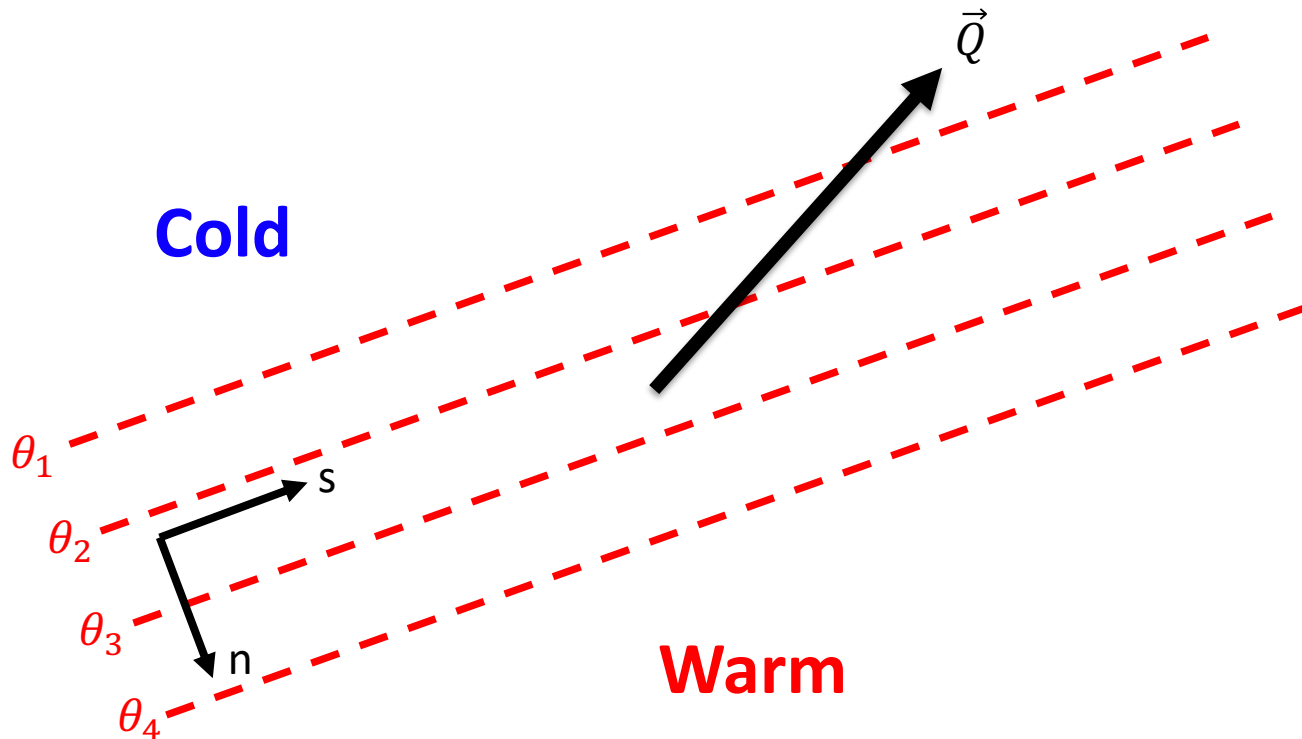
Percent of QG Descent

Along- and Across-Front Vertical Motion

Along- and Across-Front Vertical Motion

$$\sigma_r \nabla^2 \omega + f_0^2 \frac{\partial^2 \omega}{\partial p^2} = -2 \nabla \cdot \vec{Q}$$

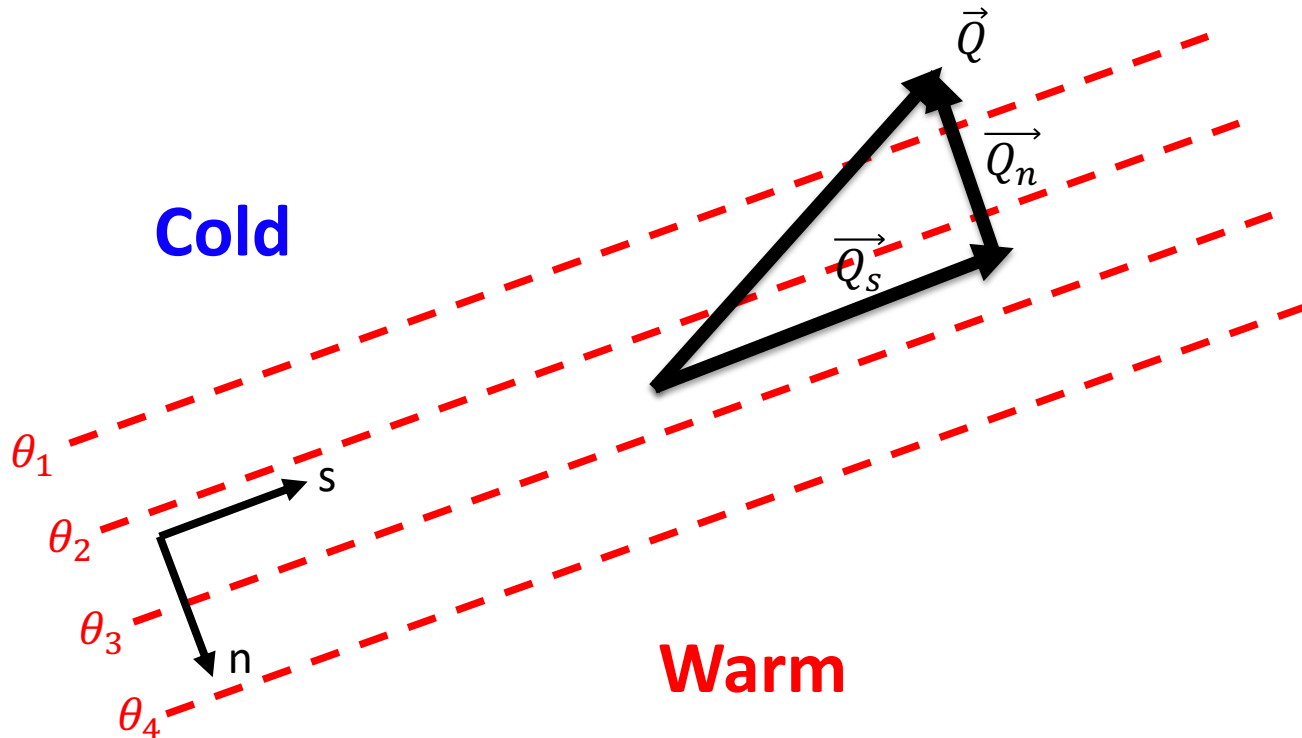
\vec{Q} can be partitioned into an along- and an across-front component.



Along- and Across-Front Vertical Motion

$$\sigma_r \nabla^2 \omega + f_0^2 \frac{\partial^2 \omega}{\partial p^2} = -2 \nabla \cdot \vec{Q}$$

\vec{Q} can be partitioned into an along- and an across-front component.

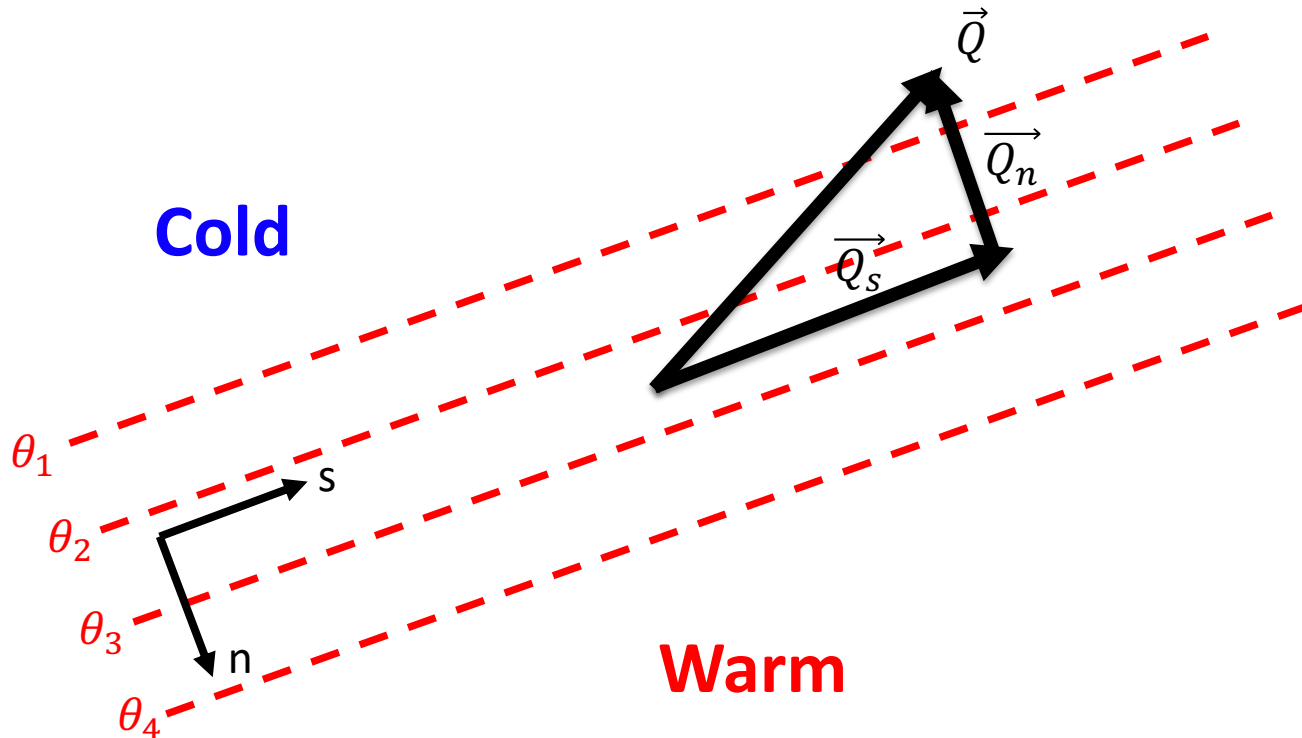


Along- and Across-Front Vertical Motion

$$\sigma_r \nabla^2 \omega + f_0^2 \frac{\partial^2 \omega}{\partial p^2} = -2 \nabla \cdot \vec{Q}$$

$$\vec{Q} = \vec{Q}_s + \vec{Q}_n$$

$$\vec{Q}_s = \left[\frac{\vec{Q} \cdot (\hat{k} \times \nabla \theta)}{|\nabla \theta|} \right] \frac{(\hat{k} \times \nabla \theta)}{|\nabla \theta|}, \quad \vec{Q}_n = \left[\frac{\vec{Q} \cdot \nabla \theta}{|\nabla \theta|} \right] \frac{\nabla \theta}{|\nabla \theta|}$$



Along- and Across-Front Vertical Motion

$$\sigma_r \nabla^2 \omega + f_0^2 \frac{\partial^2 \omega}{\partial p^2} = -2\nabla \cdot \vec{Q}$$

$$\sigma_r \nabla^2 \omega_s + f_0^2 \frac{\partial^2 \omega_s}{\partial p^2} = -2\nabla \cdot \vec{Q}_s$$

$$\sigma_r \nabla^2 \omega_n + f_0^2 \frac{\partial^2 \omega_n}{\partial p^2} = -2\nabla \cdot \vec{Q}_n$$

$$\omega = \omega_s + \omega_n$$

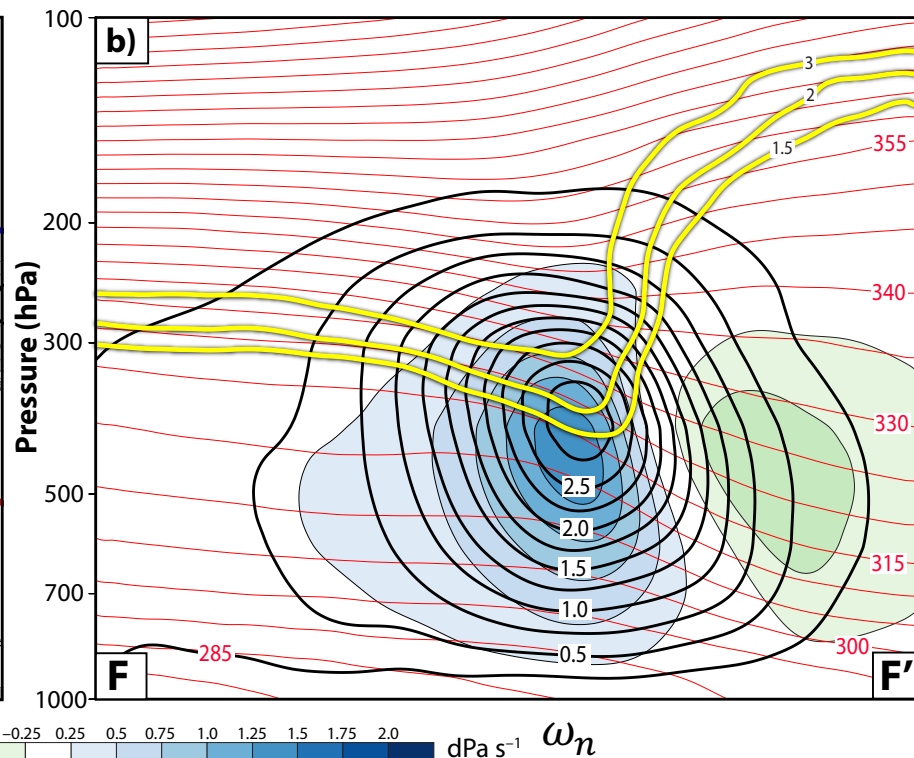
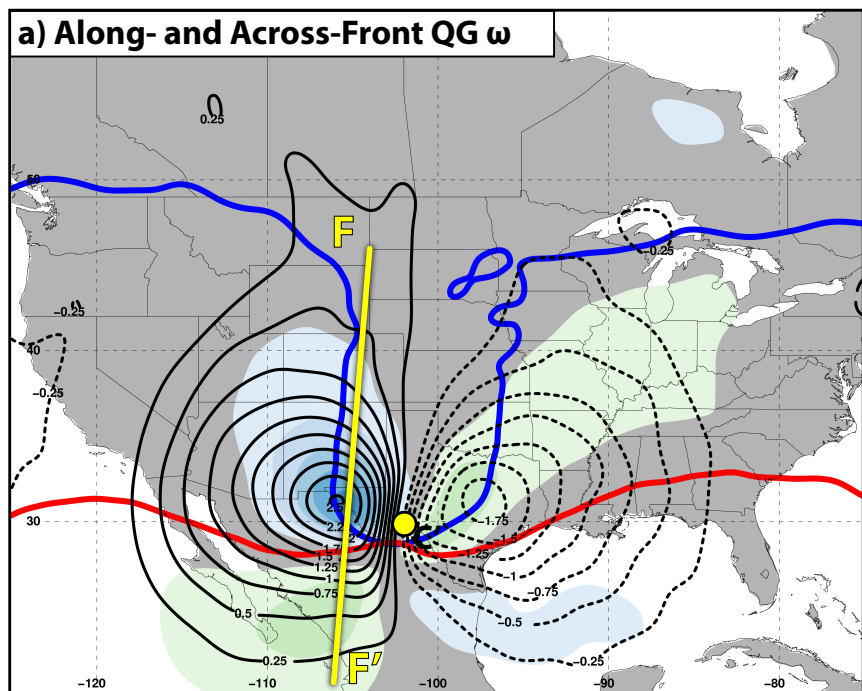
The divergence of \vec{Q}_s and \vec{Q}_n can be used to solve for the fraction of the vertical motion in the along- and across-front directions.

ω_s corresponds to vertical motion in the along-front direction and describes vertical motion on the scale of baroclinic waves.

ω_n corresponds to vertical motion in the across-front direction and describes vertical motion on the scale of frontal zones.

Along- and Across-Front Vertical Motion

Polar Dominant Events

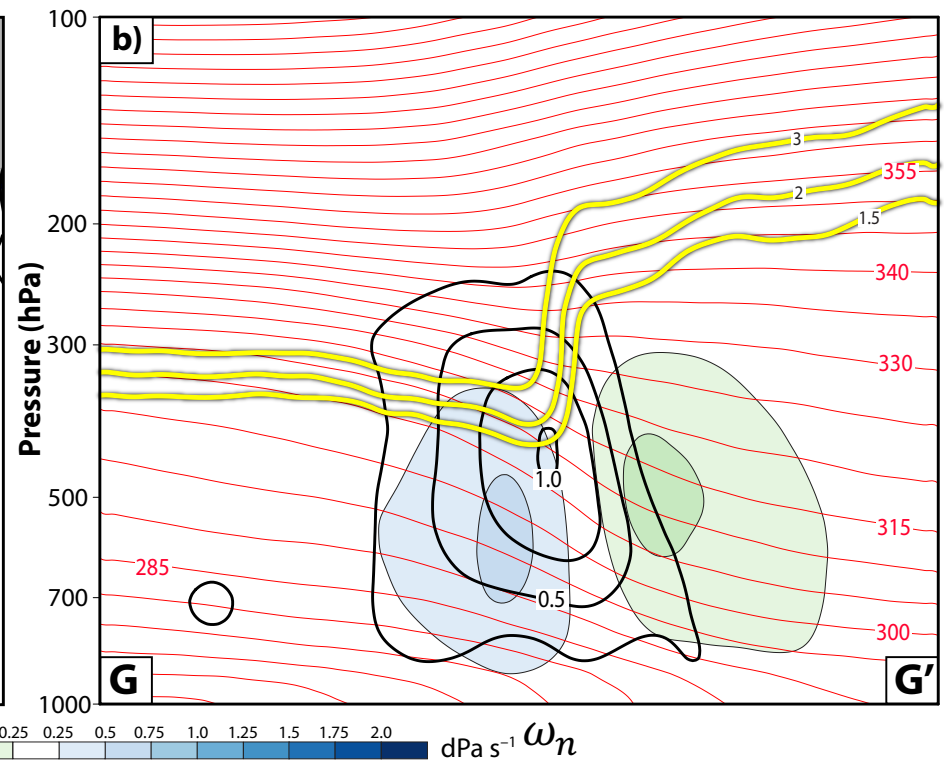
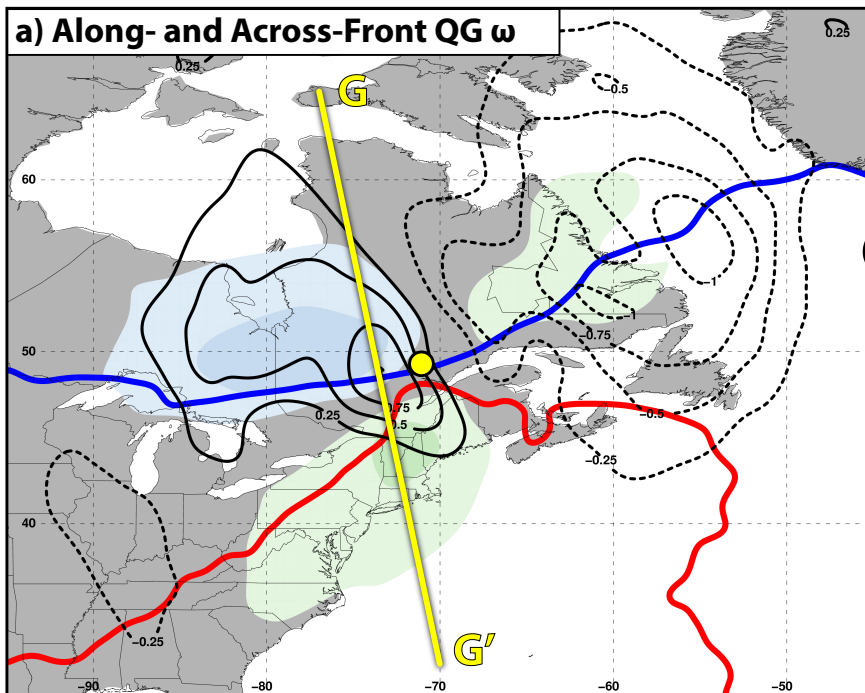


- ω_s
- 2 PVU on the 320-K surface
- 2 PVU on the 345-K surface
- Avg. Location of Jet Superposition

Both ω_s and ω_n contribute to subsidence, but ω_s is dominant.

Along- and Across-Front Vertical Motion

East Subtropical Dominant Events

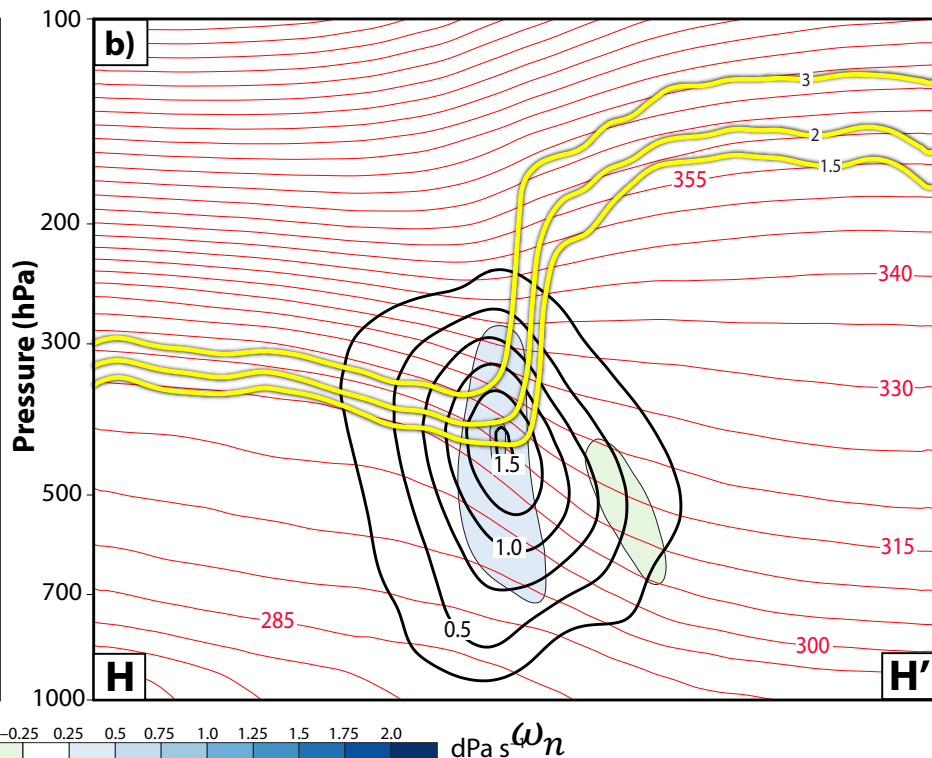
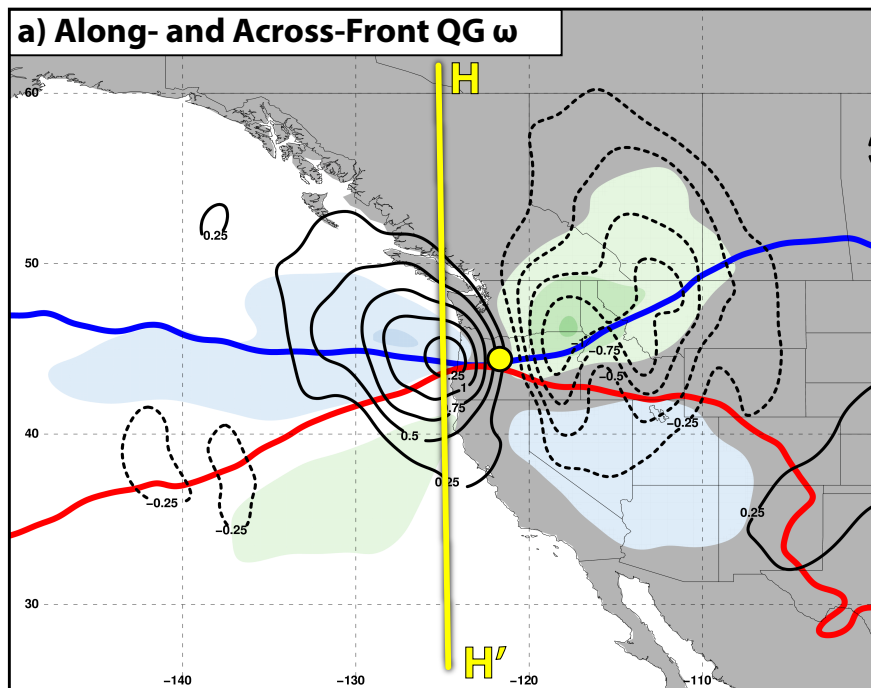


- ω_s
- 2 PVU on the 320-K surface
- 2 PVU on the 345-K surface
- Avg. Location of Jet Superposition

ω_n is closer in magnitude to ω_s compared to polar dominant events.

Along- and Across-Front Vertical Motion

West Subtropical Dominant Events



-2.0 -1.75 -1.5 -1.25 -1.0 -0.75 -0.5 -0.25 0.25 0.5 0.75 1.0 1.25 1.5 1.75 2.0 dPa s ω_n

- ω_s
- 2 PVU on the 320-K surface
- 2 PVU on the 345-K surface
- Avg. Location of Jet Superposition

ω_s is dominant compared to ω_n .

Summary

- Jet superpositions establish a dynamical and thermodynamic environment that is particularly conducive to high-impact weather.
- Descent within the jet-entrance region is a common element among jet superpositions, regardless of the event type.
- Descent is primarily associated with the geostrophic flow attributed to polar cyclonic QGPV anomalies, and the interaction of that geostrophic flow with ∇T_M and ∇T_{CYC} .
- The latter result underscores the critical role that polar cyclonic QGPV anomalies play during jet superpositions.
- Along-front subsidence, ω_s , is dominant compared to across-front subsidence, ω_n , in all event types, but ω_n is closer in magnitude to ω_s during eastern subtropical dominant events.

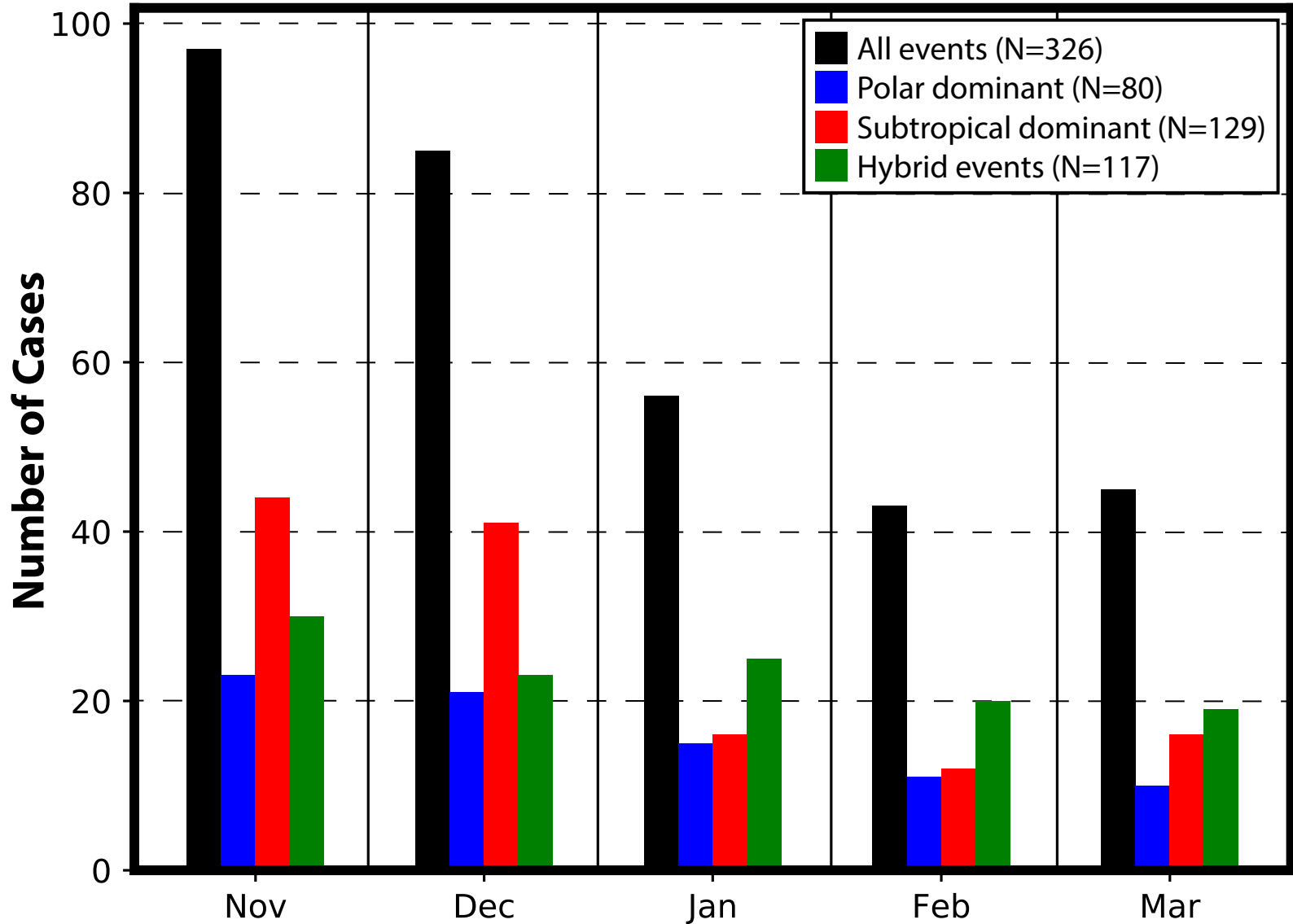
Supplementary Slides

References

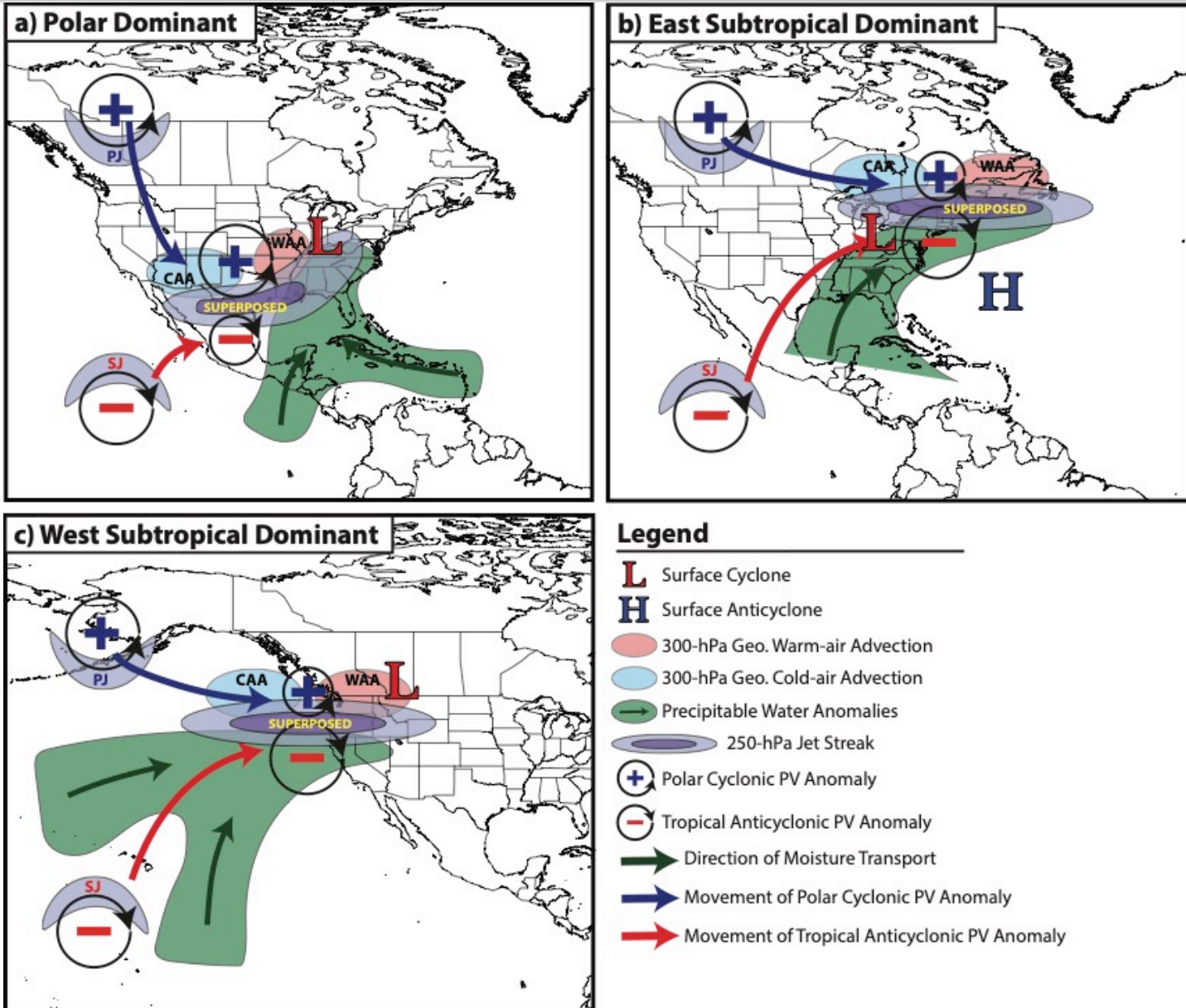
- Cavallo, S. M., and G. J. Hakim, 2010: Composite structure of tropopause polar cyclones. *Mon. Wea. Rev.*, **138**, 3840–3857.
- Christenson, C. E., and J. E. Martin, 2012: The large-scale environment associated with the 25–28 April 2011 severe weather outbreak. *16th NWA Severe Storms and Doppler Radar Conference*, Des Moines, IA, National Weather Association, 31 March 2012.
- Christenson, C. E., J. E. Martin, and Z. J. Handlos, 2017: A synoptic-climatology of Northern Hemisphere, cold season polar and subtropical jet superposition events. *J. Climate*, **30**, 7231–7246.
- Defant, F., and H. Taba, 1957: The threefold structure of the atmosphere and the characteristics of the tropopause. *Tellus*, **9**, 259–275.
- Knupp, K. R., T. A. Murphy, T. A. Coleman, R. A. Wade, S. A. Mullins, C. J. Schultz, E. V. Schultz, L. Carey, A. Sherrer, E. W. McCaul Jr., B. Carcione, S. Latimer, A. Kula, K. Laws, P. T. Marsh, and K. Klockow, 2014: Meteorological overview of the devastating 27 April 2011 Tornado Outbreak. *Bull. Amer. Meteor. Soc.*, **95**, 1041–1062.
- Moore, B. J., P. J. Neiman, F. M. Ralph, and F. E. Barthold, 2012: Physical processes associated with heavy flooding rainfall in Nashville, Tennessee, and vicinity during 1–2 May 2010: The role of an atmospheric river and mesoscale convective systems. *Mon. Wea. Rev.*, **140**, 358–378.
- Pyle, M. E., D. Keyser, and L. F. Bosart, 2004: A diagnostic study of jet streaks: Kinematic signatures and relationship to coherent tropopause disturbances. *Mon. Wea. Rev.*, **132**, 297–319.
- Saha, S. and co-authors, 2014: The NCEP Climate Forecast System Version 2. *J. Climate*, **27**, 2185–2208.
- Winters, A. C., and J. E. Martin, 2014: The role of a polar/subtropical jet superposition in the May 2010 Nashville Flood. *Wea. Forecasting*, **29**, 954–974.
- Winters, A. C. and J. E. Martin, 2016: Synoptic and mesoscale processes supporting vertical superposition of the polar and subtropical jets in two contrasting cases. *Quart. J. Roy. Meteor. Soc.*, **142**, 1133–1149.
- Winters, A. C., and J. E. Martin, 2017: Diagnosis of a North American polar/subtropical jet superposition employing piecewise potential vorticity inversion. *Mon. Wea. Rev.*, **145**, 1853–1873.
- Winters, A.C., D. Keyser, L. F. Bosart, and J. E. Martin, 2020: Composite synoptic-scale environments conducive to North American polar–subtropical jet superposition events. *Mon. Wea. Rev.*, **148**, in revision.

Composite Characteristics

Jet Superposition Event Characteristics

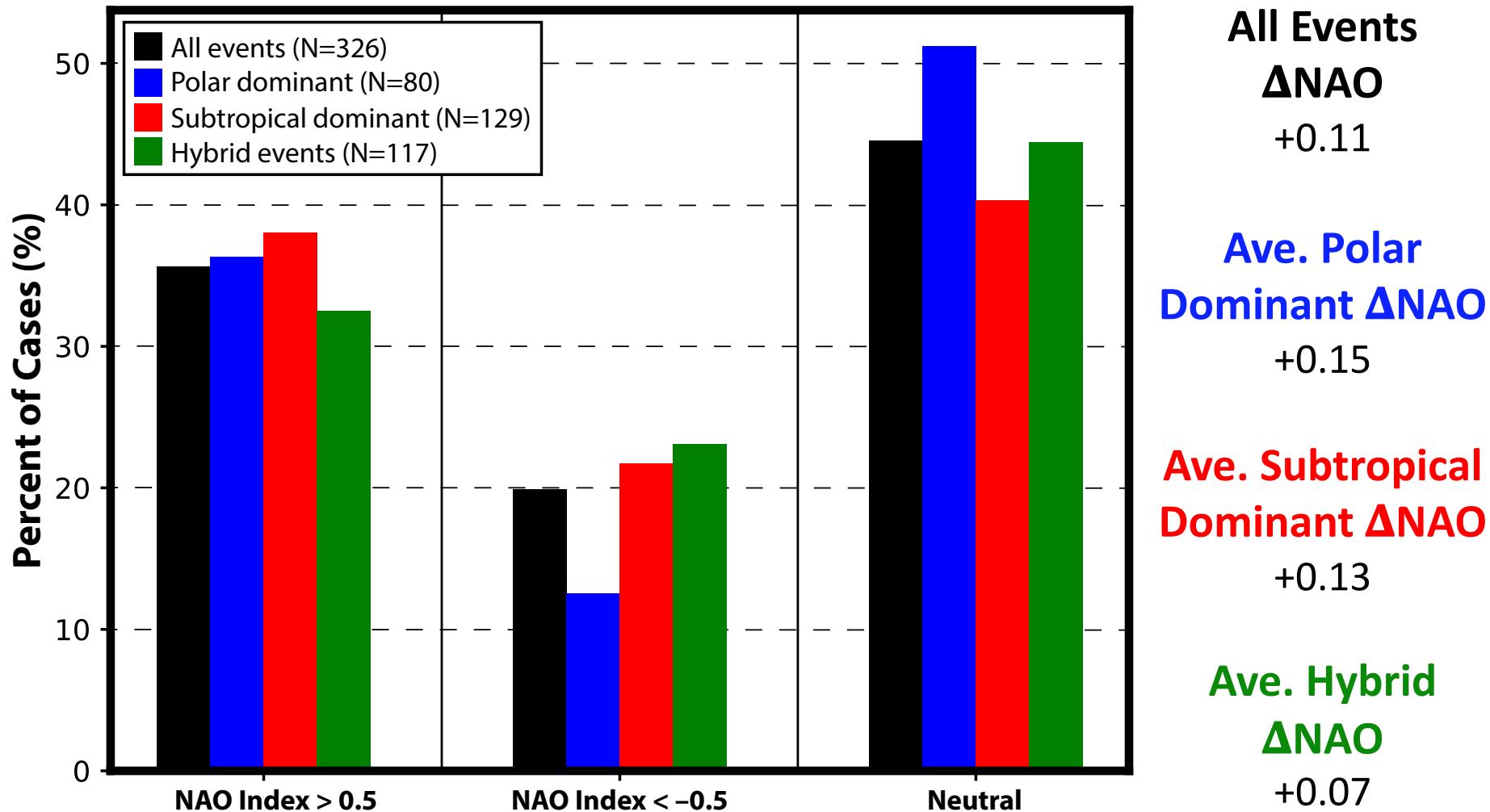


Jet Superposition Event Composites



Downstream Consequences

North Atlantic Oscillation: 5 Days After Jet Superposition



Background Material

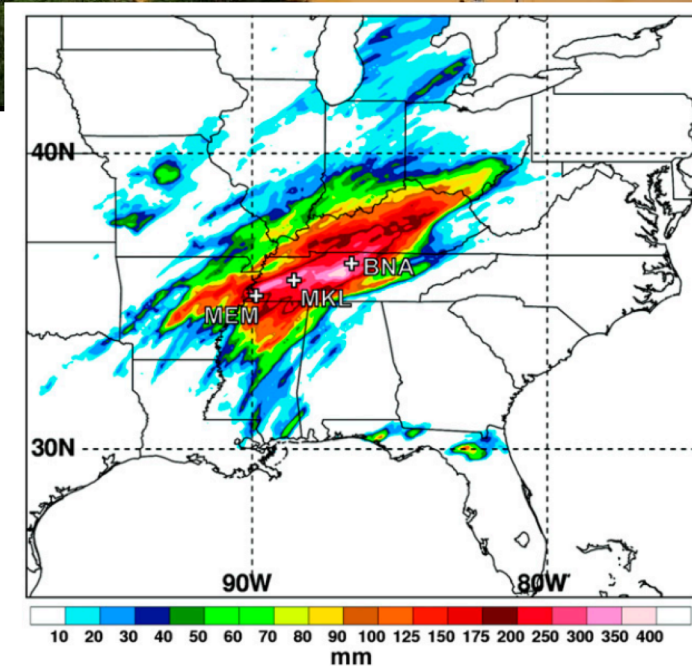
Jet Superpositions and High-Impact Weather



Jet superpositions can be an element of high-impact weather events

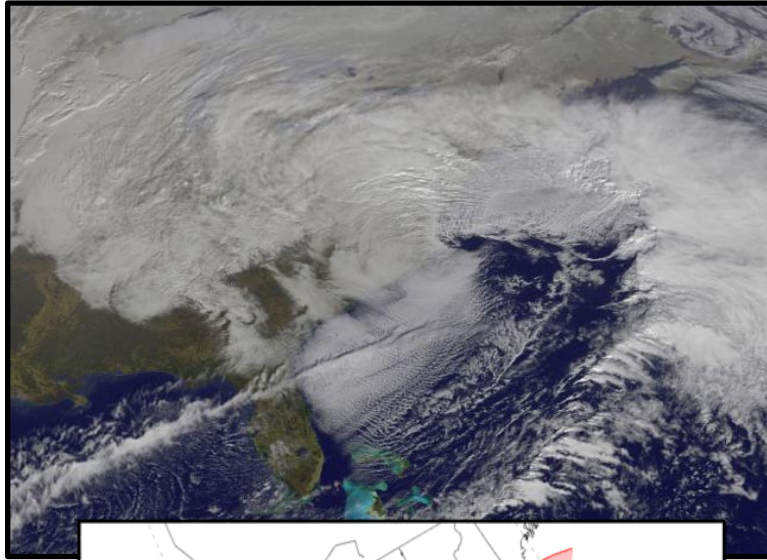
1–3 May 2010 Nashville Flood

- Jet superposition enhanced the poleward moisture transport via its associated across-front ageostrophic circulation (Winters and Martin 2014; 2016)



Moore et al. (2012; their Fig. 2)

Jet Superpositions and High-Impact Weather



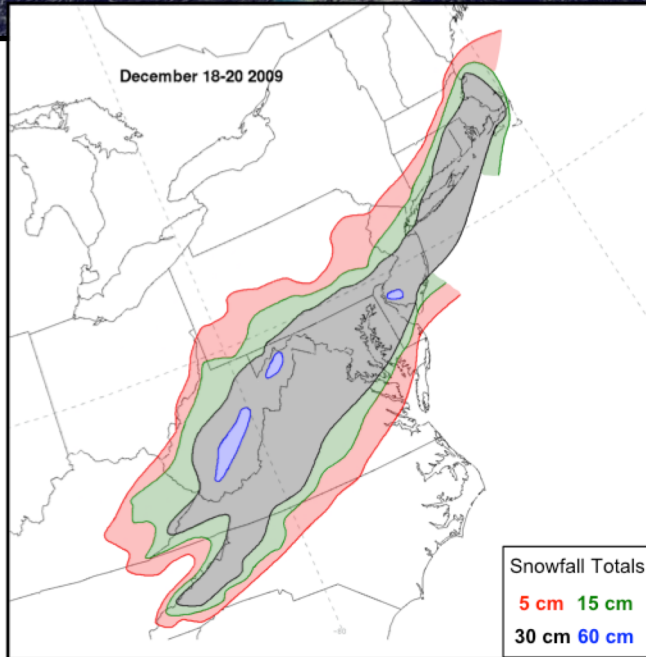
Jet superpositions can be an element of high-impact weather events

1–3 May 2010 Nashville Flood

- Jet superposition enhanced the poleward moisture transport via its associated across-front ageostrophic circulation (Winters and Martin 2014; 2016)

18–20 December 2009 Mid-Atlantic Blizzard

- Jet superposition was associated with a rapidly deepening East Coast cyclone (Winters and Martin 2016; 2017)



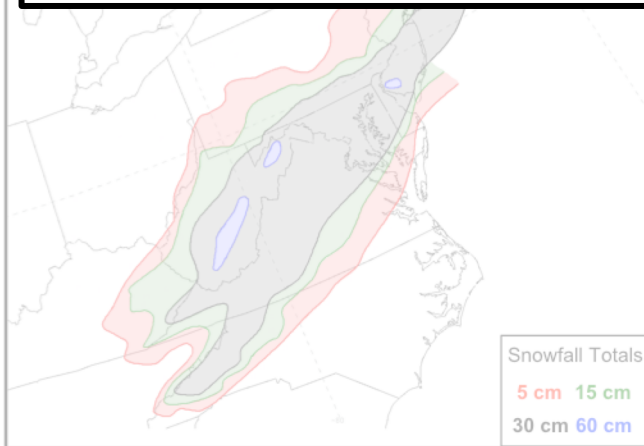
Jet Superpositions and High-Impact Weather



Jet superpositions can be an element of high-impact weather events

1–3 May 2010 Nashville Flood

How do these structures develop?

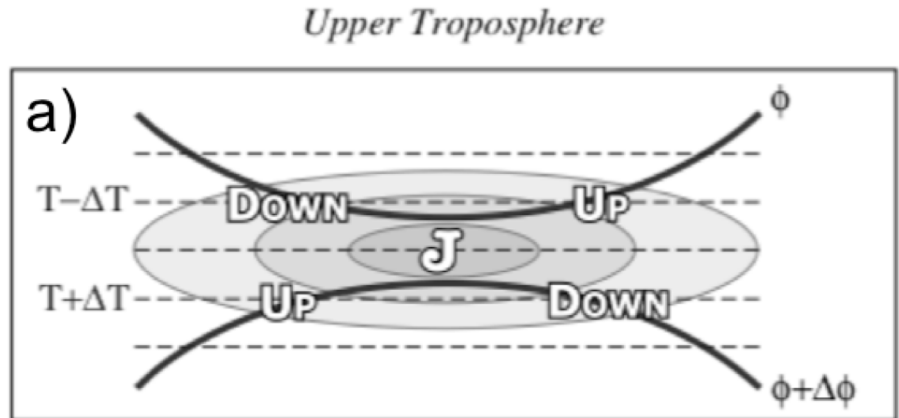


18–20 December 2009 mid-Atlantic blizzard

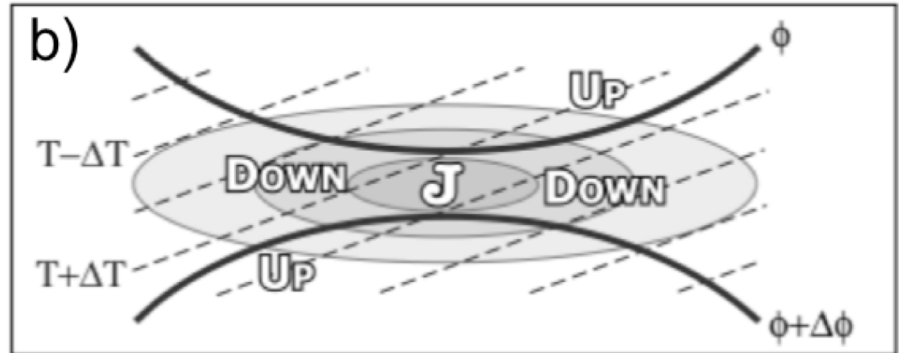
- Jet superposition was associated with a rapidly deepening East Coast cyclone (Winters and Martin 2016; 2017)

Ageostrophic Transverse Jet Circulations

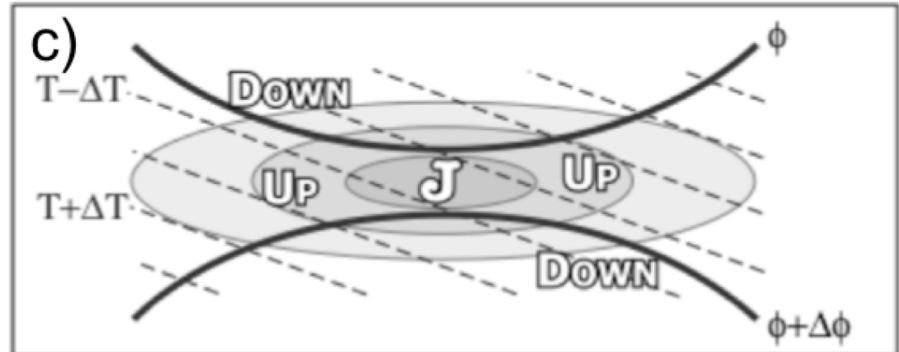
Traditional four-quadrant model



Geo. cold-air advection (CAA)
along the jet axis promotes
subsidence through the jet core



Geo. warm-air advection (WAA)
along the jet axis promotes
ascent through the jet core

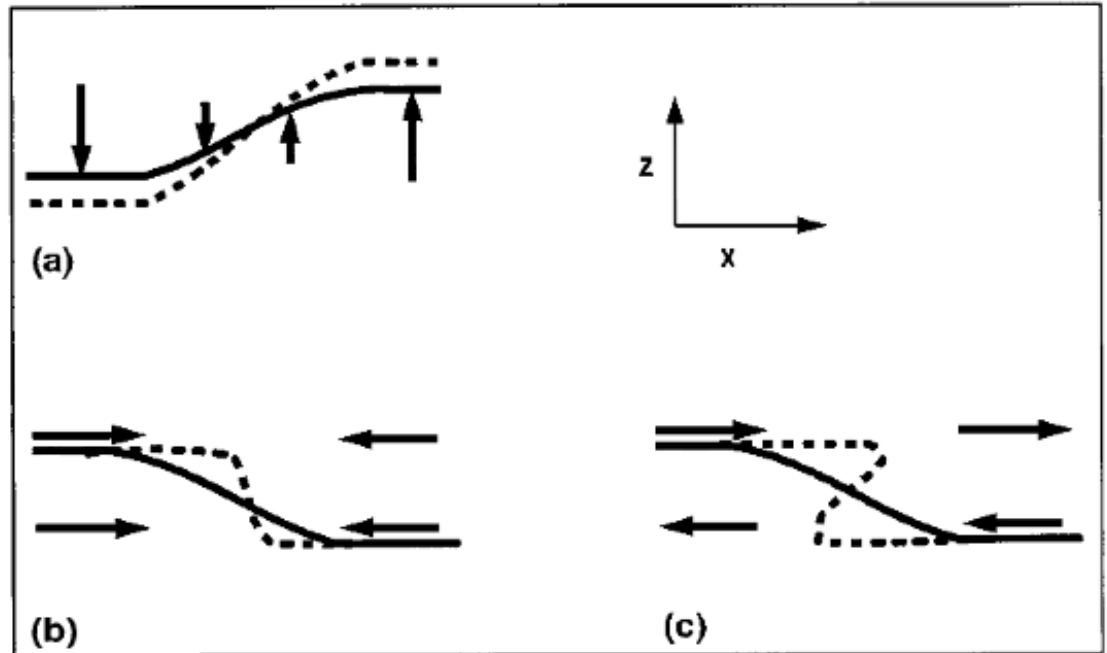


Background

Insight into how the tropopause can be restructured from a PV perspective can be found by consulting Wandishin et al. (2000)

Two processes can account for “foldogenesis”:

- 1) **Differential vertical motions** can vertically steepen the tropopause.
- 2) **Convergence or a vertical shear** can produce a differential horizontal advection of the tropopause surface.



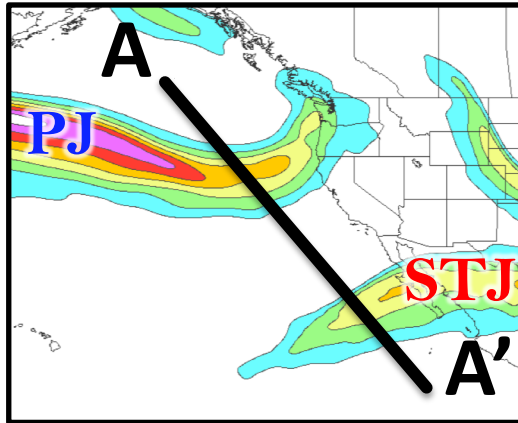
Wandishin et al. 2000

These same mechanisms are also likely to play an important role in superpositions.

Jet Identification

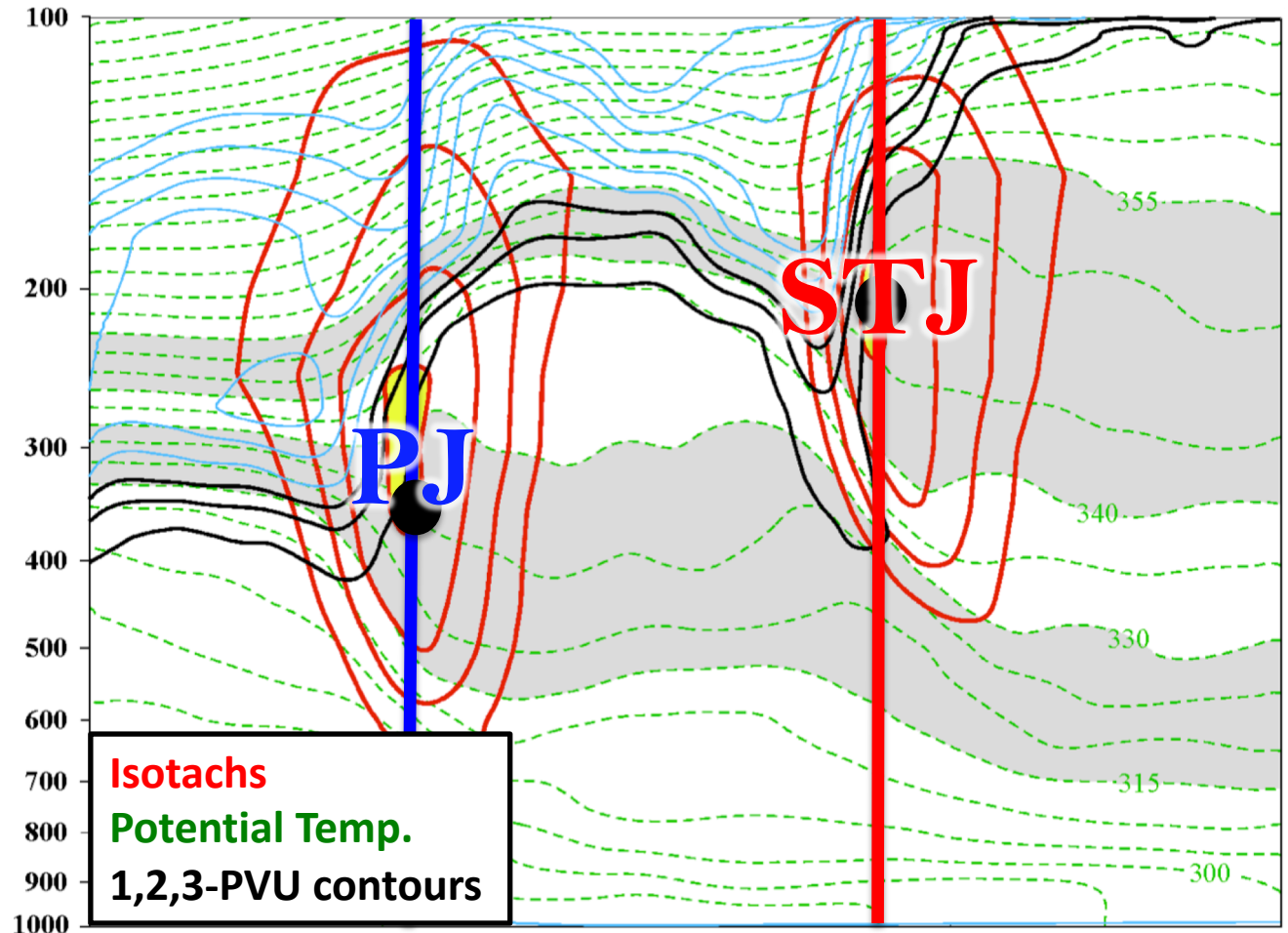
Jet Superposition Event Identification

0000 UTC 27 April 2010



250-hPa wind speed

Isolated grid points over North America in the CFSR (Saha et al. 2014) characterized by polar and subtropical jets during Nov–Mar 1979–2010.

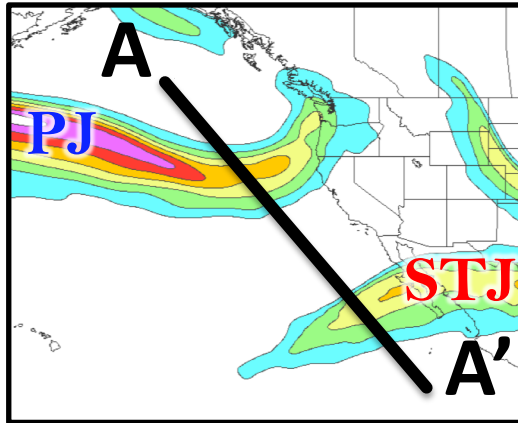


Isotachs
Potential Temp.
1,2,3-PVU contours

A Winters and Martin (2014, 2016, 2017); Christenson et al. (2017); Handlos and Martin (2016) **A'**

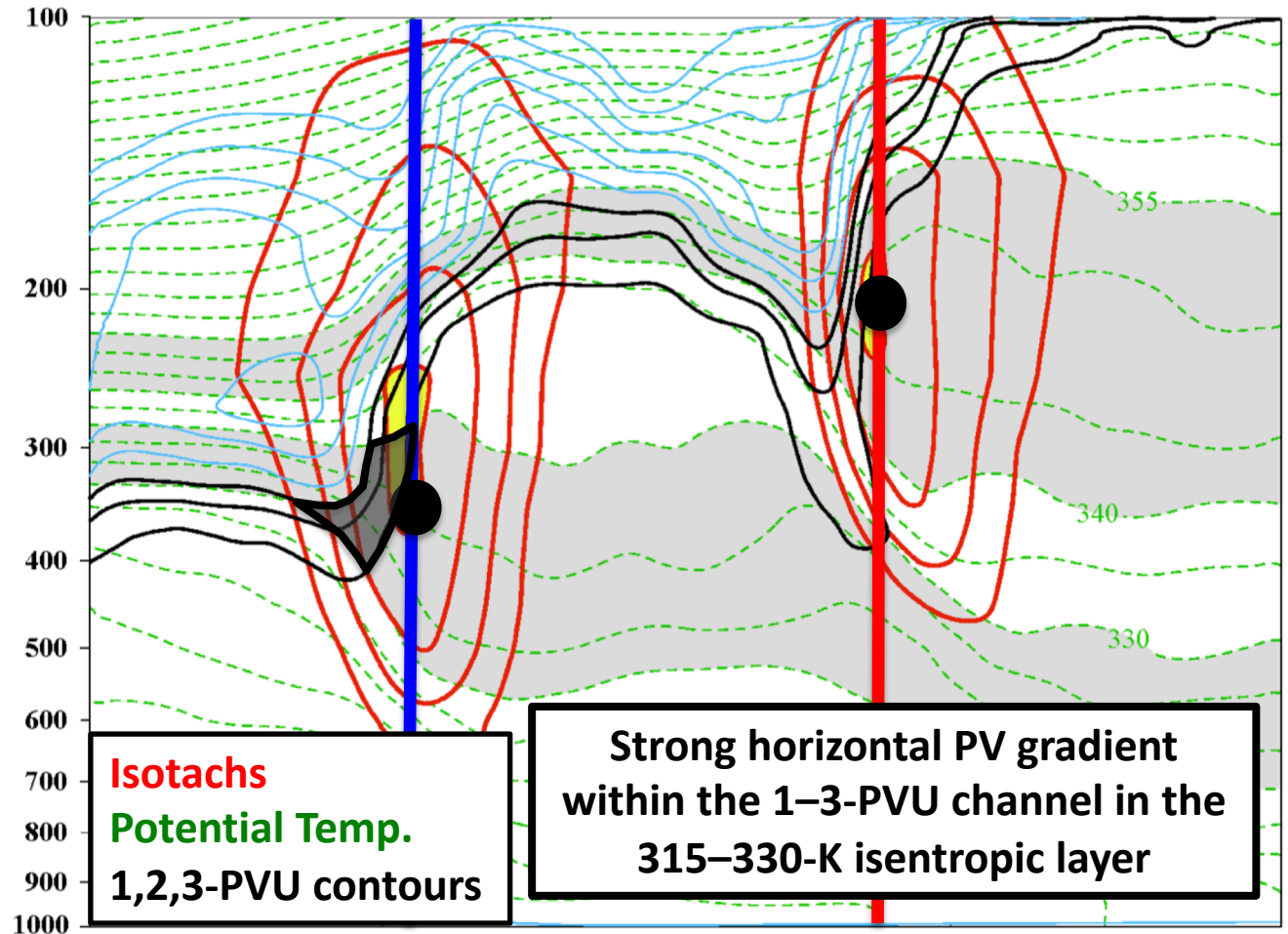
Jet Superposition Event Identification

0000 UTC 27 April 2010



250-hPa wind speed

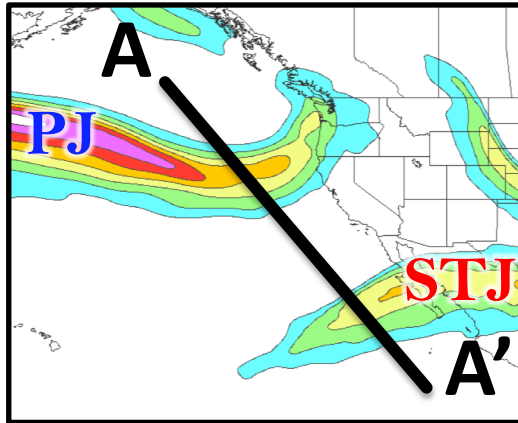
Isolated grid points over North America in the CFSR (Saha et al. 2014) characterized by polar and subtropical jets during Nov–Mar 1979–2010.



A Winters and Martin (2014, 2016, 2017); Christenson et al. (2017); Handlos and Martin (2016) **A'**

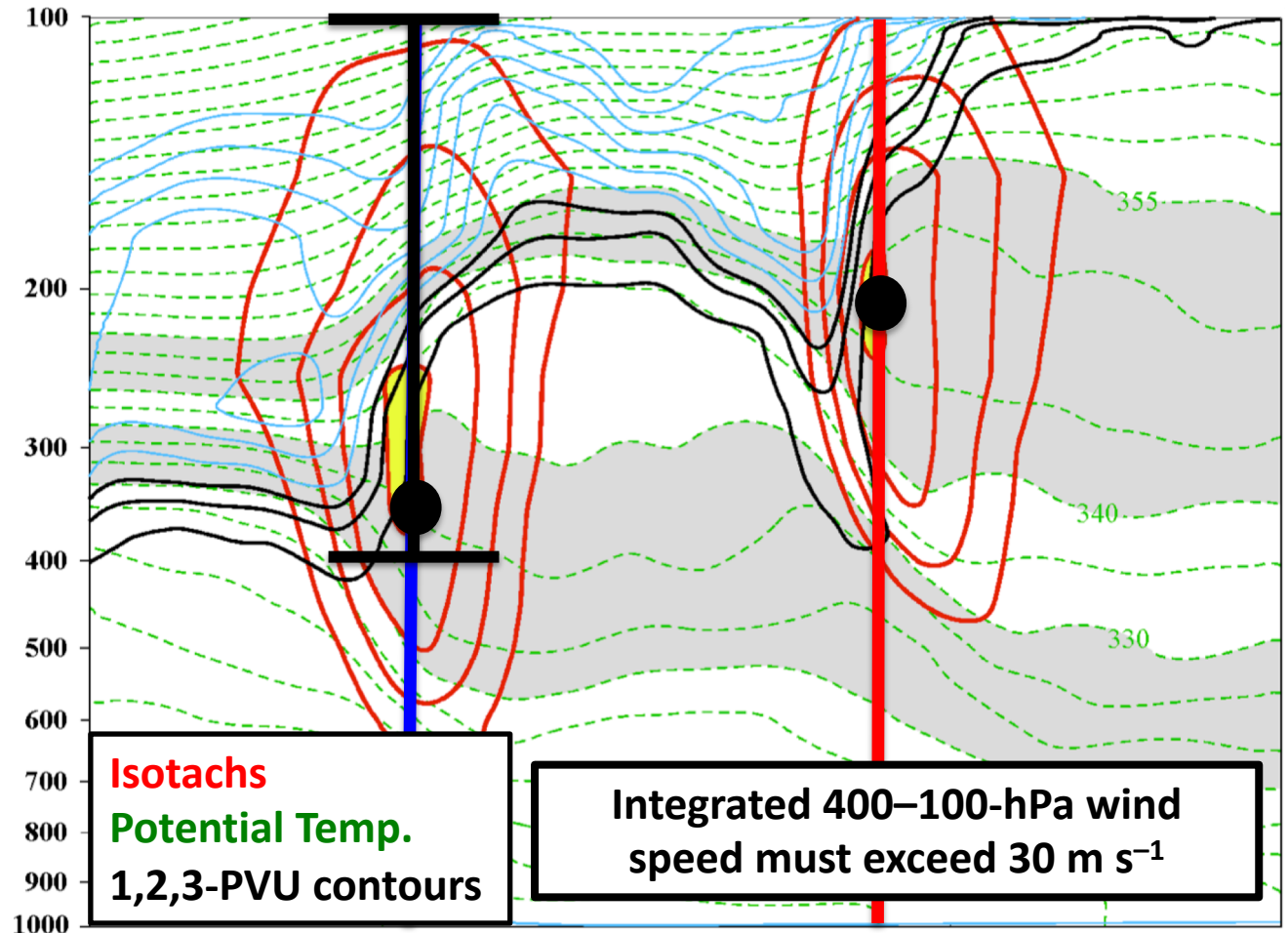
Jet Superposition Event Identification

0000 UTC 27 April 2010



250-hPa wind speed

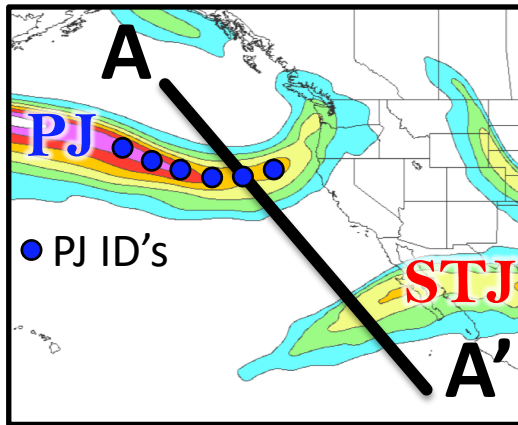
Isolated grid points over North America in the CFSR (Saha et al. 2014) characterized by polar and subtropical jets during Nov–Mar 1979–2010.



A Winters and Martin (2014, 2016, 2017); Christenson et al. (2017); Handlos and Martin (2016) **A'**

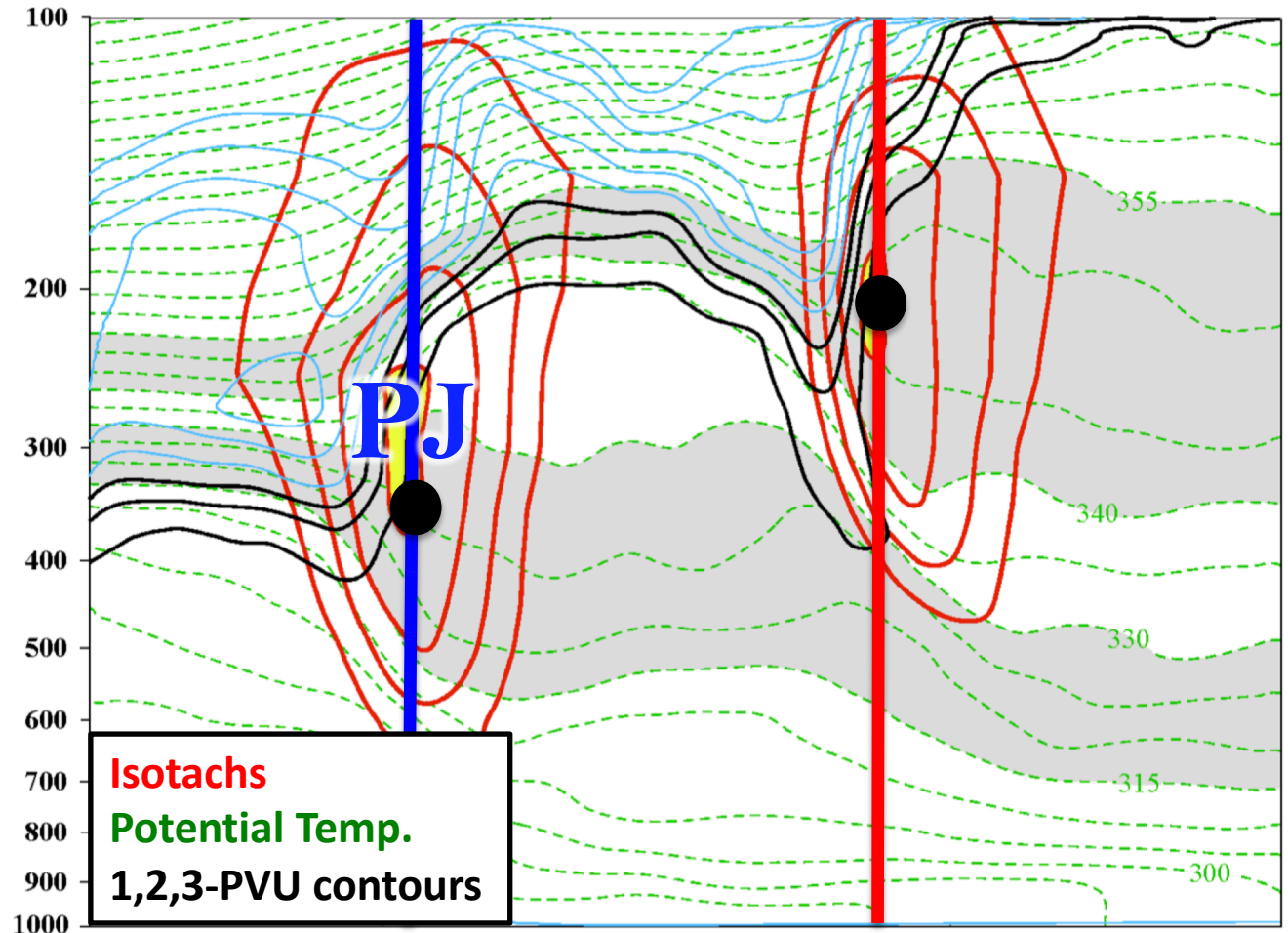
Jet Superposition Event Identification

0000 UTC 27 April 2010



250-hPa wind speed

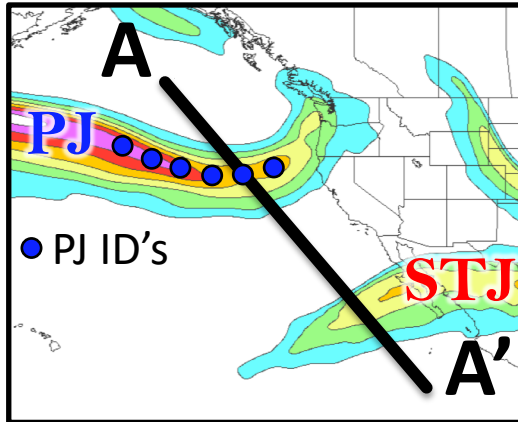
Isolated grid points over North America in the CFSR (Saha et al. 2014) characterized by polar and subtropical jets during Nov–Mar 1979–2010.



A Winters and Martin (2014, 2016, 2017); Christenson et al. (2017); Handlos and Martin (2016) **A'**

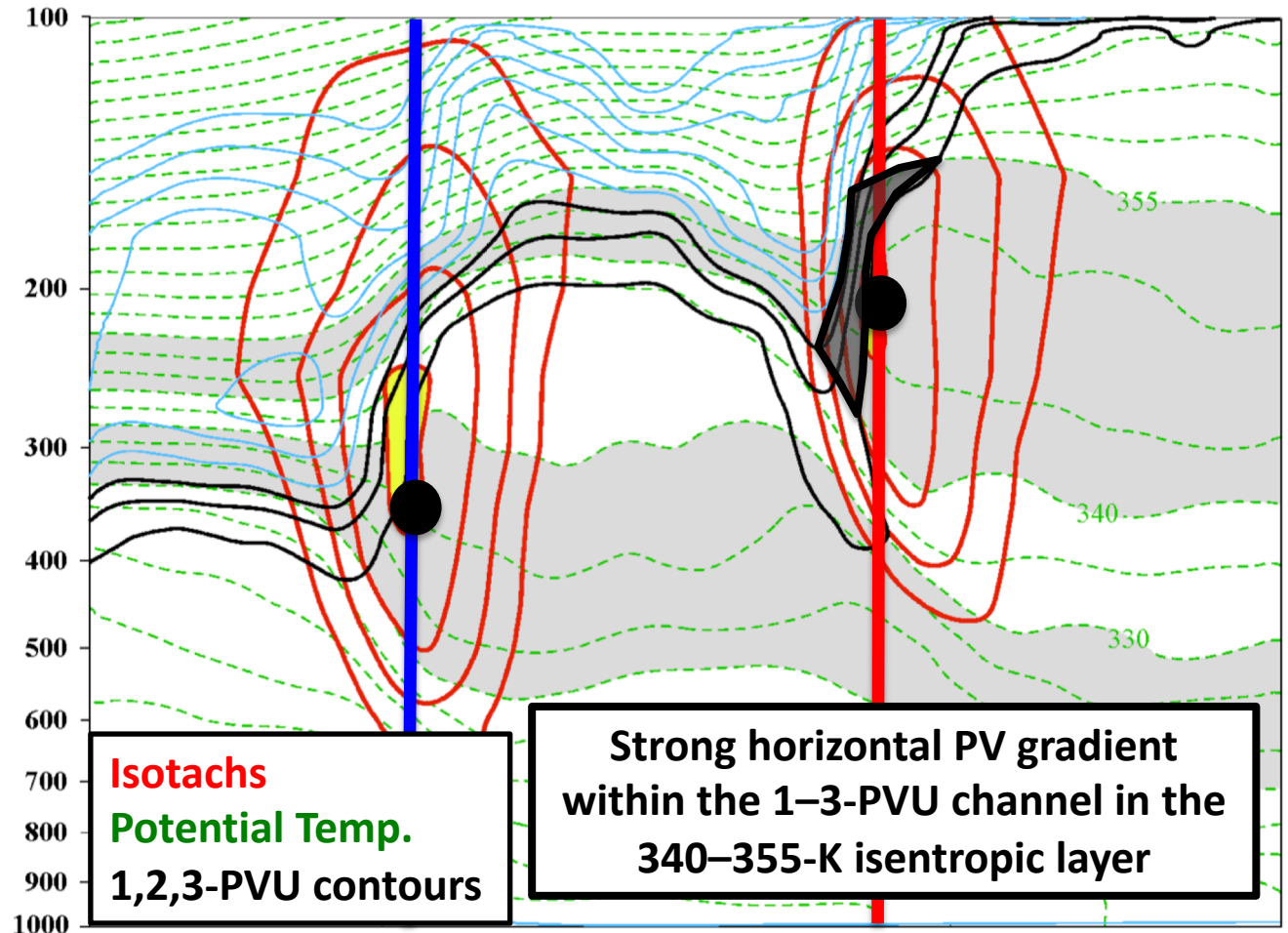
Jet Superposition Event Identification

0000 UTC 27 April 2010



250-hPa wind speed

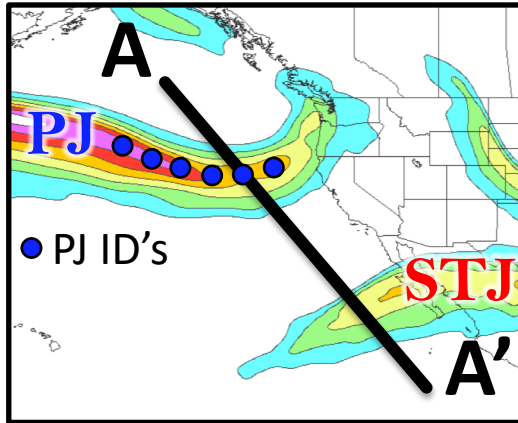
Isolated grid points over North America in the CFSR (Saha et al. 2014) characterized by polar and subtropical jets during Nov–Mar 1979–2010.



A Winters and Martin (2014, 2016, 2017); Christenson et al. (2017); Handlos and Martin (2016) **A'**

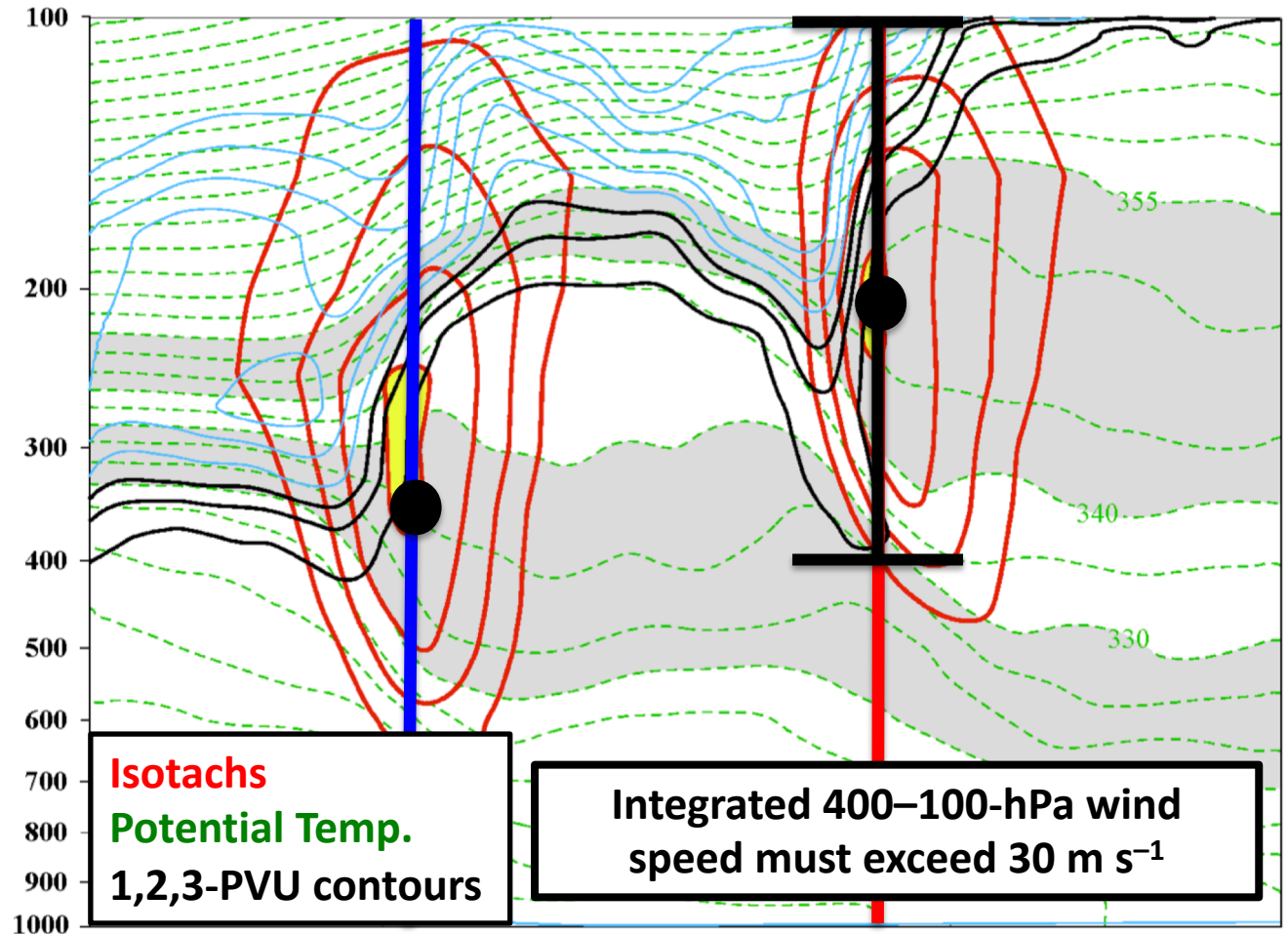
Jet Superposition Event Identification

0000 UTC 27 April 2010



250-hPa wind speed

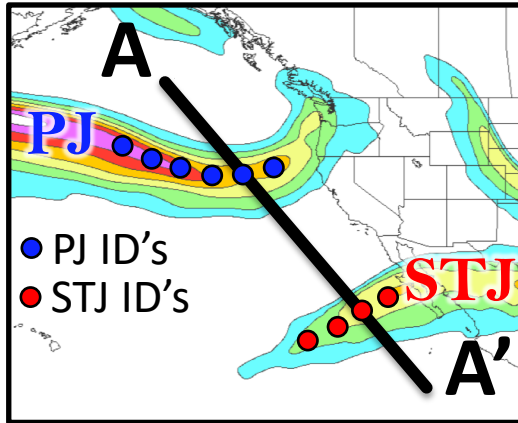
Isolated grid points over North America in the CFSR (Saha et al. 2014) characterized by polar and subtropical jets during Nov–Mar 1979–2010.



A Winters and Martin (2014, 2016, 2017); Christenson et al. (2017); Handlos and Martin (2016) **A'**

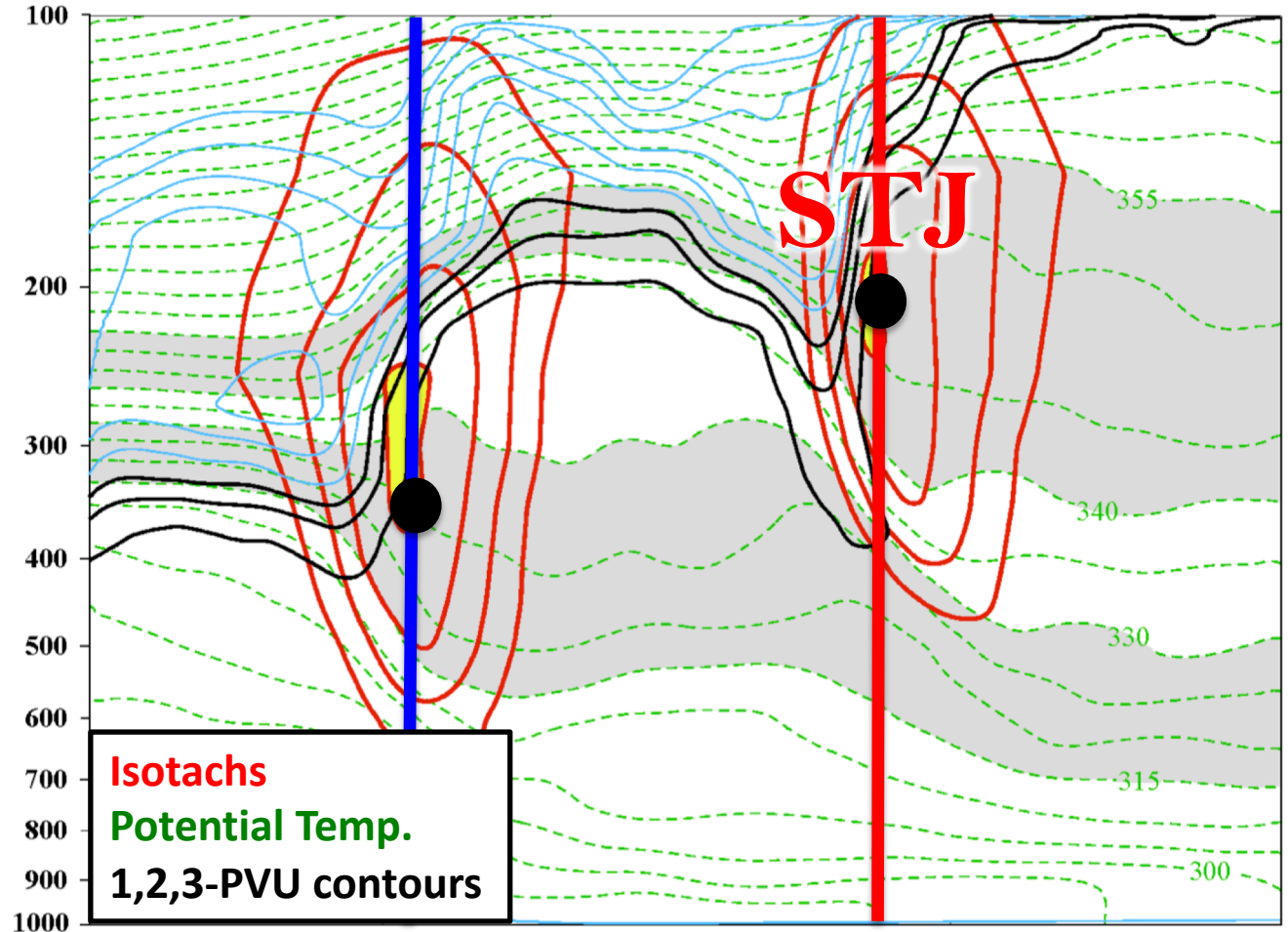
Jet Superposition Event Identification

0000 UTC 27 April 2010



250-hPa wind speed

Isolated grid points over North America in the CFSR (Saha et al. 2014) characterized by polar and subtropical jets during Nov–Mar 1979–2010.

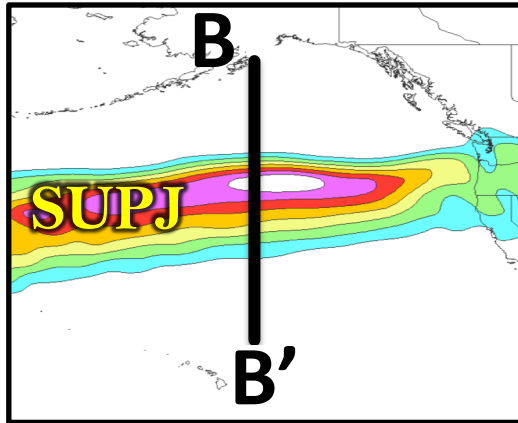


Isotachs
Potential Temp.
1,2,3-PVU contours

A Winters and Martin (2014, 2016, 2017); Christenson et al. (2017); Handlos and Martin (2016) **A'**

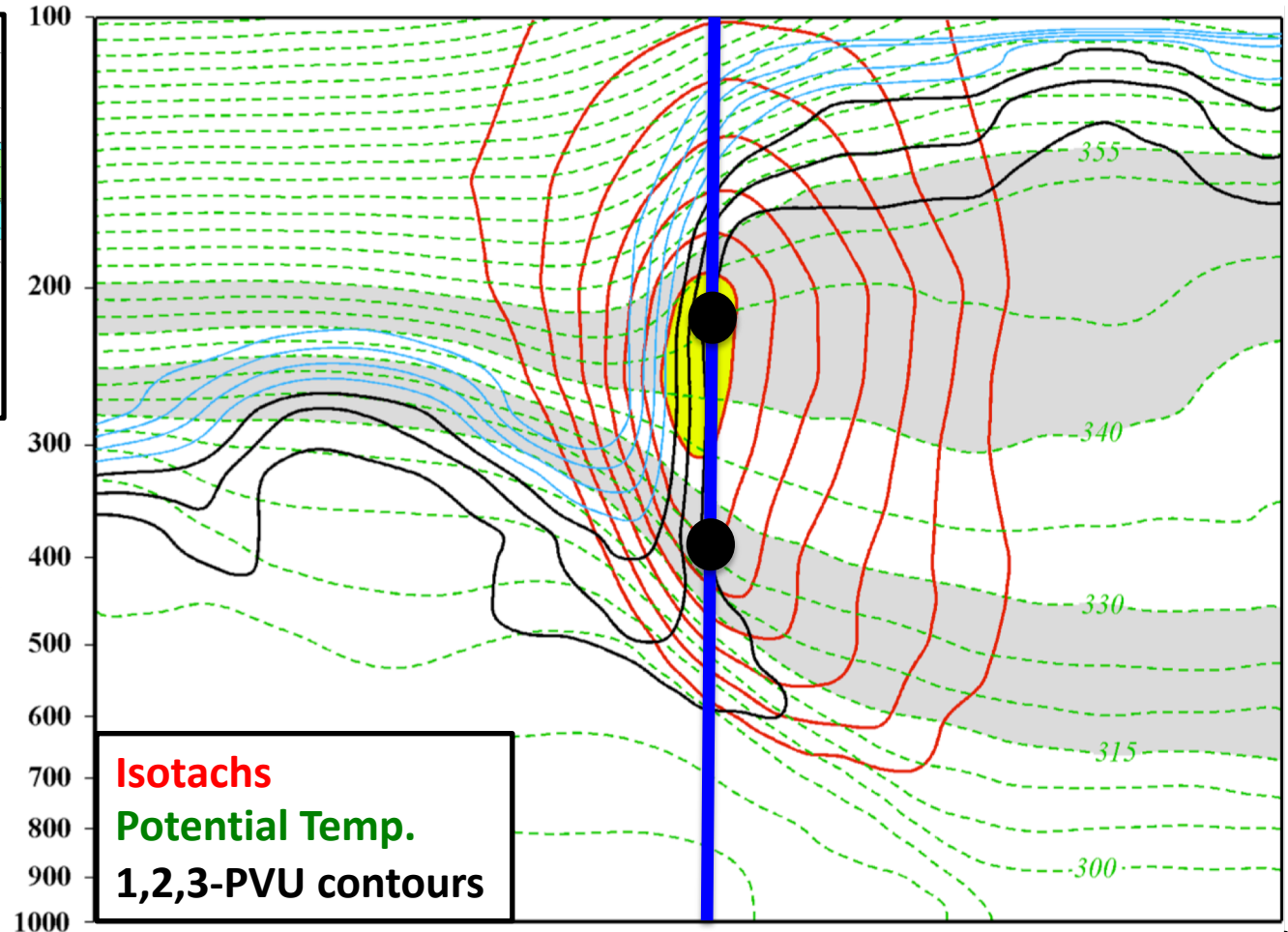
Jet Superposition Event Identification

0000 UTC 24 October 2010



250-hPa wind speed

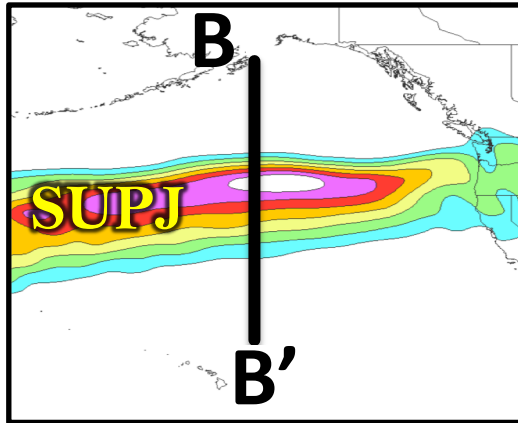
Isolated grid points over North America in the CFSR (Saha et al. 2014) characterized by a jet superposition during Nov–Mar 1979–2010.



B Winters and Martin (2014, 2016, 2017); Christenson et al. (2017); Handlos and Martin (2016) **B'**

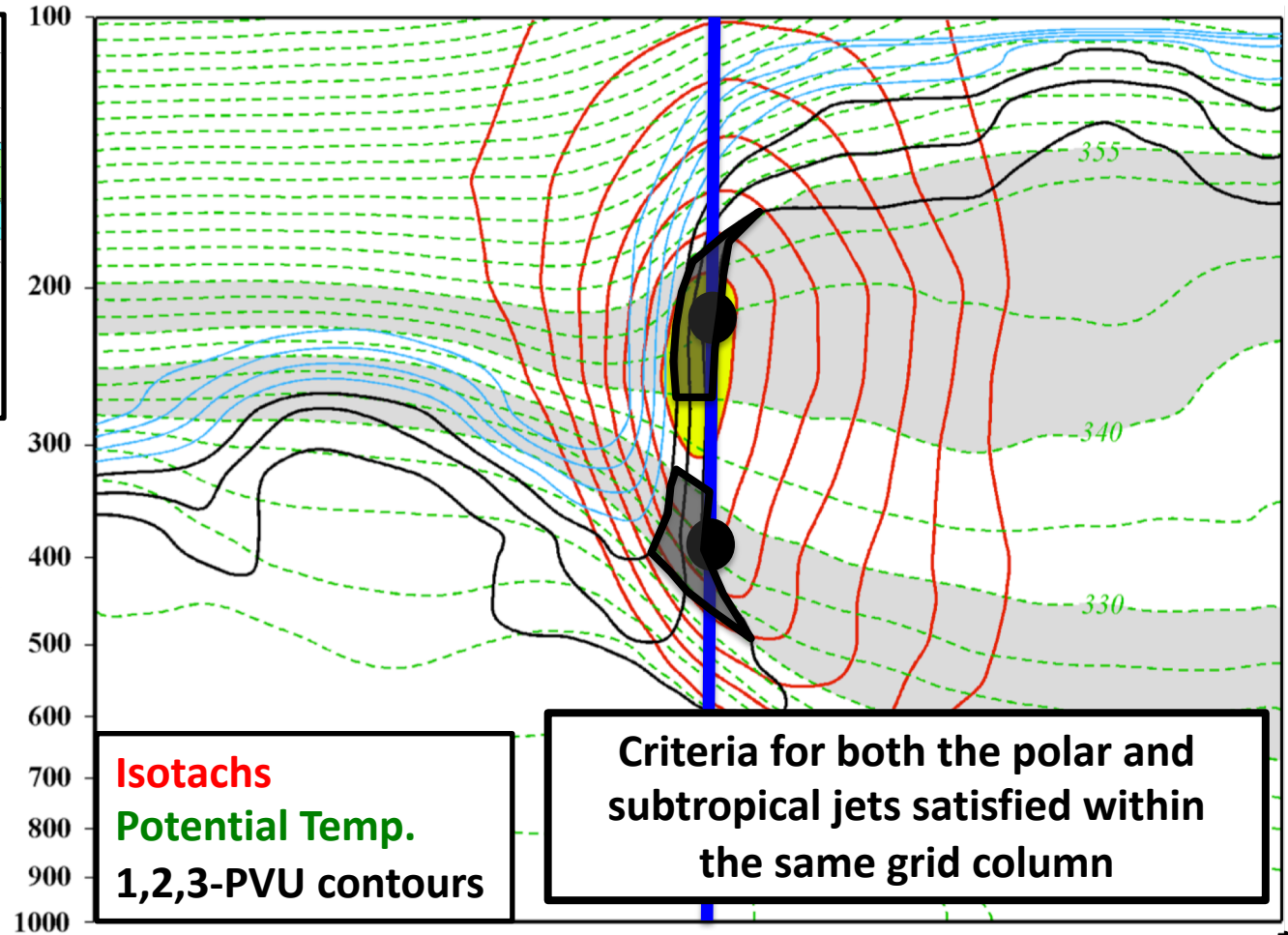
Jet Superposition Event Identification

0000 UTC 24 October 2010



250-hPa wind speed

Isolated grid points over North America in the CFSR (Saha et al. 2014) characterized by a jet superposition during Nov–Mar 1979–2010.



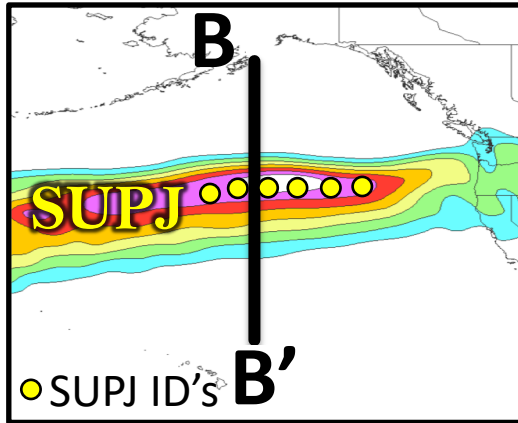
Isotachs
Potential Temp.
1,2,3-PVU contours

Criteria for both the polar and subtropical jets satisfied within the same grid column

B Winters and Martin (2014, 2016, 2017); Christenson et al. (2017); Handlos and Martin (2016) **B'**

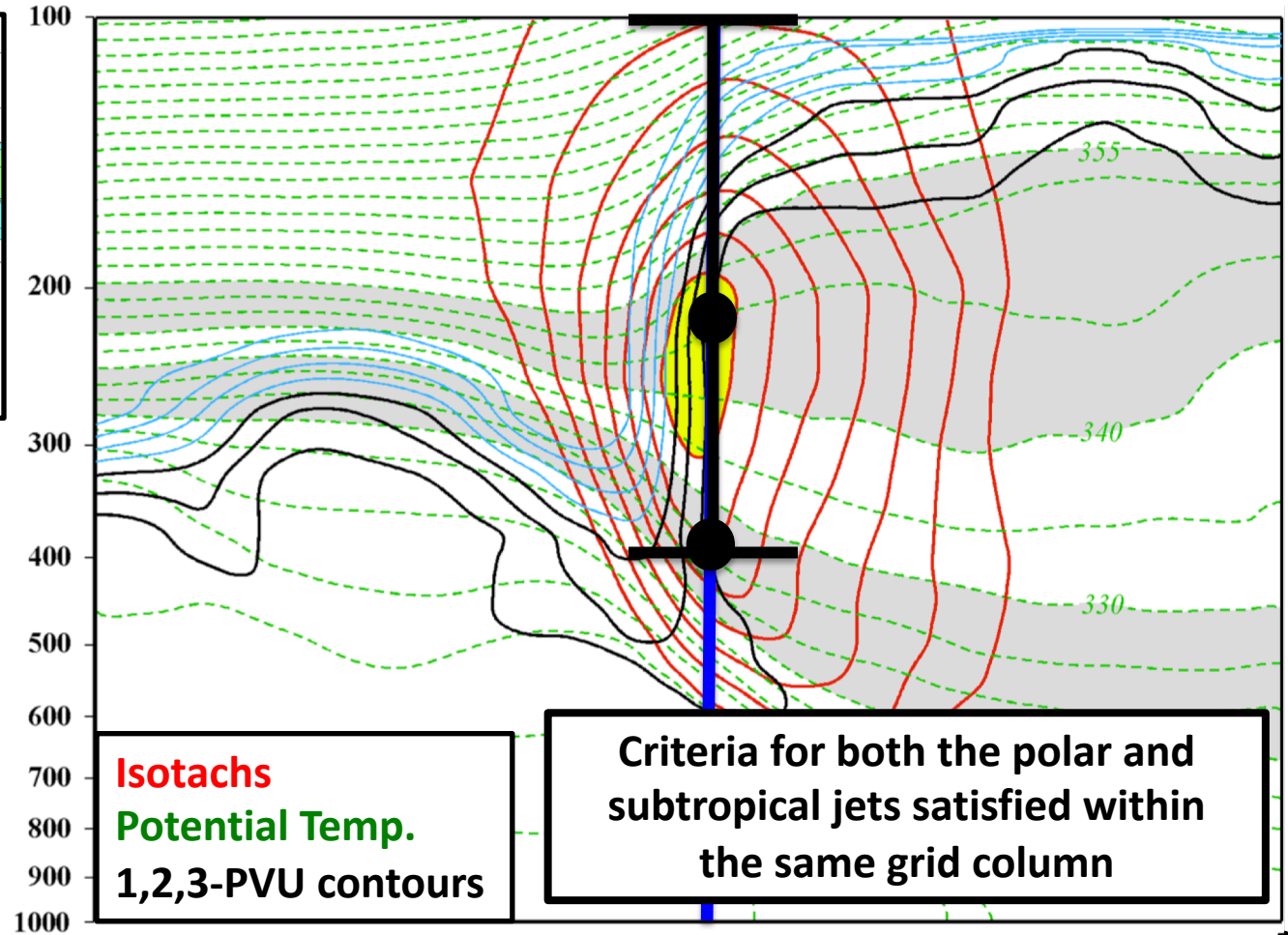
Jet Superposition Event Identification

0000 UTC 24 October 2010



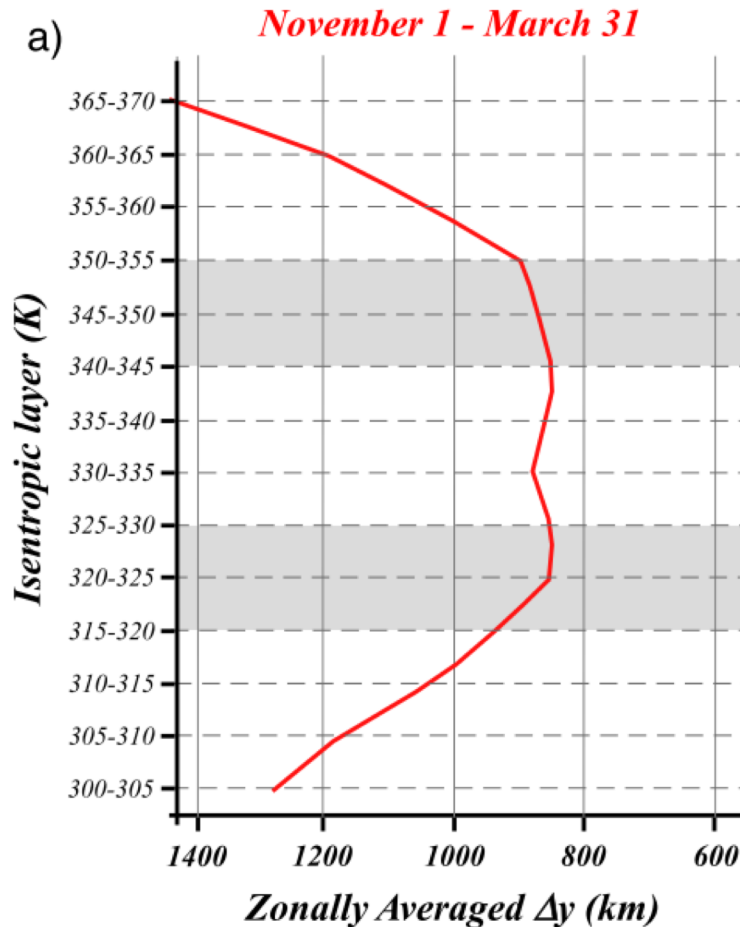
250-hPa wind speed

Isolated grid points over North America in the CFSR (Saha et al. 2014) characterized by a jet superposition during Nov–Mar 1979–2010.



B Winters and Martin (2014, 2016, 2017); Christenson et al. (2017); Handlos and Martin (2016) **B'**

Background



Christenson et al. (2017)

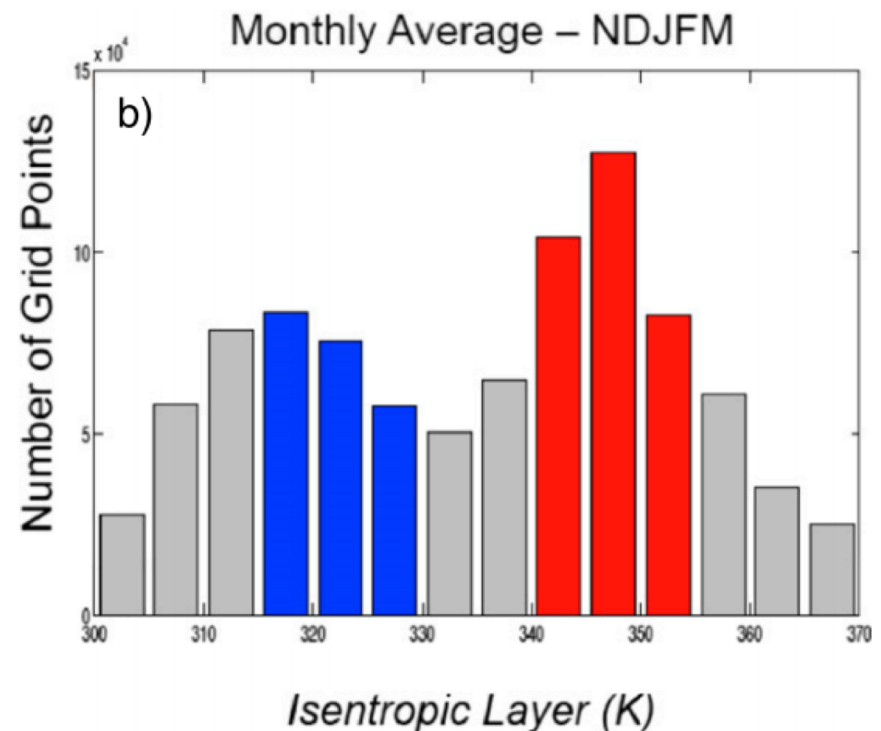
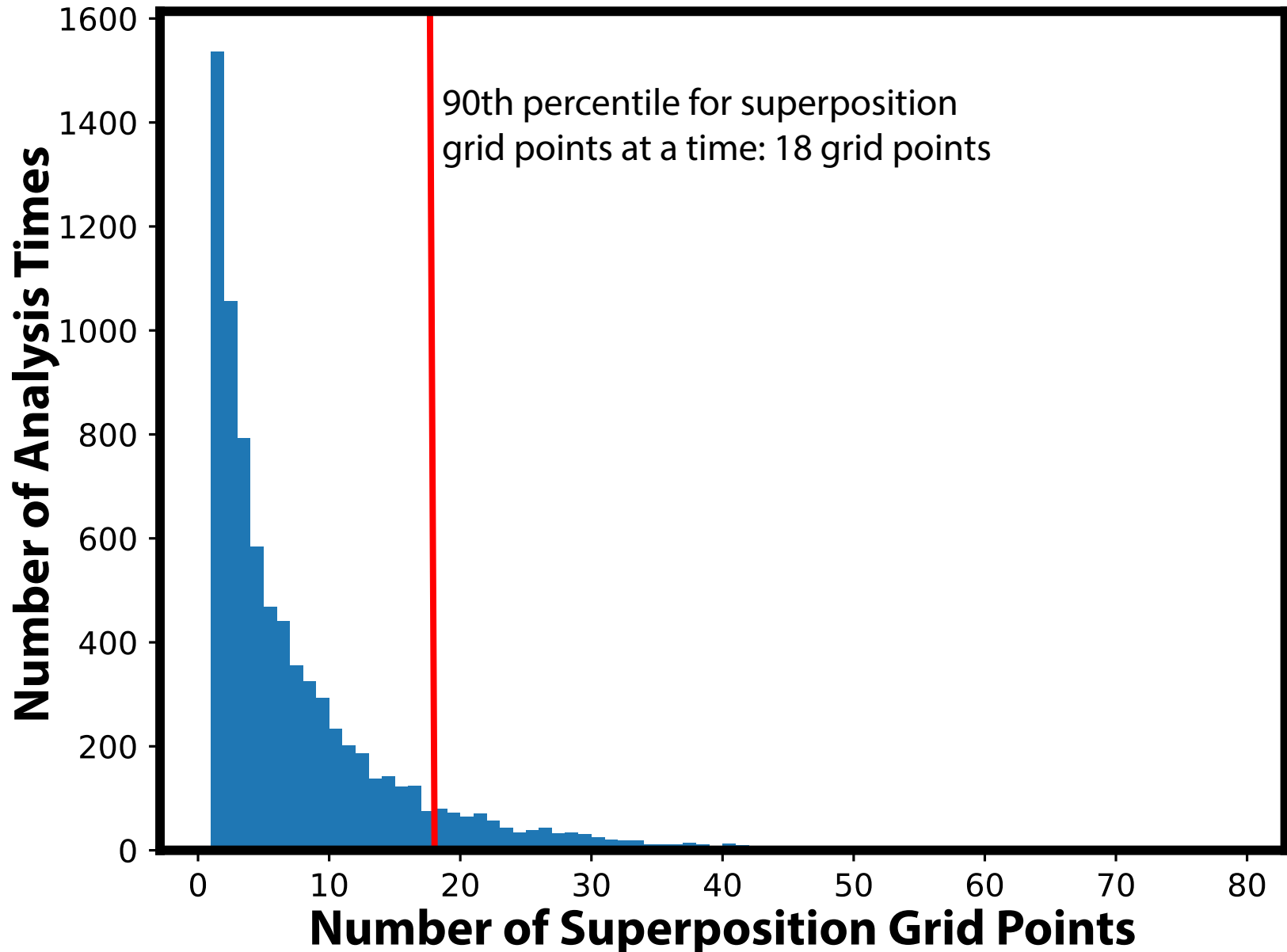


FIG. 2. (a) Cold season average of zonally averaged Δy (km) for 5-K isentropic layers ranging from 300–305 to 365–370 K. The 315–330- and 340–355-K layers are highlighted in light gray shading. (b) The average frequency of occurrence of grid points with a maximum wind speed value within the 5-K isentropic layers along the abscissa per cold season. The 315–330- and 340–355-K layers are shaded in blue and red, respectively.

Jet Superposition Event Identification

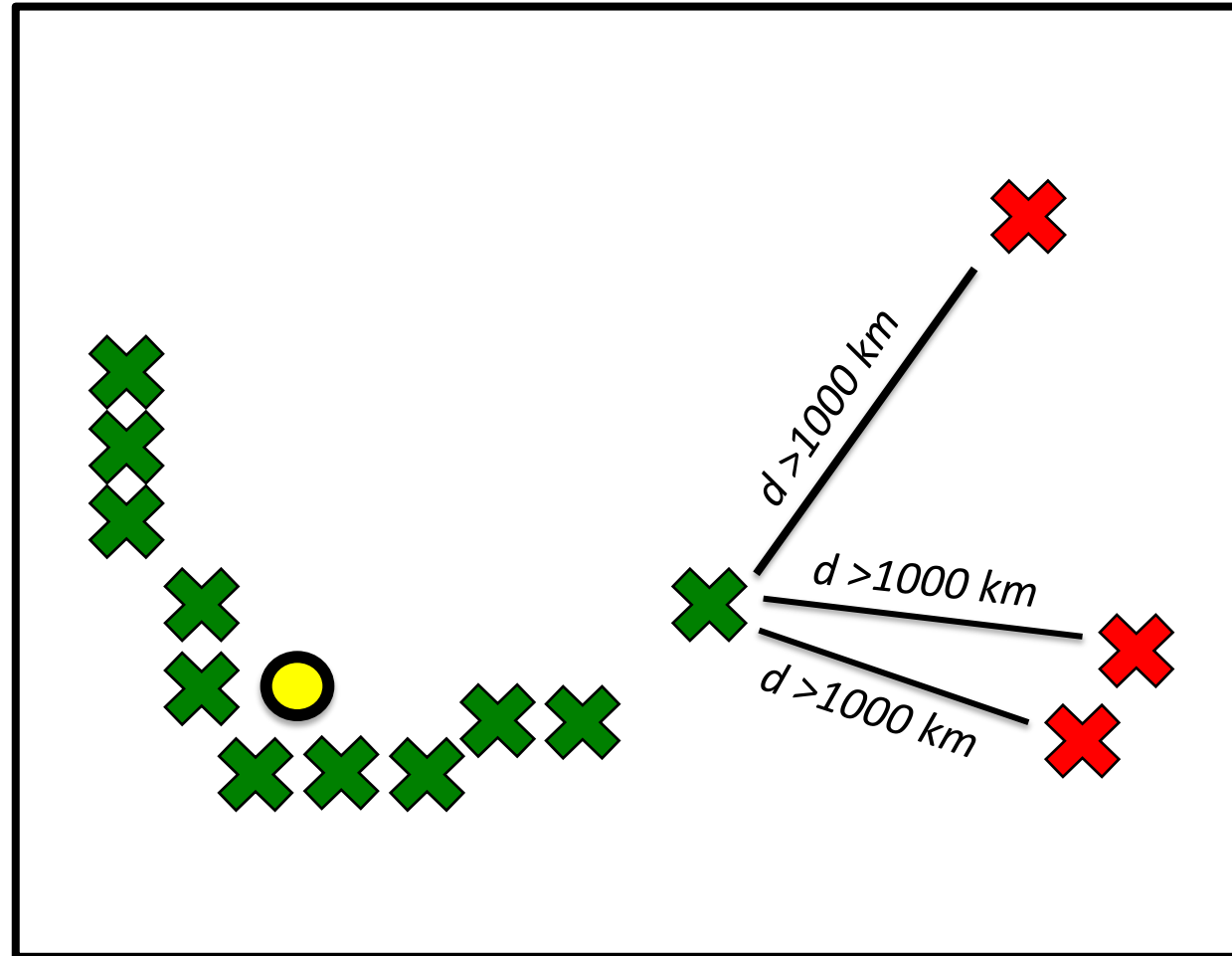


Jet Superposition Event Identification

Sample Jet Superposition Centroid Calculation

Calculated the centroid of each jet superposition based on all valid grid points at a particular analysis time.

To calculate the centroid, there must exist a group of 18 superposition grid points, of which no superposition grid point is >1000 km away from another superposition grid point.



✕ Used for calculation

✕ Not used for calculation

● Jet superposition centroid